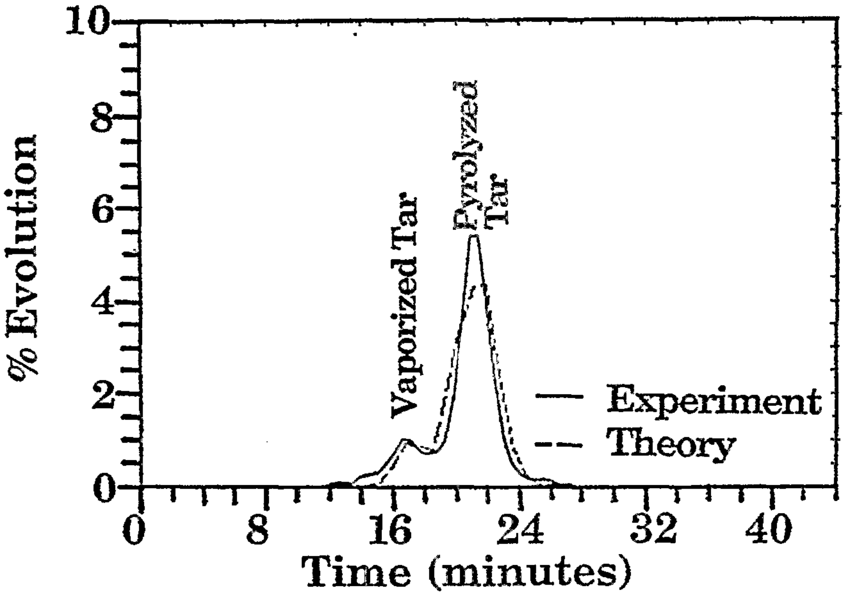

Figure II.A.7-1. Comparison of FG-DVC Model Predictions for Tar Evolution Rate from Upper Freeport Coal with TG-FTIR Data.

A prediction for the total tar yield including polymethylenes is compared in Fig. II.A.7-1 with measurements from a TG-FTIR experiment (Solomon et al., 1989a). The agreement is good. Comparisons between the predicted and measured (Freihaut et al., 1988) tar hydrogen compositions are shown in Fig. II.A.7-2. The prediction is good for high rank coals and shows the correct trend with rank. The tar hydrogen composition is, however, overpredicted for lower rank coals. This is due to an error in the way Freihaut plotted his data. The correct data compares well with the model. The relative contribution of polymethylenes is then more important. By improving the tar predictions with adjustments of DVC parameters, we should be able to obtain more accurate values of the tar hydrogen composition.

II.A.8. Crosslinking

The measurement and modeling of crosslinking phenomena in pyrolysis and how this process affects the evolved product distributions has been presented in Solomon, et al., (1990a). The abstract for this paper is presented below.

Abstract

During coal conversion, the breakup of the coal macromolecular network and resulting product formation are controlled by relative rates of bond breaking, crosslinking, and mass transport. The objective of this work was to systematically study the variations in crosslinking with several parameters (rank, temperature, heating rate, pretreatment, etc.), to identify the factors that control crosslinking, to try to identify the reactions responsible for crosslinking, and to determine the crosslinking rates. This paper describes a study of crosslinking behavior in which chars of a number of coals (including the Argonne premium coal samples) have been pyrolyzed under a variety of temperature histories and analyzed at intermediate extents of pyrolysis for solvent swelling behavior and functional group compositions. The variations in these properties were correlated with the tar molecular weight distribution measured by field ionization mass spectrometry and with the gas evolution. The study of crosslinking as a function of coal rank and pyrolysis temperature shows that there are at least two distinct crosslinking events: one occurs at low temperature prior to tar evolution (in low rank coals only) and the second occurs at moderate temperatures slightly above that for tar evolution. The low temperature crosslinking process results in low tar yields, low fluidity, (e.g., measured by Geissler plastometer), low extract yields, and low molecular weight tar. Low temperature crosslinking is increased by oxidation of the coal and reduced by methylation. Studies that compare char solvent swelling behavior to gas evolution have shown that low temperature crosslinking occurs simultaneously with CO_2 and H_2O evolution. Moderate temperature crosslinking appears to correlate best with methane formation. Studies that compare char swelling behavior to changes in char functional group concentrations have shown that crosslinking reactions occur with the loss of carboxyl groups present in the coal. A clear role for hydroxyl grups in low temperature crosslinking could not be established, nor could it be ruled out.

II.A.9. Char Reactivity Measurements

Introduction

Understanding char reactivity is important since the consumption of char is the slowest and, therefore, the controlling process in combustion or gasification. Reviews of char reactivity (Essenhigh, 1981; and Smth, 1982) demonstrate that there is a wide variation in observed reactivities. Work described by Wells, et al., (1982) highlights the very large variations (two orders of magnitude) in char reactivity with method of formation. Similarly, Ashu, et al., (1978) found an enhanced reactivity of char caused by rapid heating of the precursor coal. In work done in a vertical tunnel furnace, Essenhigh and Farzan (1982) measured very rapid burnout times for small coal particles. They ascribed this to the firing condition which gave rates of heating in the 10^6 K/s regime, compared with the more usual value of 10^4 K/s in slower burning flames. Nsakala has reported a wide variation in reactivity associated with rank (Nsakala, et al., 1982).

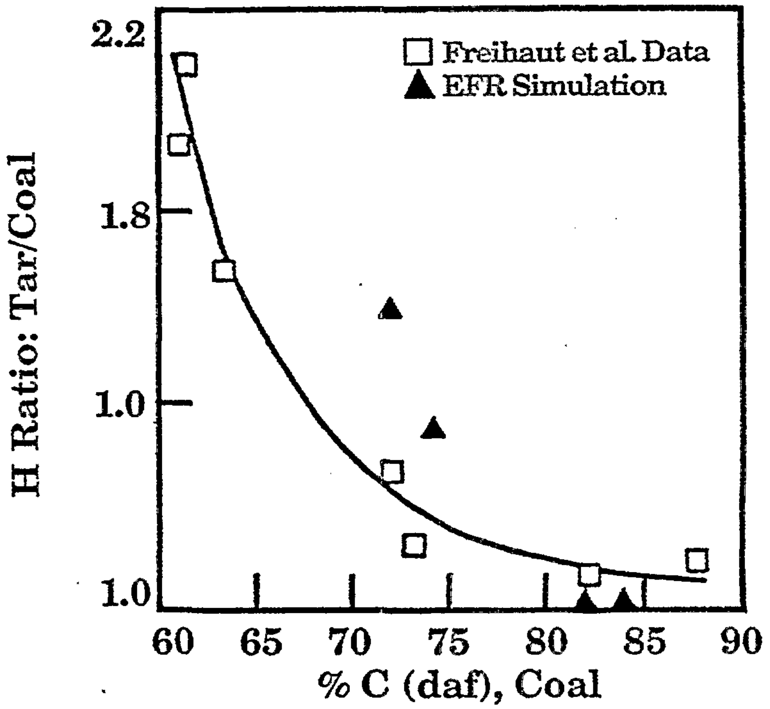

Figure II.A.7-2. Ratio of % H in Tar to % H in Coal as a Function of Coal Rank. (from Freihaut et al. (1988).

The intrinsic reactivity of the char is important in combustion experiments since most studies indicate that the char combustion at high temperatures occurs at less than the external diffusion limit (Field, 1970; Smith, 1971; Mitchell and McLean, 1982; Tichenor, et al., 1985; Waters, et al., 1988; and Leslie, et al., 1989). It has also been observed that char combustion exhibits a negative temperature coefficient (Essenhigh, 1981), which may be due to annealing which occurs during combustion at high temperatures. The effects of coal pyrolysis conditions on intrinsic combustion reactivity have not been studied over a wide range of conditions. One problem is the difficulty in making these measurements accurately at high temperatures. These experiments usually require a fairly complex apparatus and large quantities of coal, and the effects of heat and mass transport must be considered to back out intrinsic reactivity. A convenient experiment for measuring intrinsic reactivity is a thermogravimetric analyzer (TGA). However, two problems must be considered. One is how to develop a TGA test which can make measurements over a wide range of reactivities. The second problem is how to relate the low temperature reactivity measurements to the high temperature conditions of interest in pulverized fuel (p.f.) or fluidized bed combustion.

This section reports on a study of the combustion (oxidation) reactivity of a set of chars from five different coals prepared by pyrolysis at heating rates between 0.5 and 20,000°C/sec to temperatures between 400 and 1600°C. A new TGA technique was developed in which the weight loss was measured while the sample was heated at a constant heating rate in the presence of the reactive gas. The results for the present paper are for reactivity in air. This method has the advantage that the same conditions can be used for chars of widely varying reactivity. As discussed below, these low temperature measurements give reasonable predictions of high temperature char reactivities.

The development of the TGA reactivity measurement was done under previous DOE-METC Contracts (Nos. DE-AC21-84MC21004, DE-AC21-85MC22050) and applied to a larger set of coals and chars (including the Argonne Premium coals) under the current contract. The previous work is summarized below in order to provide background for the char reactivity model development that was the main focus of the current contract (see also Section II.A-10).

Experimental Procedure

Char Preparation - Chars for this study were prepared from the 200 x 325 mesh sieved fractions (~ 60 μm mean diameter) of coals and lignites listed in Table II.A.9-1. The chars were prepared by pyrolysis in an inert atmosphere in one of four reactors: 1) an atmospheric pressure entrained flow reactor (EFR) (Solomon, et al., 1982; and Solomon and Hamblen, 1985b) with coal particle temperatures between 650 and 1600°C at heating rates of ~ 10,000°C/sec; 2) a heated tube reactor (Solomon, et al., 1986c) with coal particle temperatures between 650°C and 950°C at heating rates of ~ 20,000°C/sec; 3) a thermogravimetric analyzer (TGA) with coal particle temperatures of 450°C to 900°C at heating rates of 0.5°C/sec; and 4) a high pressure entrained flow reactor (HPR) with coal temperatures of 600°C to 1400°C at heating rates of ~ 10,000°C/sec and pressures up to 200 psig (Solomon, et al., 1984).

Reactivity Measurements - Initial char reactivity measurements were made using the isothermal measurement technique developed at Pennsylvania State University (Mahajan, et al., 1978). In this method, the char is heated in a TGA in nitrogen to the desired temperature, usually 400-500°C. The temperature level is chosen to make sure no oxygen diffusion limitations are present, i.e., by varying the flow rate, bed depth and particle size. After the weight of the sample has stabilized at the selected temperature level, the nitrogen flow is switched to air and the weight loss is monitored. The time for 50% burnoff, $\tau_{0.5}$, is used as the reactivity index. Another group at Penn State has used the maximum rate of weight loss as a reactivity index, which is determined in a similar isothermal experiment (Jenkins, et al., 1973). In our char characterization work, we had difficulty applying the isothermal techniques to chars formed over a wide range of conditions. A temperature level selected for one char was inappropriate for another. The temperature was either too high for the rate to be chemically controlled or too low for the $\tau_{0.5}$ to be reached in a reasonable time period.

Table II.A.9-1.

SAMPLE PROPERTIES

WT% DAF

	Zap, North Dakota Lignite	Montana Rosebud Subbituminous	Illinois #6 Bituminous	Pittsburgh Seam Bituminous	Kentucky #9 Bituminous
Carbon	66.5	72.1	73.6	82.1	81.7
Hydrogen	4.8	4.9	4.7	5.6	5.6
Nitrogen	1.1	1.2	1.4	1.7	1.9
Sulfur	1.1	1.2	3.8	2.4	2.4
Oxygen (Diff.)	26.5	20.3	16.5	8.2	8.4
Ash (Dry Wt%)	7.1	10.0	11.0	9.2	14.1

In order to overcome this difficulty, a non-isothermal technique was developed. A Perkin-Elmer TGA 2 was initially used for this method. Recent measurements have been made using a Bomem TG/plus, which couples a Dupont 951 TGA with a Bomem Michelson 100 FT-IR spectrometer (Solomon, et al., 1989b). The sample size is about 1.5 mg. The sample is heated in air at a rate of 30 K/min until a temperature of 900°C is reached. The TGA records the sample weight continuously and, at the end of the experiment, the weight and derivative are plotted. Some representative curves for chars from the North Dakota (Zap) lignite and the Pittsburgh Seam bituminous coal are shown in Fig. II.A.9-1. The Zap and Pittsburgh chars were prepared in the EFR, in which it was calculated that the particles were heated at about 7000 K/s to 700°C before being quenched. The samples were oxidized with an air flow of 40 cc/min and a nitrogen purge flow of 400 cc/min. The derivative curve for the Zap lignite coal (Fig. II.A.9-1a) shows a sharp downward spike, indicating that the particle ignited. The Zap lignite also indicates burnout of several components of the char of different reactivity, while the Pittsburgh coal shows a more homogeneous burnout at higher temperatures.

The characteristics of the weight loss curve can be understood as follows: 1) At low temperature, there is an initial weight loss as moisture is removed, then a small weight gain due to oxygen chemisorption; 2) As the temperature is raised, the reactivity of the char increases until the fractional weight loss rate is sufficiently large to be observed. The sample size and oxygen flows are chosen so that the initial ~ 10-15% of the oxidation weight loss occurs under intrinsic reactivity control; 3) As the temperature continues to increase, the reactivity increases until eventually all the oxygen reaching the sample bed is consumed and the weight loss is controlled by the oxygen supply to the sample bed alone. Then the fractional weight loss rate becomes constant for all samples; 4) When the char has components of different reactivity, the weight loss can switch between being oxygen supply limited and being intrinsic reactivity limited as each component is consumed.

Figure II.A.9-2 compares the weight loss curves for the same char sample but with different sample sizes. The curves are identical for the initial weight loss which is controlled by the intrinsic reactivity. This is the region in which the reactivity measurements are made. As expected, the fractional rate of weight loss $df/dt = (1/m_o)\ (dm/dt)$ decreases with increasing sample size in the oxygen supply limited regime.

Theoretical Analysis

Comparison of Isothermal and Constant Heating Rate Reactivity Tests - The temperature (T_{cr}) at which the derivative of the fractional weight loss with respect to time reaches a value of 0.065 wt. fraction/min $\approx$ 0.001 wt. fraction/s was chosen as an index of reactivity to be compared with the $\tau_{0.5}$ values measured by the isothermal technique. The actual critical slope used is arbitrary. A value is chosen which is large enough to be unambiguously determined, but small enough so that reaction occurs in the chemically controlled regime. Values of $\ln \tau_{0.5}$ were plotted against $1/T_{cr}$ and a good correlation was observed.

It was subsequently decided that a comparison to $\tau_{0.1}$ (time for 10% burnoff) would be more relevant since the initial reactivity indicated by T_{cr} would be measured, rather than an integral reactivity over a large extent of conversion which could be affected by reactivity variations due to changes in the pore structure or sample inhomogeneity. A plot of $\ln \tau_{0.1}$ vs $1/T_{cr}$ is shown in Fig. II.A.9-3. This plot includes data for chars from three different coals (Lignite, Subbituminous, Bituminous) in four reactors. The experimental conditions covered the following ranges: heating rate = 0.5 to 20,000 K/sec; temperature = 400 to 1600°C; residence time = .020 s to 30 min; pressure = 0 to 1400 kPa.

It can be shown that a plot of $\ln \tau_{0.1}$ vs $1/T_{cr}$ will be linear with a slope equal to E/R, where E is the global activation energy for the intrinsic oxidation rate and R is the gas constant. For the reaction

$$C\ (\text{solid}) + O_2\ (\text{gas}) = CO_2\ (\text{gas}) \qquad (\text{II.A.9-1})$$

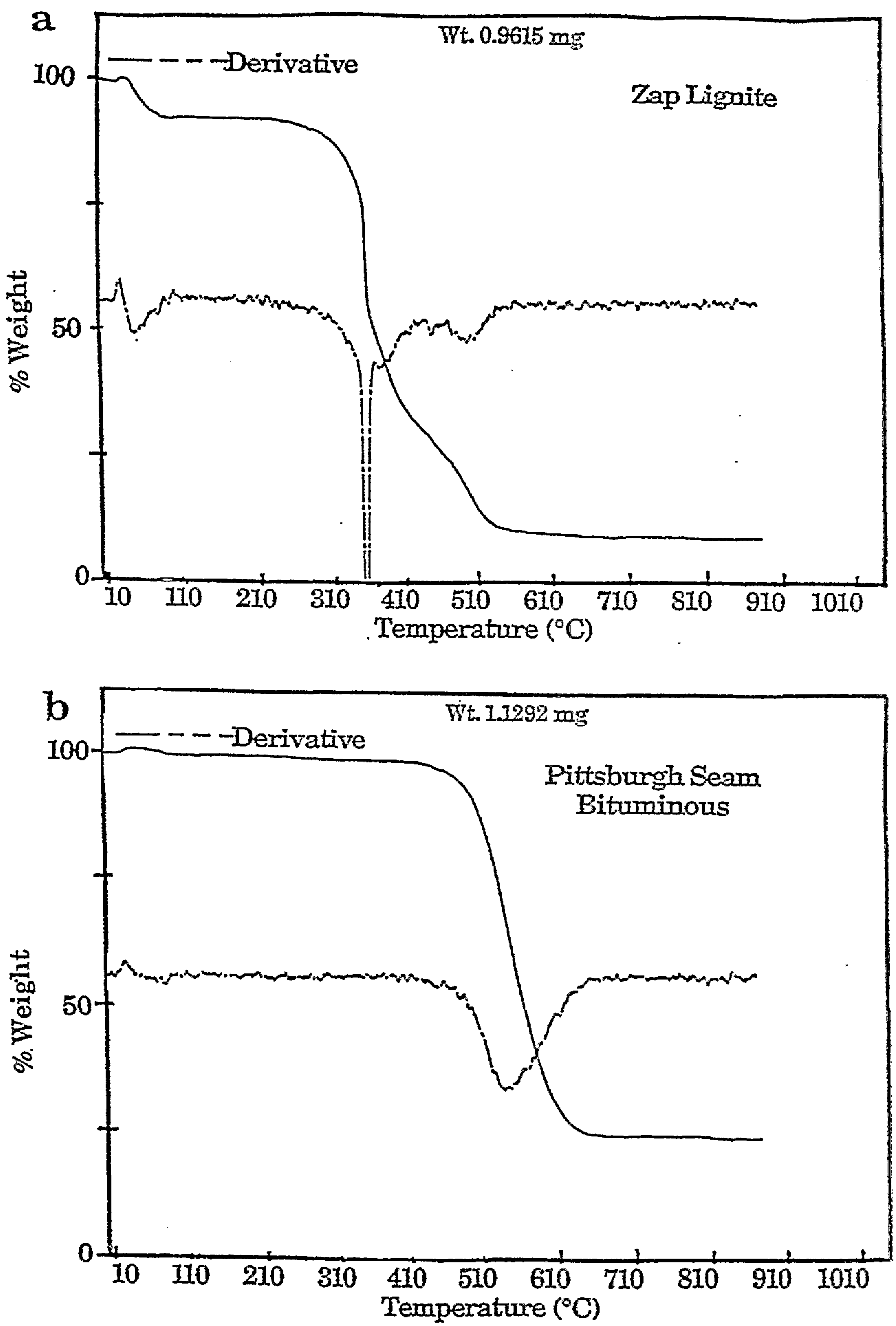

Figure II.A.9-1. Non-Isothermal TGA Reactivity Tests at 400 cc/min Air Flow; Heated at 30°C/min. a) High Reactivity Zap Lignite Char, b) Low Reactivity Pittsburgh Seam Bituminous Char.

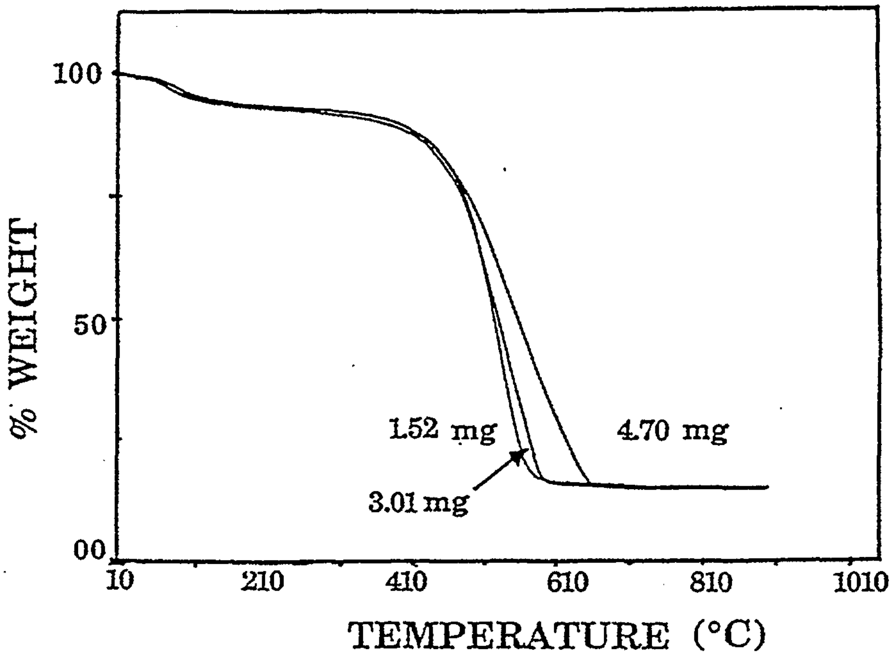

Figure II.A.9-2. TGA Weight Loss Curves for Zap Lignite Char at 3 Sample Weights.

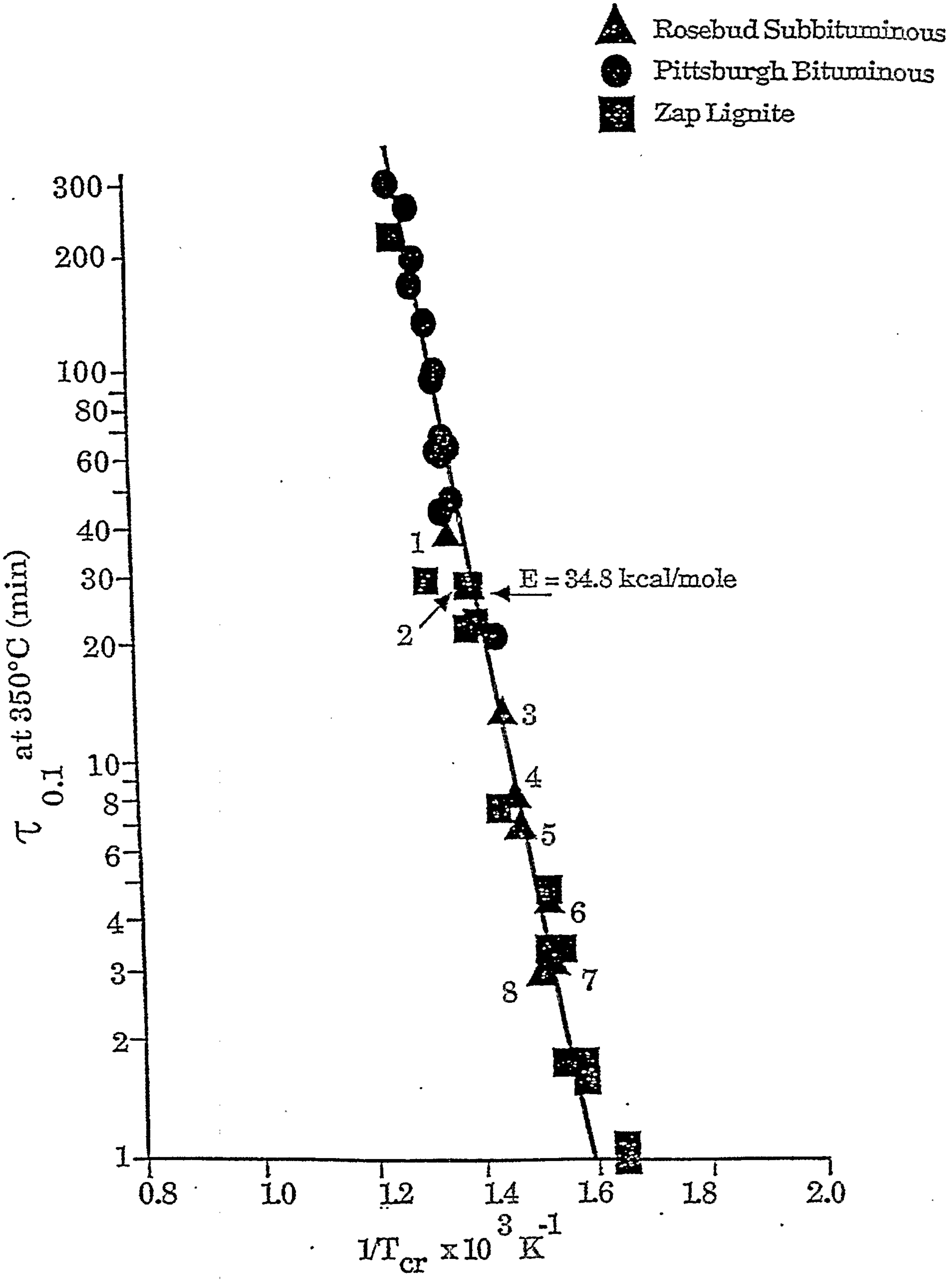

Figure II.A.9-3. $\tau_{0.1}$ (time for 10% burnoff) vs. $1/T_{cr}$. T_{cr} is the Temperature at which the Weight Loss Rate Equals −0.001 wt. Fraction/sec.

the initial fractional rate of disappearance of mass (under the condition of chemical reaction control) can be represented as follows (McKenzie, et al., 1974):

$$df/dt = 6\ R_e/(d_o\ \rho_o) \qquad \text{(II.A.9-2)}$$

where df/dt is the fractional loss of mass per particle in unit time (1/sec), R_e is the reaction rate based on external surface area (g/cm^{2}s), d_o is the initial particle diameter (cm), and ρ_o is the initial particle density. Following the treatment by Smith (1982), the relationship between the intrinsic and external reaction rate is as follows:

$$R_e = d_o\ \rho_o\ A_g\ R_i \qquad \text{(II.A.9-3)}$$

where R_i is the "intrinsic" reaction rate based on the internal surface area and A_g is the specific surface area in cm^2/g for the reaction. The parameter A_g can be thought of as the product of (βA_a), where β is the ratio of active area per unit accessible surface area (cm^2/cm^2) and A_a is the accessible surface area in cm^2 per gram. By making the above substitutions, one can arrive at a new expression for the initial fractional weight loss rate.

$$df/dt = 6\ A_g\ R_i = 6\ [\beta A_a]\ R_i \qquad \text{(II.A.9-4)}$$

In the isothermal experiment, the fractional burn-off rate is nearly constant up to ~ 10% weight loss:

$$df/dt \approx \Delta f/\Delta t \simeq -\ 0.1\ /\tau_{0.1} \qquad \text{(II.A.9-5)}$$

Substituting Eq. II.A.9-4 for df/dt:

$$6\ [\beta A_a]R_i = 0.1\ /\tau_{0.1} \qquad \text{(II.A.9-6)}$$

$$R_i = k_iC_s^m = k_i(T_o)C_s^m \qquad \text{(II.A.9-7)}$$

where T_o is the temperature of the experiment and C_s is the surface oxygen concentration.

Therefore:

$$6\ [\beta A_g]\ k_i(T_o)C_s^m = 0.1/\tau_{0.1} \qquad \text{(II.A.9-8)}$$

Solving for $\tau_{0.1}$:

$$\tau_{0.1} = 0.1/[6\ k_i(T_o)C_s^m] \cdot [1/[\beta A_a]] \qquad \text{(II.A.9-9)}$$

$$= K_1\ [1/\beta A_a] \qquad \text{(II.A.9-10)}$$

The quantities in the first set of brackets in Eq. II.A.9-9 are nearly constant for a given isothermal experiment (temperature = T_o) at low conversions and independent of coal type, while the second set of brackets contain quantities which vary with coal type and char formation conditions.

For the non-isothermal experiment, the relative rate of mass loss is constant at some critical temperature, T_{cr}:

$$df/dt = -\ 0.001 = 6\ [\beta A_a]\ k_i\ (T_{cr})C_s^m \qquad \text{(II.A.9-11)}$$

$$k_i(T_{cr}) = -0.001/[6\ C_s^m] \cdot [1/[\beta A_a]] \qquad \text{(II.A.9-12)}$$

$$= K_2\ [1/[\beta A_a]] \qquad \text{(II.A.9-13)}$$

The result obtained is that k_i (T_{cr}) is proportional to an experimental constant and inversely proportional to char properties.

For data collected on the same char sample, $[\beta A_s]$ can be eliminated between Eqs. II.A.9-9 and II.A.9-12:

$$\tau_{0.1} = [0.1/[6\ k_i(T_o)C_s^m]] \cdot [k_i\ (T_{cr})\ 6\ C_s^m/\text{-}0.001] \qquad \text{(II.A.9-14)}$$

or

$$\tau_{0.1} = 100 \exp [-E/R\ [1/T_{cr} - 1/T_o]] \qquad \text{(II.A.9-15)}$$

assuming that k_i can be expressed as an Arrhenius expression $k_i(T) = k_o \exp(-E/RT)$.

Consequently, a plot of ln $\tau_{0.1}$ vs $1/T_{cr}$ will have a slope equal to -E/R of the intrinsic global oxidation rate. In the absence of catalytic effects, the value of E should be the same for chars from all coals and chars from the same coal prepared under a wide variety of conditions. The nearly linear data in Fig. II.A.9-3 appears to support this conclusion. A problem may arise if T_{cr} and T_o are significantly different. The mechanism of the oxidation reaction probably changes with temperature, as indicated by the wide range of activation energies and reaction orders reported for the char oxidation reaction in the literature (Larandeau, 1978). The best fit value of about 35 kcal/mole determined from Fig. II.A.9-3 is intermediate in reported values and close to the value of ~ 31 kcal/mole determined by Radovic et al. (1983), and Wells et al. (1982) for a wide range of chars from U.S. coals in TGA experiments. It also agrees with the value of 34 kcal/mole determined by Smith (1982) for the intrinsic global activation energy of several U.S. coals.

The formation conditions for the Montana Rosebud Chars which are labeled in Fig. II.A.9-3 are given in Table II.A.9-2. This provides an indication of the range of pyrolysis conditions required to provide the variation of $\tau_{0.1}$ and T_{cr} observed in Fig. II.A.9-3.

Results

Reactivity vs. Extent of Pyrolysis - Figure II.A.9-4 summarizes the results for chars from T_{cr} measurements on five coals produced over a wide range of pyrolysis conditions. The critical temperature (T_{cr}), which varies inversely with reactivity, is plotted as a function of the (daf) hydrogen content, which is used as a measure of the extent of pyrolysis. For each char type, there is a trend for increasing T_{cr} (decreasing reactivity) with decreasing hydrogen. Most of the change occurs below 2.5% hydrogen, after the evolution of aliphatic hydrogen is complete. That is, T_{cr} appears to vary primarily with the concentration of aromatic hydrogen. This variation could be due to a variation in the active site concentration (β), possibly correlated with the ring condensation accompanying the elimination of aromatic hydrogen. There does not appear to be any drastic effects due to heating rate for low rank coals containing minerals, as chars for a wide range of conditions all fell along the same curve. The results for bituminous coals and demineralized low rank coals do not show the same heating rate independence (Serio, et al., 1989). It should be noted that there is also ring oxygen in the char which is removed at about the same rate as the hydrogen and which may be related to the reactivity changes. Similar correlations were observed with oxygen concentration for chars produced from a single coal, i.e., the reactivity decreases with decreasing char oxygen concentration (Solomon, et al., 1984). However, it is thought that the hydrogen is a better indicator of reactivity, since it is present at about five times the level of oxygen on an atomic basis and can be more easily and accurately measured.

The upper solid line in Fig. II.A.9-4 is a "best fit" line drawn through the data for Kentucky No. 9 and Pittsburgh Seam bituminous chars. The lower solid line is a best fit line drawn through the Zap lignite chars. The differences in the values of T_{cr} with the extent of pyrolysis allows one to assess the importance of this parameter on reactivity. In the case of the Zap lignite, the range of T_{cr} from about 350°C to 525°C corresponds to a factor of ~ 500 in reactivity (assuming the 35 kcal/mole activation energy). In the case of the two bituminous coals, the range of T_{cr} from about 450°C to 575°C corresponds to a factor of ~ 40

Table II.A.9-2.

Key to Montana Rosebud Data in Figure II.A.9-3.

Datum No.	Reactor	Heating Rate[a] °C/s	Maximum Temperature °C	Residence Time[b] (s)	Pressure (psig)
1	TGA	0.5	900	---	0
2	EFR	10,000	1300	0.2	0
3	HPR	10,000	817	0.3	100
4	HTR	20,000	800	0.2	0
5	HPR	10,000	817	0.3	26
6	HTR	20,000	800	0.1	0
7	HTR	20,000	800	---	0
8	HTR	20,000	600	---	0

NOTES:

TGA	Thermogravimetric Analyzer
EFR	Atmospheric Pressure Entrained Flow Reactor
HPR	High Pressure Entrained Reactor
HTR	Heated Tube Reactor
a	Heating rates are nominal
b	Residence time at final temperature

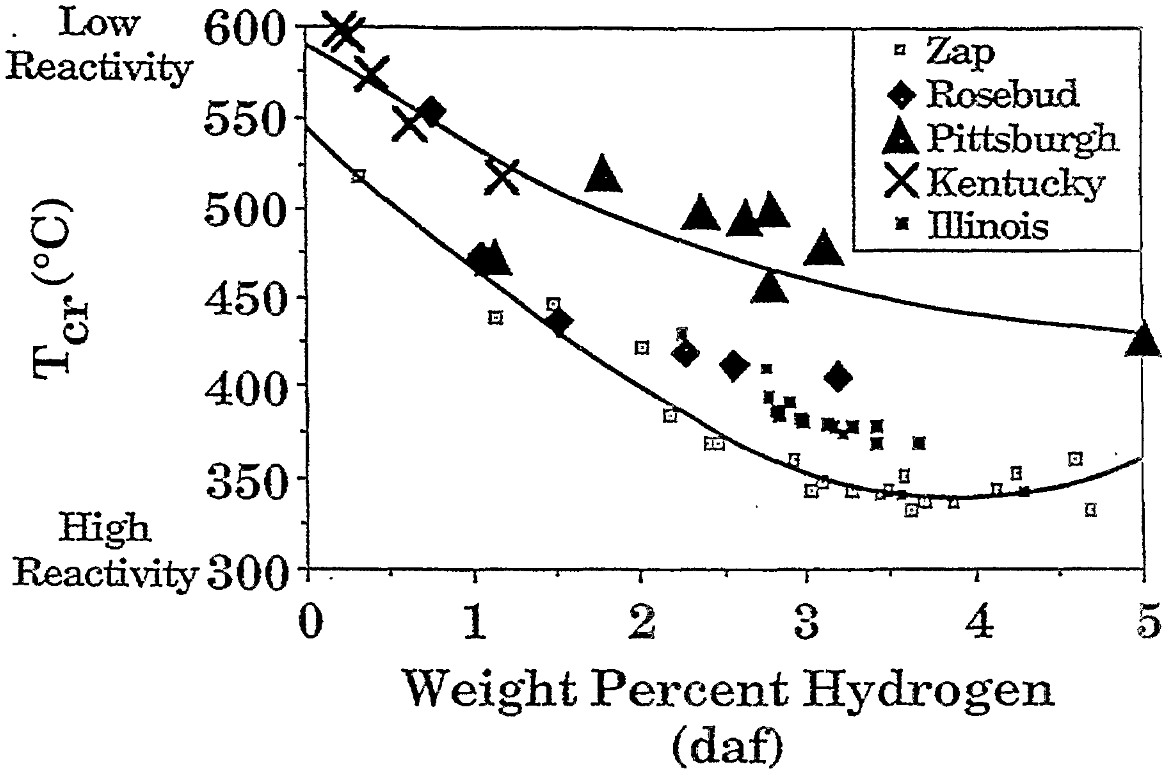

Figure II.A.9-4. Comparison of Reactivity for Chars from Five Various Ranks as a Function of Hydrogen Concentration. Tcr Varies Inversely with Reactivity.

in reactivity. Using the same method, one can track the maximum difference in reactivities with coal types as being a factor of 120 (350°C, 475°C) while the minimum difference is about a factor of 4 (525°C, 575°C).

Reactivity vs. Mineral Content - It is known that the vertical displacement of the curves in Fig. II.A.9-4. is at least partly due to the variations in catalytic activity of minerals. This effect has been observed in previous studies which have been reviewed by Mahajan and Walker (1978). The most reactive chars are for the Zap lignite which are known to have a high Na and Ca content. The results for T_{cr} versus daf hydrogen content for chars produced from demineralized Zap by the Bishop and Ward technique (Tichenor, et al., 1985) are similar to chars from bituminous coals (Serio, et al., 1989).

Reactivity vs. Surface Area - Our previous work has suggested that the rank differences in reactivity in Fig. II.A.9-4 are primarily due to differences in mineral content and not from differences in surface area (Solomon, et al., 1989b; Serio, et al., 1989; and Solomon, et al., 1988c). Similarly, the trends with the hydrogen concentration are due to changes in the molecular order (active site concentration) and not from changes in surface area.

The fact that reactivities differences between chars from different coals do not correlate well with BET surface area is not surprising. As discussed by Walker and coworkers (Radovic and Walker, 1983), it is the active surface area (ASA) as measured by oxygen chemisorption which is important. However, the utility of oxygen chemisorption as a technique for measuring the ASA of "young" chars in question (Suuberg, et al., 1986). In this work, we have not attempted to measure ASA's.

Reactivity vs. Burnout - Measurements have been made of T_{cr} versus the extent of burnout for chars from a Montana Rosebud and a Pittsburgh Seam coal (Solomon, et al., 1988d). In this case, the values of T_{cr} must be corrected for the increase in the ash content. The value of T_{cr} increases systematically with increasing burnout for both coals, which indicates that more reactive components are removed first (or that the burnout process anneals the remaining material).

Correlation of T_{cr} Measurements with High Temperature Combustion Reactivities - Of course the measurement of T_{cr} would not be of much good to those interested in p.f. combustion unless it can be shown that these measurements correlate with intrinsic reactivities measured at high temperatures. The T_{cr} measurement provides a temperature at which df/dt = 0.001 s^{-1}. For a ~ 60 μm mean diameter fraction of Montana Rosebud coal, the measured T_{cr} was 429°C (702K) while the measured initial CO_2 BET surface area was 152 m^2/g. The problems of using the BET surface area as a correlating parameter have been discussed previously (Serio, et al., 1989). However, since the intrinsic reactivity data in the literature have been derived using such measurements, this approach is consistent. The CO_2 area varies the least over a wide range of burnoffs, for most coal chars, and is used here. Using equation II.A.9-4, one would calculate $R_i = 1.1 \times 10^{-10} g/cm^2s$ at $T_p = 702K$. The most comprehensive compilation of intrinsic reactivity data for a range of carbons is that provided by Smith (1982). The correlation of Smith would predict a value of $R_i = 1.0 \times 10^{-11} g/cm^2s$. However, this correlation underpredicts the data for brown coal chars and lignites in this temperature range, so the agreement is actually within a factor of 2 of the relevant data in Fig. 9 of Smith (1982). The extrapolation to high temperatures can be done by using E = 35 kcal/mole which gives $R_i = 2 \times 10^{-4}$ g/cm^2s at $T_p = 1650K$. This estimate is about a factor of two lower than Smith's correlation and about a factor of two higher than his data for brown coal chars. A similar agreement is observed for the other chars that were studied. Consequently, it appears that the T_{cr} measurement is capable of giving meaningful results when extrapolated to high temperatures using an activation energy of E = 35 kcal/mole.

Recent work in our laboratory with a laminar coal flame experiment has shown a correlation of T_{cr} with the ignition point above the nozzle (Solomon, et al., 1988c) and with the interval of time required to achieve 100% burnout (Solomon, et al., 1989c).

Correlation of T_{cr} Measurements for Reactivity Modeling - As discussed in Section II.A.10, most of the work under the current contract has involved using the T_{cr} database to develop a char reactivity submodel for use in a comprehensive entrained gasification and combustion code (Charpenay, et al. 1992 a,b, 1993). Since T_{cr} is inversely proportional to the reactivity, $1/T_{cr}$ was found to be a more appropriate quantity to use to develop correlations. Good linear correlations of $1/T_{cr}$ vs. the char hydrogen concentration were obtained for all of the coals examined, as shown in Fig. II.A.9-5. This includes some additional data which is not included in Fig. II.A.9-4. The points which fall below the bottom line for the Pittsburgh Seam coal are from chars which were produced at low heating rate in a TGA. For fluid coal, the pyrolysis heating rate can affect the reactivity by at least one order of magnitude.

Conclusion

A new reactivity test has been developed which allowed relative rates of reactivity to be determined for chars of widely varying reactivity. The method was applied to study the dependence of reactivity on coal properties and pyrolysis conditions. Reactivities are seen to decrease dramatically with decreasing aromatic hydrogen concentration. Reactivities were insensitive to pyrolysis heating rate for a lignite but were sensitive to heating rate for a bituminous coal. Mineral catalytic effects explain most of the rank variations. The test provides a measure of the reaction rate which agrees well with literature data for chars from similar coals. The measured intrinsic reactivities also extrapolate well to high temperature measurements if an activation energy of 35 kcal/mole is used. The test can also predict the reactivity differences between coals in a laminar coal flame experiment.

II.A.10. The Prediction of Coal Char Reactivity Under Combustion Conditions

The main objective of the char reactivity work under this contract was to develop a char reactivity submodel that could be used in a comprehensive code for entrained coal combustors and gasifiers. The requirement of a char reactivity model is to predict the reactivity of chars from a wide range of coals, over a wide range of temperatures, and for various degrees of burnoff. In order to predict intrinsic reactivity, correlations of reactivity with char hydrogen content, coal oxygen content and coal mineral content were used. A random pore model (high rank coals) and a volumetric model (low rank coals) were included to predict variations of intrinsic reactivity with burnoff. The correlations combined with those models gave good predictions of reactivity (within a factor of 2 to 4) and reactivity variations with burnoff (within 20%) for the range of chars studied.

In the pore diffusion regime, the model uses the Thiele modulus to calculate the reaction rates as a function of intrinsic rate (obtained using the correlations) and char properties such as porosity, tortuosity, and the mean pore radius. Predictions of reactivity required an estimate of the tortuosity and the mean pore radius. The tortuosity was kept constant at a value of 2. Using a value of 6Å (corresponding to the size of micropores) for the mean pore radius led to good predictions of the onset of diffusion limitations for low heating rate, fluid chars. For high heating rate chars, pore size distribution measurements showed that values of approximately 100Å were more appropriate. The corresponding predictions using this value gave a fairly good fit to the literature data investigated. This analysis shows that it may be possible to extend a low temperature reactivity model to high temperatures.

A complete description of this model appears in Charpenay et al. (1992a,b). The extension of the model to better account for the influence of char structure is discussed in Charpenay et al. (1993).

II.A.11. Analysis of the Argonne Premium Coal Samples by Thermogravimetric Fourier Transform Infrared Spectroscopy

We have developed a TG-FTIR instrument that combines thermogravimetric analysis (TGA) with evolved products analysis by Fourier Transform Infrared (FT-IR) spectroscopy. FT-IR analysis of evolved products has advantages over mass spectroscopy in allowing analysis of very heavy products and over gas chromatography in speed. The paper by Solomon et al. (1990a) describes the most recent improvements in the apparatus and presents is application in characterizing the Argonne premium coal samples. The TG-FTIR apparatus for pyrolysis, oxidation of pyrolysis products, and oxidation of the sample is described. To analyze coal, a sequence of drying, pyrolysis, and combustion is employed to

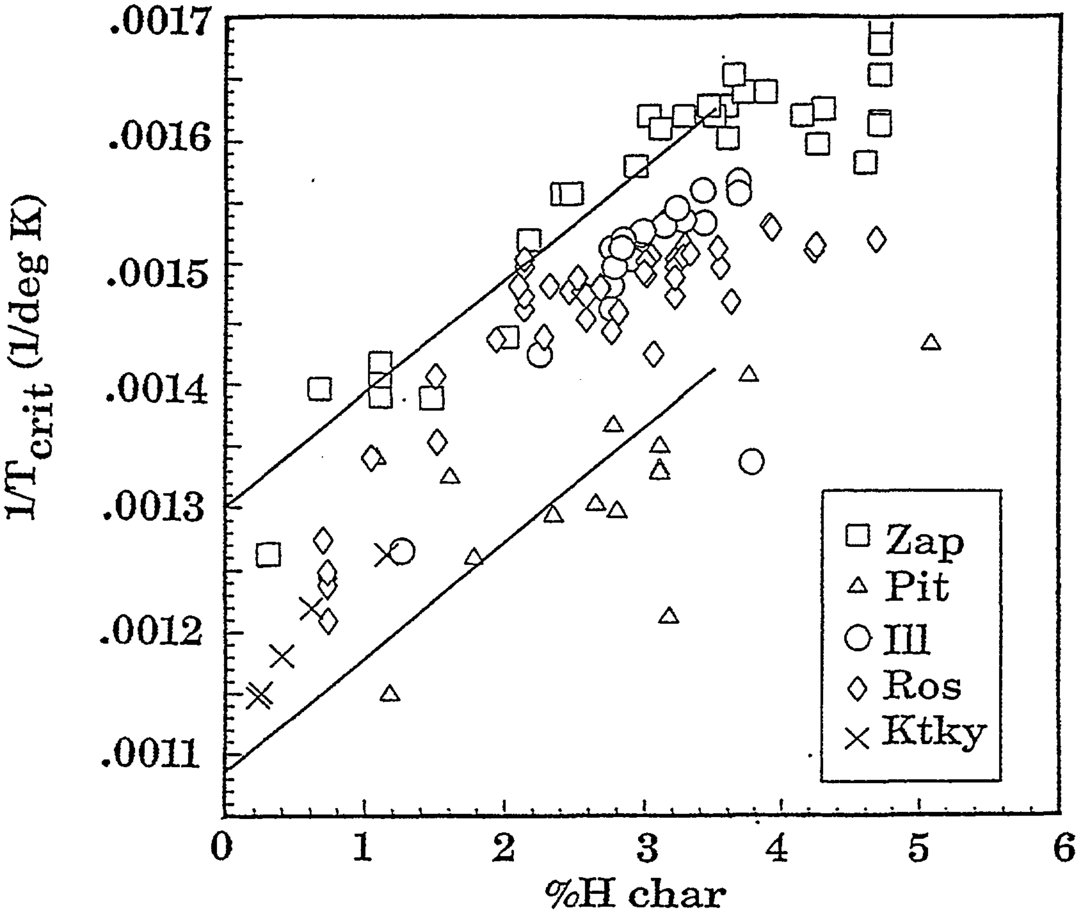

Figure II.A.9-5. Correlation of $1/T_{crit}$ with the Percent (daf) Hydrogen Content of the Char (H_{char}) for Zap, Rosebud, Illinois No. 6 and Pittsburgh No. 8 Coals.

obtain proximate analysis, volatile composition, volatile kinetics, and relative char reactivity. Pyrolysis results are presented for the eight Argonne coals, several demineralized coals, and two oxidized samples of Pittsburgh Seam coal. A kinetic analysis was applied to species evolution data collected at several different heating rates. There is a systematic variation in rate with rank. The rate for tar evolution from Pittsburgh Seam coal is in good agreement with that of Burnham et al. (1989) using a similar set of data. Analysis of the amounts of evolved products also show a systematic variation with rank consistent with the coal's elemental and functional group compositions. Postoxidation of the volatile products has been successful in providing elemental composition information on the volatile products as well as showing the evolution of H_2, which is not infrared active, and H_2S (in the postoxidized SO_2 profile), which is a weak infrared absorber. Oxidation of the char yields an ash amount as well as two measures of the char's reactivity, the oxygen absorbed by the char, and the temperature at which significant oxidation of the char occurs. This work is described in detail in Solomon et al. (1990a).

References for Subtask 2.a.

Annual Book of ASTM Standards, Sec. 5 Petroleum Products, Lubricants, and Fossil Fuels, Vol. 05.05 Gaseous Fuels; Coal and Coke, pp. 356-360 (1985)

Ashu, J.T., Nsakala, N.Y., Mahajan, O.P., and Walker, P.L., Jr.: Fuel, **57**, 251 (1978).

Baumann, H., and Moller, P., Erdol, Erdgas and Kohle, **44**, (1), 29-33 (1991).

Best, P.E., Carangelo, R.M., and Solomon, P.R., FT-IR Determination of Coal and Soot Particle Temperatures During Pyrolysis, ACS Div. of Fuel Chem. Preprtins, **29**, (6), 249 (1984).

Best, P.E., Carangelo, R.M., Markham, J.R., and Solomon, P.R., Extension of Emission-Transmission Technique to Particulate Samples Using FT-IR, Combustion and Flame, **66**, 47 (1986).

Bohren, C.F., and Huffman, D.R., Absorption and Scattering of Light by Small Particles, John Wiley & Sons, NY (1983).

Bose, A.C., Dannecher, K.M., and Wendt, J.O.L., Energy & Fuels, **2**, 301-308 (1988).

Boudou, J.P., Boulegue, J., Malechaux, L., Nip, M., de Leeuw, J.W., and Boon, J.J., Fuel, **66**, p 1558 (1987).

Burchill, P., Some Observations on the Variation of Nitrogen Content and Functionality with Coal Rank, Proceedings of the Int. Conf. on Coal Science, (J.A. Moulign, et. al., Eds.), Elsevier Science Publishers, BV Amsterdam, The Netherlands pp 5-8 (1987).

Burnham, A.K., Oh, M.S., Crawford, R.W., and Samoun, A.M., Energy & Fuels, **3**, 42 (1989).

Calkins, W.H., Hagaman, E., and Zeldes, H., Fuel, **63**, 1113 (1984a).

Calkins, W.H., Tyler, R.J., Fuel, **63**, 1119 (1984b).

Calkins, W.H., Fuel, **63**, 1125 (1984c).

Calkins, W.H., Hovsepian, B.K., Drykacz, G.R., Bloomquist, C.A.A., and Ruscic, L., Fuel, **63**, 1226 (1984d).

Calkins, W.H., Energy & Fuels, **1**, 59-64 (1987).

Carangelo, R.M., Solomon, P.R., and Gerson, D.J., Fuel, **66**, 960 (1987).

Charpenay, S., Serio, M.A., Solomon, P.R., The Prediction of Coal Char Reactivity Under Combustion Conditions, 24th Symposium (Int) on Combustion, The Combustion Institute, Pittsburgh, PA, 1189-1197 (1992).

Che, S.C., et al., Flash Pyrolysis Coal Liquefaction Process Development, Final Report for July 1976 to June 1978, DOE Report No. FE-2244-26 (1978).

Chen, S.L., Heap, M.P., Pershing, D.W., and Martin, G.B., Nineteenth Symposium (International) on Combustion, 1271-1280, The Combustion Institute, Pittsburgh, PA (1982).

Chiou, M.J. and Levine, H.B., Investigation of Structural Deformation of Coal Particles in Pyrolysis, Internal Report JAYCOR.

Essenhigh, R.H., *Chemistry of Coal Utilization*, (M.A. Elliott, Ed.), John Wiley & Sons, 2nd Supplementary Vol., p. 1162 (1981).

Essenhigh, R.H. and Farzan, H., Nineteenth Symposium (International) on Combustion, 1105-111, The Combustion Institute (1982).

Field, M.A., Combust. Flame, **14**, 237 (1970).

Foster, P.J. and Howarth, C.R. *Carbon*, **6**, 719, and references therein (1968).

Freihaut, J.D, Proscia, W.M., and Seery, D.J., ACS Div. Fuel Chem. Preprints, **33**(2), 262 (1988).

Gan, H., Nandi, S.P., and Walker, P.L., Jr., Fuel, **51**(4), 272 (1972).

Gorbaty, M.L. Kelemen, S.R., George, G.N., and Kwiatek, P.J., Fuel, **71**, 1255 (1992).

Huffman, G.P., Mitra, S., Hugguns, F.E., Shah, N., Vaidya, S., and Lu, F., Energy & Fuels, **5**, 574-581 (1991).

Jenkins, R.G., S.P. Nandi, and P.L. Walker, Jr., Fuel, **52**, 288 (1973).

Kelemen, S.R., Gorbaty, M.L., Vaughn, S.N., and George, G., Preprint, Am. Chem. Soc., Div. of Fuel Chem., **36** (3), 1225-1232 (1991).

Khan, M.R., Fuel, **68**, 1439 (1989).

Knight, R. A., Gissy, J., Onischak, M., Babu, S.P., Wooten, J.M., and Duthie, R.G., Development of an Advanced, Continuous Mild Gasification Process for the Production of Co-Products, Topical Report for Contract No. DE-AC21-87MC24266 (1990).

LaCount, R.B., Kern, D.G., King, W.P., Trulli, T.K., Walker, D.K., ASC Div. of Fuel Chem. Preprints, 1992, **37** (3), 1083 (1992).

Larandeau, N.M., Prog. Eng. Combust. Sci., **4**, 221 (1978).

Leslie, I.H., M. Jost, and C.H. Kruger, Combust. Flame, **78**, 195 (1989).

Litt, R.D., Paisely, M.A., and Tewksbury, T.L., Experimental Development of a Multi-Solid Fluidized-Bed Reactor Concept, Topical Report for Contract No. DE-AC21-87MC23293 (1990).

Mackie, J.C., Colket, M.B., and Nelson, P.F., Phys. Chem., **94**, 4099 (1990).

Mackie, J.C., Colket, M.B., Nelson, P.F., and Esler, M., Int. J. Chem. Kinetics, **23**, 733 (1991).

Mahajan, O.P., and Walker, P.J., Jr., *Analytical Methods for Coal and Coal Products*, (C. Karr, Ed.), Vol. II, Ch. 32, pp. 465-492, Academic Press (1978).

Mahajan, O.P., R. Yarzab, and P.L. Walker, Jr., Fuel, **57**, 643 (1978).

McKenzie, A., I.W. Smith, and G.A.D. Szpindler, J. Inst. Fuel, **47**, 75 (1974).

Mehldi Taghiei, M., Hugguns, F.E., Shah, N., and Huffman, G.P., Am. Chem. Soc., Div. Fuel Chem. Preprints, **36**, (2), 757-764 (1991).

Mitchell, R.E. and J.W. McLean, 19th Symposium (Int) on Combustion, The Combustion Institute, 1113 -1122 (1982).

Nelson, P.F., Fuel, **66**, 1264 (1987).

Nelson, P. F., Buckley, A. N. and Kelly, M. D., Twenty Forth Symposium (Int) On Combustion, The Combustion Institute, Pittsburgh, PA, 1259-1267 (1992).

Nsakala, N.Y., Patel, R.L., and Lao, T.C.: Final Report, Electric Power Research Institute, Report No. 1654-6 (1982).

Oh, M.S., Burnham, A.K., and Crawford, R.W., Am. Chem. Soc. Div. of Fuel Chem. Preprints, **33**. (1), 274 (1988).

Radovic, L.R., P.L. Walker, Jr., and R.G. Jenkins, Fuel, **62**, 849 (1983).

Scotti, L.J., et al., Char Oil Energy Development Interim Report No. 5, DOE Report No. FE-1212-5 (1975).

Serio, M.A., Hamblen, D.G., Markham, J.R., and Solomon, P.R., Kinetics of Volatile Product Evolution in Coal Pyrolysis: Experimental and Theory, Energy and Fuel, **1**, 138 (1987).

Serio, M.A., P.R. Solomon, R. Bassilakis, and E.M. Suuberg, ACS Div. of Fuel Chem. Prepr., **34**, (1), 9 (1989).

Smith, I.W, Combust. Flame, **17**, 421 (1971).

Smith, I.W., 19th Symposium (Int) on Combustion, The Combustion Institute, 1045-1065 (1982).

Solomon, P.R., Coal Structure and Thermal Decomposition, in *New Approaches in Coal Chemistry*, ACS Symposium Series, **169**, 61 (1981).

Solomon, P.R., Hamblen, D.G., Carangelo, R.M., and Krause, J.L., 19th Symposium (International) on Combustion/The Combustion Institute, Pittsburgh, PA, pp. 1139-1149 (1982).

Solomon, P.R., Hamblen, D.G., and Carangelo, R.M. Analytical Pyrolysis, (K.J. Voorhees, Ed.), Ch. 5, p. 121, Butterworths (1984).

Solomon, P.R., Hamblen, D.G., Carangelo, R.M., Markham, J.R., and Chaffee, M.R., Application of FT-IR Spectroscopy to Study Hydrocarbon Reaction Chemistry, ACS Div. of Fuel Chem. Preprints, **30** (1), **1** (1985a).

Solomon, P.R. and Hamblen, D.G. in *Chemistry of Coal Conversion*, (R.H. Schlosberg, Ed.), Ch. 5, p. 121, Plenum Press (1985b).

Solomon, P.R., Carangelo, R.M., Hamblen, D.G., and Best, P.E., Infrared Analysis of Particulates by FT-IR Emission/Transmission Spectroscopy, Applied Spectroscopy, **40** (6), 746 (1986a).

Solomon, P.R., Carangelo, R.M., Best, P.E., Markham, J.R., and Hamblen, D.G., Analysis of Particle Composition, Size and Temperature by FT-IR Emission/Transmission Spectroscopy, ACS Div. of Fuel Chem. Preprints, **31**, (1), 141 (1986b).

Solomon, P.R., Serio, M.A,. Carangelo, R.M., and Markham, J.R., Very Rapid Coal Pyrolysis, Fuel, **65**, 182, (1986c).

Solomon, P.R., Carangelo, R.M., Best, P.E., Markham, J.R., and Hamblen, D.G., The Spectral Emittance of Pulverized Coal and Char, 21st Symposium (Int) on Combustion, The Combustion Institute, Pittsburgh, PA, 437 (1986d).

Solomon. P.R., Carangelo, R.M., Best, P.E., Markham, J.R., and Hamblen, D.G., Analysis of Particle Emittance, Composition, Size, and Temperature for FT-IR Emission/Transmission Spectroscopy, Fuel, **66**, 897 (1987a).

Solomon, P.R., Hamblen, D.G., Serio, M.A., Smoot, L.D., and Brewster, S., Measurement and Modeling of Advanced Coal Conversion, First Annual Report, DoE/METC Contract No. DE-AC21-86MC23075 (1987b).

Solomon, P.R., Hamblen, D.G., Carangelo, R.M., Serio, M.A., and Deshpande, D.V., A General Model of Coal Devolatilization, Energy and Fuels, **2**, 405 (1988a).

Solomon, P.R., Hamblen, D.G., Carangelo, R.M., Serio, M.S., and Deshpande, D.V., Models of Tar Formation During Coal Devolatilization, Combustion and Flame, **71**, 137 (1988b).

Solomon, P.R., P.L. Chien, R.M. Carangelo, P.E. Best, and J.R. Markham, 22nd Symposium (Int) on Combustion, The Combustion Institute, 211-221 (1988c).

Solomon, P.R., Serio, M.A., Hamblen, D.G., Markham, J.R., Best, P.R., and Bassilakis, R., Chemical and Physical Develpoment of Char Particles During Devolatilization, DOE/METC Final Report under Contract No. DE-AC21-85MC22050 (1988b).

Solomon, P.R., Best, P.E., Yu, Z.Z., and Deshpande, G.V., ACS Div. of Fuel Chem. Prepr., **34,** (3), 895 (1989a).

Solomon, P.R., M.A. Serio, R.M. Carangelo, and R. Bassilakis, International Conference of Coal Science Proceedings, p. 67, IEA, Japan (1989b).

Solomon, P.R., M.A. Serio, D.G. Hamblen, L.D. Smoot, and B.S. Brewster, DOE/METC Third Annual Report under Contract No. DE-AC21-86MC23075 (1989c).

Solomon, P.R., Serio, M.A., Deshpande, G.V., and Kroo, E., Crosslinking Reactions During Coal Conversion, Energy and Fuel, **4**, 402 (1990a).

Solomon, P.R., Hamblen, D.G., Yu, Z., and Serio, M.A., Fuel, **69**, 754 (1990a).

Solomon, P.R., Serio, M.A., Carangelo, R.M., Bassilakis, R., Gravel, D., Bailargeon, M., Baudais, F., and Vail, G., Energy & Fuels, 4 (3), 319 (1990b).

Solomon, P.R., Best, P.E., Yu, Z.Z., and Charpenay, S., An Empirical Model for Coal Fluidity Based on a Macromolecular Network Pyrolysis Model, Energy and Fuel, **6**, 143 (1992).

Solomon, P.R., Hamblen, D.G., Serio, M.A., Yu, Z.Z., and Charpenay, S., A Characterization Method and Model for Predicting Coal Conversion Behavior, Fuel, **72** (4), 469 (1993).

Suuberg, E.M., Calo, J.M., and Mojtowciz, M.: ACS Div. of Fuel Chem. Prepr., **31**, (3), 186 (1986).

Tichenor, D.A., R.E. Mitchell, K.R. Hencken, and S. Niksa, 20th Symposium (Int) on Combustion, The Combustion Institute, 1213-1221 (1985).

Tyler, R.J., Flash Pyrolysis of Coals. Devolatilization of Bituminous Coals in a Small Fluidized Bed Reactor, Fuel, **59**, 218 (1980).

Users Guide for FG-DVC Model, PC version, Advanced Fuel Research, Inc., East Hartford, Connecticut, USA (February, 1992).

Usman Ghani, M., and Wendt, J.O.L. Twenty-Third Symposium (International) on Combustion, 1281-1288, The Combustion Institute, Pittsburgh, PA (1990).

Vorres, K.S., Users Handbook for the Argonne Coal Sample Program, (1989).

Wallace, S. Bartle, K.D., and Perry, D.L., Fuel, **68**, 1450 (1989).

Waters, B.J., R.E. Mitchell, R.G. Squires, and N.M. Laurendeau, 22nd Symposium (Int) on Combustion, The Combustion Institute, 17-27 (1988).

Wells, W.F., S.K. Kramer, L.D. Smoot, and A.U. Blackham, 19th Symposium (Int) on Combustion, The Combustion Institute, 1539-1546 (1982).

Whelan, J.K., Solomon, P.R., Deshpande, G.V., and Carangelo, R.M., Energy & Fuels, **2**, 65 (1988).

Zygourakis, K., Pyrolysis and Gasification of Coal Particles at High Temperatures, Proceedings of the Ninth Annual Gasification and Gas Stream Cleanup Systems Contractor's Review Meeting (1989).

II.B. SUBTASK 2.B. - FUNDAMENTAL HIGH-PRESSURE REACTION RATE DATA

Senior Investigators - Geoffrey J. Germane and Angus U. Blackham
Brigham Young University
Provo, Utah 84602
(801) 378-2355 and 6536

Student Research Assistants - Charles R. Monson, Gary Pehrson, and Kenneth Bateman

Introduction

Most of the coal currently being consumed is combusted in atmospheric pressure utility furnaces, but a large number of other processes are also being used and developed for either direct combustion of coal or conversion of coal into other products. A number of these processes, including coal gasification, operate at elevated pressure. Gas turbine and diesel engines, which typically use liquid petroleum fuels, operate at high pressures and prove to be candidates for coal fuel. Practical research is being conducted on the use of coal in these applications, yet little is known about the basic nature of coal combustion at elevated pressure. A great deal of research has been conducted on char combustion at atmospheric pressure but the data obtained by these experiments cannot be extrapolated to higher pressures because of the intricate coupling of transport phenomena and chemical kinetics during combustion. The effect of pressure on char reactions has been examined by only a few researchers during the past 25 years. These studies have been limited by experimental apparatus and have produced conflicting results. Careful research is needed to characterize the fundamental effects of pressure on char oxidation.

To this end a high pressure facility was designed and constructed for use in both preparing char and carrying out fundamental char oxidation experiments. Chars were prepared in sufficient quantities for oxidation tests and oxidation experiments were conducted at both atmospheric and elevated pressures. Simultaneous in-situ measurements of particle size, velocity and temperature in a controlled temperature environment were made for char particles for a range of oxygen partial pressures and total pressures.

Objectives

The overall objectives of this subtask are to determine the effects of pressure on the mass reactivities and reaction rates of coal chars combusting in oxidizing environments at high temperatures.

Specific objectives for the project included:

1. Design, construct and characterize a high-pressure, controlled-profile (HPCP) drop tube furnace for char preparation and oxidation studies at atmospheric and high pressure.
2. Prepare and characterize chars from the coals selected for this study, using the HPCP for char production.
3. Conduct high pressure and atmospheric oxidation tests in the HPCP reactor with chars produced from several of the coals selected for study.

Accomplishments

Three components of the subtask have been identified to accomplish the objectives outlined above: 1) design and construction of a laminar-flow, high-pressure, controlled-profile (HPCP) reactor, 2) char preparation at high temperature and high pressure, and 3) determination of the kinetics of char-oxygen reactions at high pressure.

High Pressure Facility

The controlled conditions required for high temperature, pulverized coal char oxidation experiments place great demands on a test facility. Not only must the initial heating rates (10^4-10^5 K/s) and high particle temperatures (1700-2200 K) encountered in pulverized fuel combustors be simulated, but facility temperatures must be controllable over a wide range. It is also desired to maintain constant particle temperature during the oxidation process. The particle reaction must proceed in a consistent manner, with quenching occurring at various stages during the short time of particle burnout (<200 ms). The temperature and composition of the gas surrounding a particle must also be known and variable. The overall conditions of the oxidation process must allow subsequent correction for mass transfer effects, limiting experiments to single particles rather than group events. Also required is the ability to measure particle properties, especially temperature, during the reaction. The difficulties associated with implementing these requirements were compounded in the present study by the additional requirement of high-pressure operation.

A High-Pressure, Controlled temperature Profile (HPCP), drop-tube reactor was designed and constructed as part of this study for use in both devolatilization and char oxidation tests. The reactor has the following capabilities: pressure from 1 to 30 atm, gas temperature from 1000 to 1700 K, controllable temperature profile along the reaction tube length, particle residence times from 30 to 1000 ms, variable gas compositions of inert and oxidizing gases, and optical access ports for *in-situ* diagnostics. Fig. II.B-1 shows a cross-sectional view of the HPCP reactor. A particle imaging system, providing *in-situ* measurement of individual particle temperature, size and velocity was developed for use in conjunction with the reactor. The instrument was patterned after a pyrometer developed at Sandia National Laboratories (Tichenor et al., 1984; Niksa, et al., 1984), and further by Wells and Smoot (1989) with modifications made to allow the measurement of smaller (30 to 150 μm), cooler particles and to allow proper functioning with the heated wall reactor. Details of the HPCP reactor, the optical pyrometer and other components of the high-pressure facility were presented in progress reports for this study (Solomon et al.).

Char Oxidation Experiments

Approximately 100 oxidation experiments were performed with two bituminous coal chars. The bulk gas O_2 and total pressure ranges covered in the experiments were larger than any reported in the literature. Independent measurement of both particle temperature and reaction rates allowed an internal check of the data consistency and insight into the products of combustion. Details of the experiments and the results follow.

Char Preparation - Char oxidation experiments were performed with three fuels: two size fractions of UT Blind Canyon HVB coal (63-74 μm, 37-44 μm) and one size fraction of Pittsburgh HVA coal (63-74 μm). These are common U.S. coals that have been used in a number of char oxidation studies and are included in the Penn State, the Department of Energy and the Argonne National Laboratory coal banks. They are also standard ACERC coals. The UT coal was obtained from the Huntington power plant and the Pittsburgh coal was obtained from Argonne National Laboratories as tailings from the premium sample preparation process.

Samples of the coals were ground, dried and size-classified with a combination of sieving and aerodynamic classification (using a Vortec classifier) to produce tight size fractions of 200x230 mesh (63-74 μm) and 325x400 mesh (37-44 μm). The size fractions were verified by scanning electron microscope

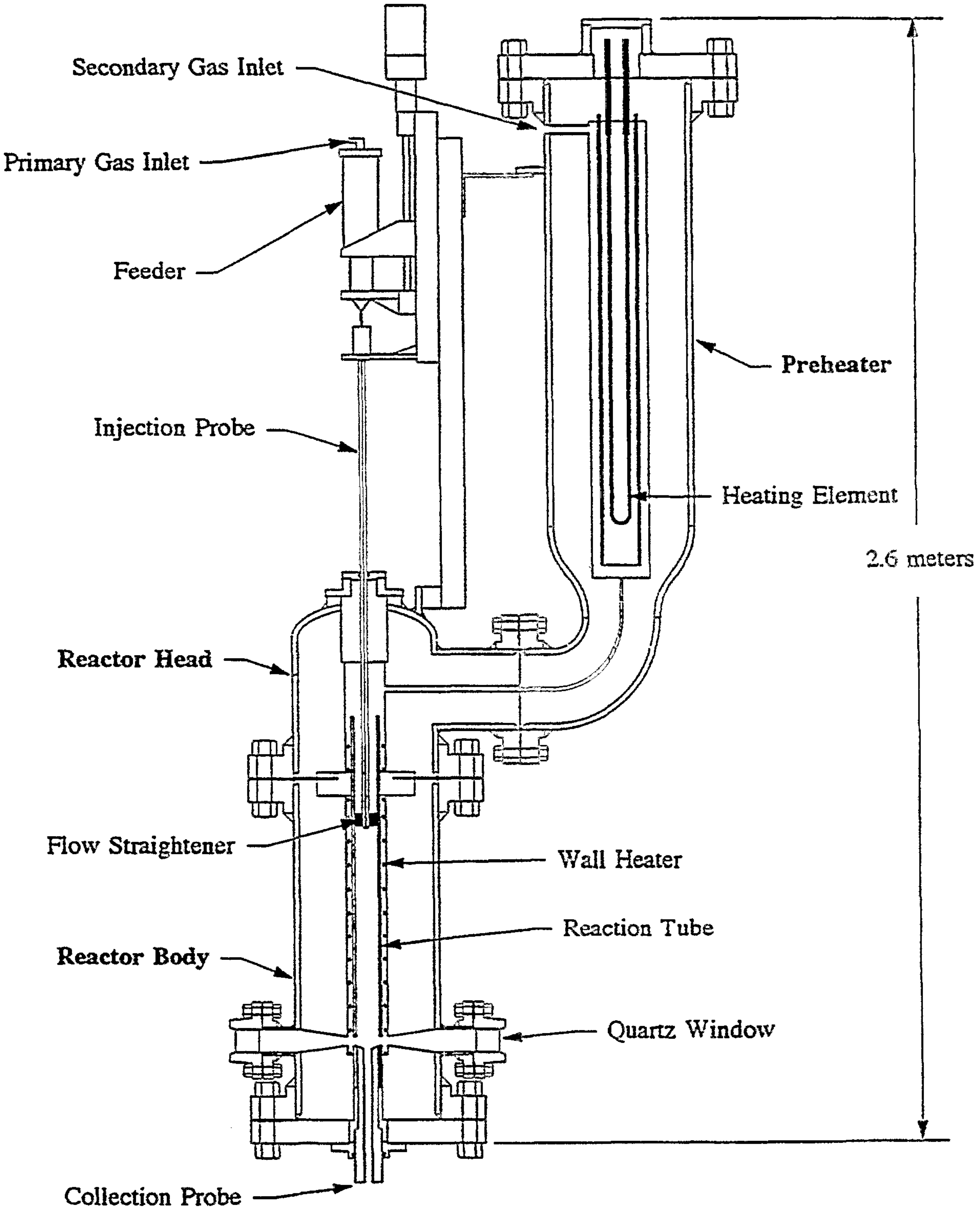

Figure II.B-1. Reactor cross section.

(SEM) and Coulter Counter measurements. Figure II.B-2 shows SEM photographs of each of the three coals along with their respective size histograms from the Coulter measurements. The sizing is seen to be excellent for the larger size fractions while the smaller size fraction exhibits a wider distribution, including a portion of smaller fines. Proximate and ultimate analyses, performed according to ASTM standards, are listed in Table II.B-1 for each of the coals.

Chars for the oxidation experiments were prepared in the HPCP furnace in a nitrogen environment. Since devolatilization conditions greatly affect char characteristics, all of the chars were prepared at the same reactor conditions. These conditions, chosen to produce complete devolatilization, were as follows: atmospheric pressure, wall and gas temperatures of 1500 K, an initial particle heating rate of 10^4 K/s (calculated using gas and wall temperature measurements), and a particle residence time of 300 ms. A number of properties for each of the resulting chars are listed in Table II.B-2 and SEM photographs and histograms are shown in Fig. II.B-3. In each case, the original coal softened during devolatilization, rounding the sharp edges and producing char particles that were quite spherical. The predominant structure for both UT chars was a 'lacy-cenosphere' type particle with no appreciable swelling. The mean size of the 70 µm UT char appears to have decreased somewhat, likely a result of the rounding of the nonspherical coal. The mean size of the 40 µm UT char was essentially unchanged, as were the distributions for both UT chars. The Pitt. char, on the other hand, exhibited thin and thick wall cenosphere formation with noticeable swelling. Its size distribution also widened substantially. While all of the raw coals had similar densities, the apparent density of the Pitt. char (0.43 g/cc) was about half that of the UT chars (0.80 and 0.86 g/cc).

Experimental Conditions - In order to obtain accurate results, a number of requirements pertaining to the particle temperature history had to be met. In the analysis of the results, it was assumed that the particle temperature was constant as it passed through the reaction zone. In order to approach this in the actual experiments, the gas temperature had to be carefully controlled. It was required that the preheated secondary flow enter the reaction zone somewhat hotter than the desired gas temperature to provide a rapid heatup of the primary gases and particles. Also, the temperatures of the gases and the particles were required to rapidly drop at the end of the reaction zone, upon entry into the collection probe. Conformance to these temperature requirements was monitored using a thermocouple probe to measure the gas temperature profiles before the experiments were performed.

The particle temperature history was also required to be similar for all particles during a given test. Because the gas motion was developing from plug flow to laminar flow, the gas and particle velocities at the reaction tube axis were greater than at some off-axis location. Particle dispersion was, therefore, held to a minimum so that all particles would experience approximately the same residence time. The particle dispersion was visually observed through the reactor windows and seldom ever approached 1 cm over a reaction length of 0.75 m.

Another requirement for reliable measurements was a constant oxygen concentration in the bulk gas. In order to ensure that this concentration was not affected by particle reactions, it was required that the char feed rate be at least 100 times smaller than the gas flow rate (Annamalai and Ramalingham, 1987). The char feedrate was 2 cc/hr (1.7 g/hr for the UT chars and 0.9 g/hr for the Pitt. char) for all of the tests and the slowest gas flow rate was 12 SLPM (850 g/hr), easily meeting the requirement. The low feedrate was also necessary to produce the small particle loading required by the optical pyrometer.

The plan for the char oxidation experiments consisted of a number of atmospheric pressure tests to both establish a baseline for the effect of pressure and to validate the procedure by comparison with other published data. These atmospheric tests then followed by higher pressure tests designed to allow examination of the effect of total pressure on the char oxidationprocess. The following parameters were varied during the experiments (with the corresponding number of levels shown in parentheses): fuel type (2), fuel size (2), total pressure (4), reactor temperature (3), bulk O_2 composition (3), and burnoff (3). An extensive test set was performed with the 70 µm UT char to provide a detailed description of the effects of

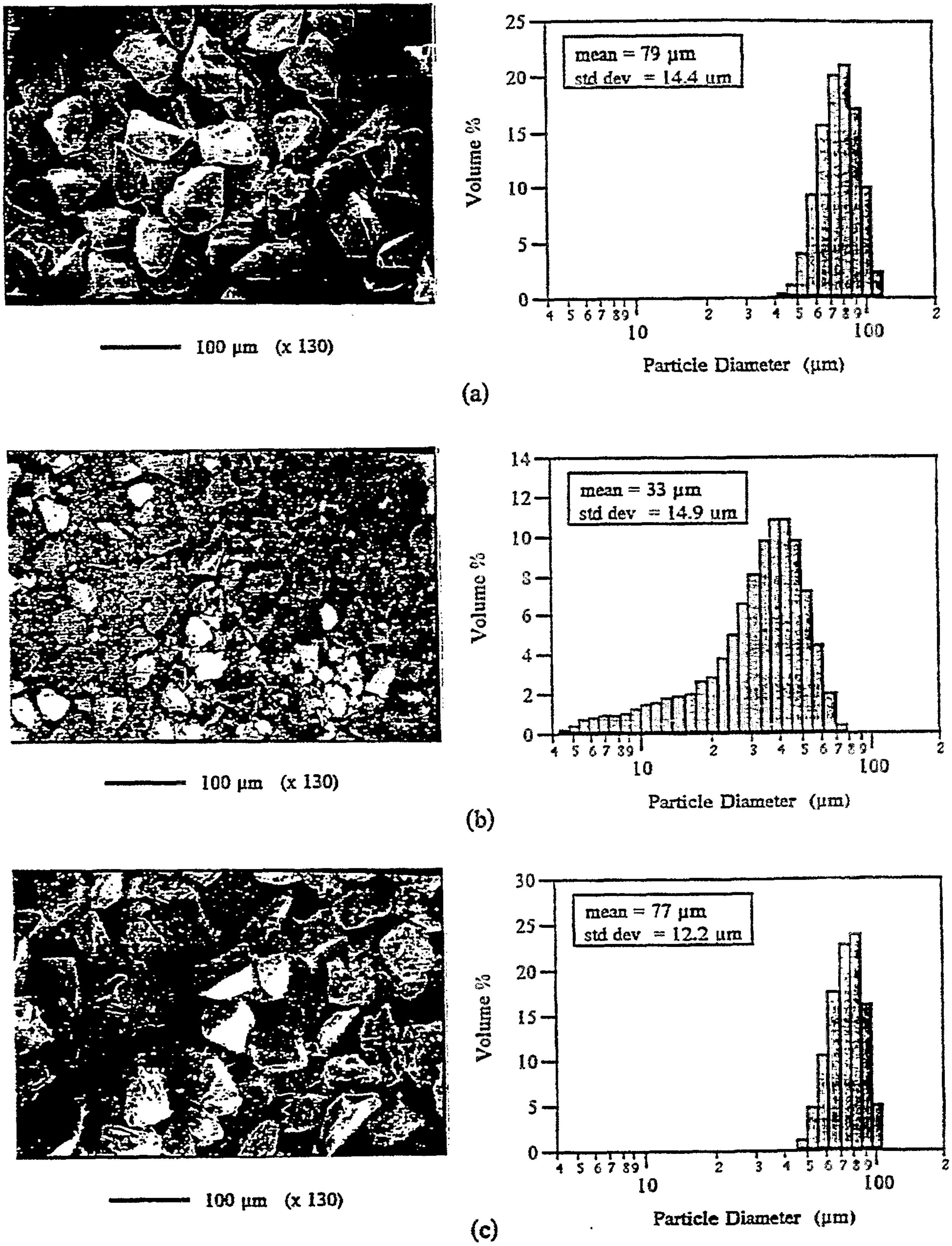

Figure II.B-2. SEM photographs and size histograms of the size- classified coals. a) 63-74 µm UT, b) 37-44 µm UT, c) 63-74 µm Pitt.

TABLE II.B-1
COAL ANALYSIS

	Proximate (%)				Ultimate (%)				
Char	Moisture	Volatiles	Carbon	Ash	C	H	N	S	O
UT (63-74 mm)									
UT (37-44 mm)									
Pitts. (63-74 mm)									

TABLE II.B-2
CHAR PROPERTIES

Char	Char Yield[1]	H/C	Ash Fraction (daf)	Apparent Density (g/cc)	Particle Diameter (mean, µm)[2]
UT (63-74 µm)	0.57	0.016	0.335	0.804	64
UT (37-44 µm)	0.57	0.016	0.236	0.860	36
Pitts. (63-74 µm)	0.64		0.248	0.431	73

1. m/mo

2. Calculated from $d_p = d_{p_o}\left(\frac{m/m_o}{\rho/\rho_o}\right)^{1/3}$

pressure on not only the reactivity and reaction rates of the char but also on the char's physical characteristics. The other chars were then tested at a limited number of conditions to observe their general pressure behavior. The experimental conditions for the three test sets are listed in Tables II.B-3 to II.B-5.

Because the burning behavior of the char was unknown over the wide range of conditions called for in the experimental plan, the particle residence length could not be specified beforehand. Determination of the length was made at the time of testing for each test condition in the following manner. The injection probe was initially positioned so its exit could be viewed through the optical access of the reactor. The probe was then raised until the ignition point of the particles was observed and this distance, referred to hereafter as the ignition distance, was recorded. The probe was then raised further until complete burnout of the particles was observed. Intermediate injection probe heights were then chosen to provide a range ofburnoffs. The ignition distance varied from near zero to several cm depending mainly on the reactor temperature and bulk O_2 concentration.

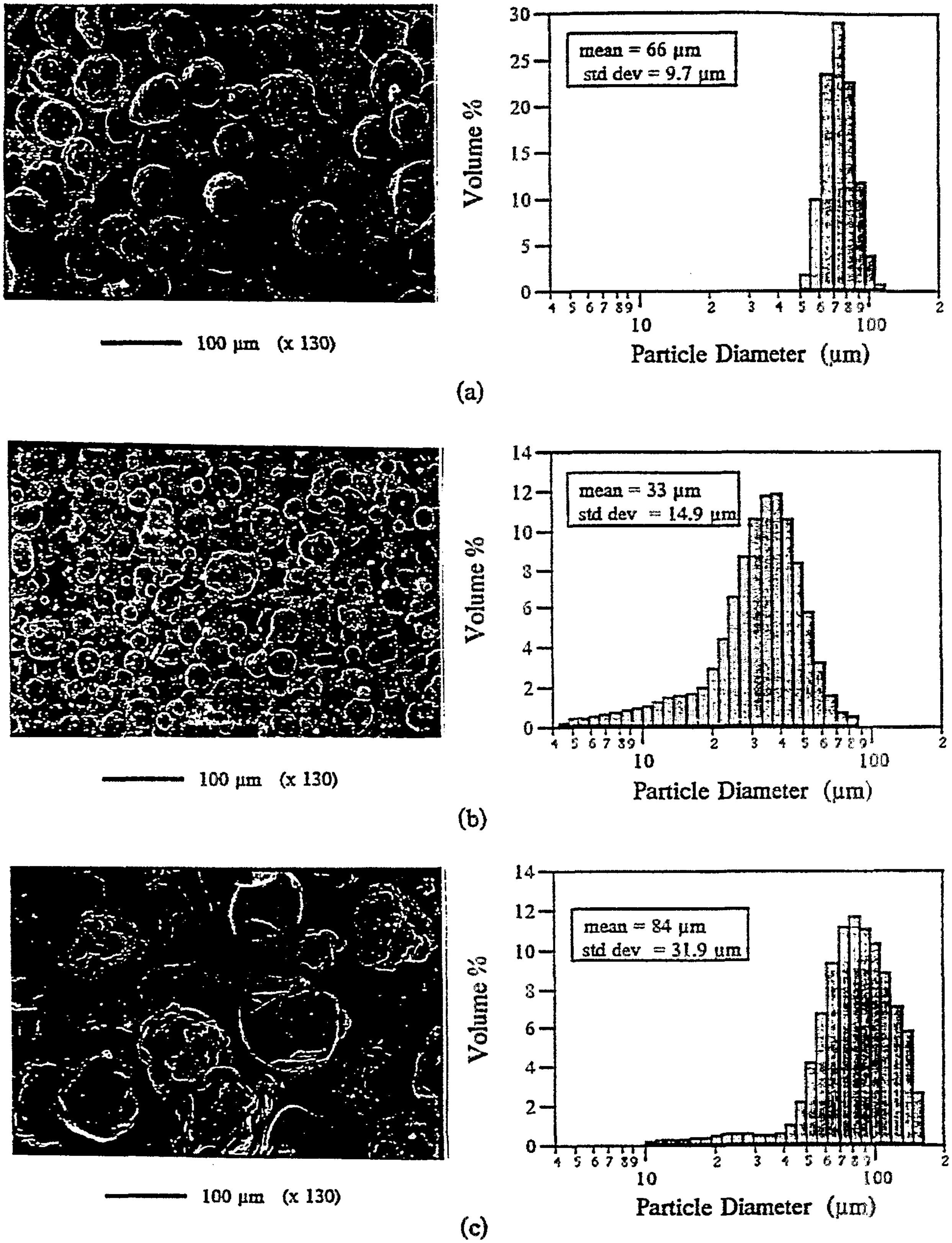

Figure II.B-3. SEM photographs and size histograms of the prepared chars. a) 63-74 µm UT, b) 37-44 µm UT, c) 63-74 µm Pitt.

TABLE II.B-3
70 µm UT CHAR EXPERIMENTAL CONDITIONS AND OVERALL RESULTS

Test	IP[1]	RL[2] (cm)	Pg (atm)	O_2 Conc (%)	T_p (K)	T_g (K)	T_W (K)	v_p (m/s)	t_r (ms)	B (%)	q_m[3]	q_a[4]	k_c[5]	χ	Sample
U1.1	U	7.5	0.92	4.40	—	1145	1143	1.1	68	9.2	1.43	—	—	—	1-53
U2.1	C	7.0	0.93	10.0	1550	1120	1100	1.19	59	15.4	2.84	2.50	9.54	0.14	1-8
.2	U	7.5	0.97	10.2	1621	1145	1143	0.94	80	38.2	5.92	4.68	19.7	0.26	1-25
.3	U	9.5	0.96	10.0	1646	1145	1143	1.00	95	49.2	6.87	5.13	22.5	0.29	1-24
U3.1	C	7.0	1.0	21.0	1827	1120	1100	1.08	64	57.3	12.4	8.85	22.9	0.22	1-7
.2	U	6.5	0.95	21.0	1853	1145	1143	1.10	59	75.3	20.4	13.0	37.7	0.32	1-22
.3	U	7.5	0.95	21.0	1819	1145	1143	1.13	66	63.0	13.9	9.59	25.9	0.24	1-20
.4	U	10.5	0.95	21.0	1815	1145	1143	1.19	88	70.3	12.3	8.12	21.2	0.20	1-21
.5	U	10.5	0.96	21.0	1804	1145	1143	1.05	100	83.4	14.3	8.66	22.9	0.21	1-23
.6	U	10.5	0.94	21.0	1953	1145	1143	1.12	94	73.6	12.4	8.02	21.0	0.20	1-47
.7	U	10.5	0.92	21.0	1942	1145	1143	1.11	95	78.1	13.5	8.47	22.7	0.21	1-50
.8	U	10.5	0.92	21.0	1962	1145	1143	1.07	98	68.4	10.6	7.08	18.4	0.18	1-51
.9	U	10.5	0.91	21.0	1962	1145	1143	1.08	97	74.1	12.1	7.80	20.7	0.19	1-52
U4.1	C	10.0	0.95	10.3	1672	1130	1130	1.21	83	45.6	7.15	5.44	23.3	0.29	1-5
U5.1	C	5.0	0.95	21.0	1892	1130	1130	1.19	42	46.6	14.5	11.0	30.0	0.27	1-4
.2	C	9.0	0.92	21.0	1812	1130	1130	1.23	87	64.6	15.1	9.41	25.9	0.23	1-12
.3	C	9.0	0.90	21.0	1812	1130	1130	1.04	73	79.1	13.0	8.89	24.0	0.22	1-9
.4	C	13.0	0.94	21.0	1846	1130	1130	1.23	106	70.4	10.3	6.79	17.2	0.17	1-3
U6.1	U	1.0	0.92	5.0	1659	1462	1462	1.35	78	0.0	—	—	—	—	1-48
.2	U	4.0	0.92	4.7	1704	1462	1462	1.51	26	23.3	10.0	8.49	—	0.90	1-49
U7.1	C	7.0	0.90	10.0	1769	1450	1428	0.98	71	57.0	11.2	8.00	38.7	0.39	1-11
.2	U	5.5	0.99	10.1	1817	1462	1469	0.87	63	65.3	15.3	10.4	52.9	0.49	1-29
.3	U	8.5	1.00	10.2	1865	1462	1469	0.86	99	59.9	—	—	—	—	1-30
.4	U	11.5	1.01	10.0	1829	1462	1469	0.94	122	85.8	12.3	7.32	30.3	0.34	1-31
U8.1	C	7.0	0.89	21.0	1970	1450	1428	0.96	73	87.0	21.1	12.4	35.0	0.27	1-10
.2	U	6.5	0.93	21.0	1951	1462	1469	1.23	52	68.4	19.7	13.2	36.9	0.29	1-26
.3	U	8.0	0.93	21.0	2014	1462	1469	0.96	83	86.7	18.4	10.9	28.9	0.24	1-27
.4	U	9.5	0.93	21.0	2017	1462	1469	1.00	95	89.5	17.1	9.91	25.9	0.21	1-28
U9.1	U	3.5	0.91	0.0	—	1143	1145	—	35	0.0	—	—	—	—	1-16
.2	U	3.5	0.95	0.0	—	1462	1469	—	35	0.0	—	—	—	—	1-19
U10.1	C	20.0	5.00	5.00	—	1100	1100	1	200	0.0	—	—	—	—	1-14
U11.1	C	10.0	4.84	9.95	1694	1100	1100	1.01	99	66.9	10.2	7.10	15.7	0.40	1-13
.2	U	8.5	5.12	10.2	1626	1131	1109	1.11	77	46.6	7.89	6.11	12.6	0.33	1-32
.3	U	11.5	5.15	10.1	1642	1131	1109	1.00	115	59.8	7.42	5.35	10.2	0.29	1-33
.4	U	14.5	5.15	10.1	1635	1131	1109	1.02	142	66.0	6.94	4.83	8.84	0.26	1-34
U12.1	U	6.5	5.21	21.0	1849	1131	1109	1.21	54	80.0	24.8	16.0	21.3	0.39	1-35
.2	U	8.0	5.32	21.0	1916	1131	1109	1.16	69	74.1	17.1	11.4	13.2	0.28	1-36
.3	U	9.5	5.38	21.0	1902	1131	1109	1.29	74	87.4	24.1	14.8	18.4	0.36	1-37
U13.1	U	8.5	5.30	4.20	1564	1136	1266	0.71	120	55.0	6.34	4.70	—	0.58	1-45
.2	U	12.5	5.00	4.00	1562	1136	1266	0.78	160	58.4	5.15	3.75	24.3	0.49	1-46
U14.1	U	7.5	5.26	10.1	1783	1336	1266	0.94	80	86.2	19.0	11.8	30.9	0.57	1-41
.2	U	9.5	5.26	10.1	1809	1336	1266	0.90	106	91.5	16.0	9.58	19.9	0.46	1-42
.3	U	11.5	5.26	10.0	1815	1336	1266	0.85	135	85.2	11.0	6.87	12.3	0.33	1-43
U15.1	U	6.5	5.25	21.0	2017	1336	1266	1.01	64	84.8	22.9	14.3	17.1	0.32	1-38
.2	U	8.0	5.33	21.0	2072	1336	1266	1.00	80	90.7	20.7	12.5	14.2	0.28	1-39
.3	U	9.5	5.31	21.0	2128	1336	1266	0.98	97	96.1	19.1	11.1	12.3	0.24	1-40
U16.1	U	3.5	4.88	0.0	—	1131	1109	—	35	0.0	—	—	—	—	1-17
.2	U	3.5	5.50	0.0	—	1336	1266	—	35	0.0	—	—	—	—	1-18
U17.1	U	6.5	9.86	5.0	1404	1006	726	0.49	133	41.7	3.97	3.14	8.68	0.40	1-58
.2	U	9.5	9.75	5.0	1424	1006	726	0.49	194	45.6	3.05	2.37	5.04	0.30	1-29
U18.1	U	6.5	9.84	10.0	1721	1006	726	0.52	125	51.8	5.59	4.22	5.22	0.25	1-56
.2	U	6.5	10.4	10.0	1622	1006	726	0.53	123	66.9	8.17	5.70	8.23	0.33	3-7
.3	U	6.5	10.4	10.0	1637	1006	26	0.49	133	60.2	6.48	4.69	6.12	0.28	3-8
.4	U	6.5	10.4	10.2	1643	1006	726	0.53	123	65.7	7.95	5.61	7.86	0.33	3-9
.5	U	6.5	10.4	10.0	1639	1006	726	0.52	125	69.3	8.48	5.84	8.38	0.34	3-10
.6	U	8.5	9.79	10.1	1687	1006	726	0.65	131	78.6	9.90	6.44	9.42	0.37	1-57
U19.1	U	5.5	10.0	21.0	1801	1006	726	0.65	85	52.5	—	—	—	—	1-54
.2	U	6.5	9.87	21.0	1938	1006	726	0.73	89	87.5	17.5	10.8	9.00	0.28	1-55
U20.1	U	7.5	10.2	5.0	1465	1173	858	0.49	153	39.8	3.25	2.59	5.48	0.30	1-61
.2	U	10.5	10.2	5.0	1540	1173	858	0.51	206	61.2	4.28	3.09	7.00	0.35	1-60

TABLE II.B-3 (CONTINUED)

Test	IP [1]	RL [2] (cm)	Pg (atm)	O_2 Conc (%)	T_p (K)	T_g (K)	T_w (K)	v_p (m/s)	t_r (ms)	B (%)	q_m [3]	q_a [4]	k_c [5]	χ	Sample
U21.1	U	8.5	10.2	10.0	1706	1173	858	0.63	135	82.6	10.4	6.60	9.24	0.35	1-62
.2	U	10.5	9.95	10.0	1759	1173	858	0.70	150	90.2	11.0	6.64	8.98	0.35	1-63
U22.1	U	6.5	10.0	21.0	1824	1173	858	0.56	116	—	—	—	—	—	1-65
.2	U	7.5	10.1	21.0	2025	1173	858	0.60	125	99.9	15.0	8.64	6.75	.20	1-64
U23.1	U	6.5	15.4	5.0	1328	987	631	0.24	271	23.4	0.98	0.84	1.07	0.11	3-5
.2	U	8.5	15.5	5.0	1376	987	631	0.25	340	43.0	1.61	1.27	1.72	0.16	3-5
U24.1	U	6.5	15.3	10.0	1545	987	631	0.25	260	70.2	4.16	2.84	2.74	0.17	3-3
.2	U	8.5	15.1	10.0	1592	987	631	0.30	283	80.7	4.77	3.06	2.98	0.18	3-4
U25.1	U	6.5	15.4	21.0	1864	987	631	0.29	224	73.0	5.13	3.45	2.03	0.09	3-1
.2	U	8.5	15.3	21.0	1914	987	631	0.34	250	92.8	6.93	4.11	2.45	0.11	3-2

1. Injection Probe: C - cooled, U - uncooled
2. Reaction Length
3. Mass Reactivity (g/g • s)
4. Area Reactivity(g/cm^2• s) •10^{-3}
5. Reaction Rate Coefficient (g/cm^2• s)(1/atm)$^{0.5}$ •10^{-3}

TABLE II.B-4

40 µm UT CHAR EXPERIMENTAL CONDITIONS AND OVERALL RESULTS

Test	IP [1]	RL [2] (cm)	Pres (atm)	O_2 Conc (%)	T_p (K)	T_g (K)	T_w (K)	v_p (m/s)	t_r (ms)	B (%)	q_m [3]	q_a [4]	k_c [5]	χ	Sample
U26.1	C	8.0	0.93	21.0	1820	1120	1100	1.22	66	57.7	12.4	5.41	12.9	0.08	2-2
.2	U	6.5	0.97	21.0	—	1145	1143	—	67	61.2	13.2	5.65	13.2	0.08	2-5
.3	u	9.5	0.96	21.0	1827	1145	1143	0.96	99	76.1	12.4	4.85	11.3	0.07	2-6
.4	u	12.5	0.96	21.0	1824	1145	1143	0.98	128	78.4	5.05	1.94	4.41	0.03	2-7
U27.1	C	4.5	0.90	21.0	1930	1428	1450	0.91	49	70.4	22.0	8.91	22.1	0.11	2-1
.2	u	6.5	0.90	21.0	1931	1469	1462	1.02	64	90.4	25.9	9.17	22.7	0.11	2-8
.3	u	7.5	0.97	21.0	1988	1469	1462	0.87	86	94.2	20.7	7.12	17.2	0.09	2-9
U28.1	U	6.0	5.16	21.0	1843	1131	1109	1.23	49	63.2	18.9	8.26	8.60	0.11	2-10
.2	U	8.5	5.04	21.0	1906	1131	1109	1.12	76	84.8	19.4	7.49	7.78	0.10	2-11
U29.1	U	6.5	5.32	21.0	1976	1336	1266	1.52	43	92.5	40.2	14.8	15.8	0.18	2-12
.2	U	9.5	5.32	21.0	2025	1336	1266	1.51	63	97.5	30.2	10.7	11.0	0.13	2-13

1. Injection Probe: C - cooled, U - uncooled
2. Reaction Length
3. Mass Reactivity (g/g • s)
4. Area Reactivity (g/cm^2• s) •10^{-3}
5. Reaction Rate Coefficient (g/cm^2• s)(1/atm)$^{0.5}$ •10^{-3}

TABLE II.B-5

70 µm PITT. CHAR EXPERIMENTAL CONDITIONS AND OVERALL RESULTS

Test	IP[1]	RL[2] (cm)	Pres (atm)	O_2 Conc (%)	T_p (K)	T_g (K)	T_W (K)	v_p (m/s)	t_r (ms)	B (%)	q_m[3]	q_a[4]	k_c[5]	χ	Sample
P1.1	U	6.0	0.93	10.0	1755	1335	1330	1.26	48	24.0	5.68	4.80	19.4	0.25	1-3
.2	U	11.0	0.93	10.0	1780	1335	1330	1.40	79	46.0	7.56	5.74	23.9	0.29	1-4
P2.1	U	8.0	0.94	21.0	1900	1335	1330	1.24	65	66.3	15.4	10.4	28.0	0.24	1-1
.2	U	13.0	0.93	21.0	1893	1335	1330	1.37	95	78.8	13.7	8.56	22.3	0.20	1-2
P3.1	U	7.0	0.91	10.0	1757	1460	1450	1.39	50	12.3	—	—	—	—	1-7
.2	U	11.0	0.91	9.9	1799	1460	1450	1.35	81	—	—	—	—	—	1-8
P4.1	U	7.0	0.92	21.0	1971	1460	1450	1.51	46	60.4	18.7	13.1	36.9	0.29	1-5
.2	U	11.0	0.91	21.0	2012	1460	1450	1.42	77	80.9	17.6	10.8	29.2	0.24	1-6
P5.1	U	7.0	9.97	10.0	1746	1100	850	0.66	106	40.0	4.72	3.76	4.44	0.21	1-9
.2	U	11.0	10.1	9.9	1725	1100	850	0.64	172	29.5	—	—	—	—	1-10
P6.1	U	7.0	10.0	21.0	2011	1100	850	0.96	73	70.5	14.9	10.2	8.27	0.25	1-11
.2	U	10.0	10.0	21.0	2088	1100	850	0.84	119	86.4	12.8	7.93	6.15	0.19	1-12
P7.1	U	10.2	10.2	10.0	1669	1270	930	0.92	76	63.8	12.3	8.71	15.8	0.45	1-15
.2	U	10.3	10.3	10.0	1742	1270	930	0.87	115	78.4	11.2	8.30	10.2	0.37	1-16
P8.1	U	10.2	10.2	21.0	1936	1270	930	0.99	56	82.2	25.1	16.0	14.5	0.37	1-13
.2	U	10.2	10.2	21.0	2081	1270	930	0.98	77	92.2	22.2	13.2	11.0	0.30	1-14

1. Injection Probe: C - cooled, U - uncooled
2. Reaction Length
3. Mass Reactivity (g/g • s)
4. Area Reactivity (g/cm^2• s) •10^{-3}
5. Reaction Rate Coefficient(g/cm^2• s)($1/atm$)$^{0.5}$ •10^{-3}

Experimental Results - Measurements taken during each test included reaction tube temperatures, bulk gas O_2 concentration, total pressure, reaction length, and individual particle temperature, size, and velocity. Gas temperatures were obtained for each reactor condition before the testing was performed. Subsequent analysis of the char residue included measurement of the ash content, elemental analysis of Ti, Al, C, and H, bulk density, true density, and N_2 surface area. Mass and area reactivities and apparent kinetic coefficients were determined for each of the fuels. The overall results for each of the tests are listed in Tables II.B-3 to II.B-5.

Analysis of Test Results

Detailed analyses of char oxidation measurements were conducted for the three fuels used. The analyses include char composition, char structure, char residence time and burnoff, and char reactivity.

Ash and Elemental Analyses - Ash and elemental analyses were performed on the residual char from each test. The fraction of ash in a given sample was determined by oxidizing the sample in a muffle furnace until only the ash component remained. Comparison was then made between the weight of the original sample and that of the final ash. The Ti and Al contents of the ash were determined by inductively-coupled plasma atomic emission spectroscopy (ICP). Elemental analysis of the char residue for the C and H contents were performed on a Leko instrument.

Particle Residence Time and Burnoff - The reaction length for a given test condition was determined as the difference between the injection-to-collection-probe length and the ignition distance. The average particle residence time was determined by dividing the reaction length by the measured, average particle velocity.

The carbon burnoff (dry, ash-free) of a sample was determined by following three tracers: ash, Ti and Al. Assuming that the given tracer does not react to form gaseous products during conversion, the burnoff can be calculated by (Pace, 1982)

$$B = \frac{x_{t_i}\left(1 - x_{a_f}\right)}{x_{t_f}\left(1 - x_{a_i}\right)} \qquad \text{II.B-1}$$

This formulation of the burnoff allows for ash loss (for minerals other than the specific tracer) when used with Ti or Al tracers. For each test, burnoffs were calculated using each of the tracers. In almost every case the three values agreed within a few percent, promoting confidence in the ash analyses. The three values were averaged to produce the burnoffs listed in the tables and used in subsequent calculations.

Particle Temperature, Velocity and Size Measurements - Approximately 50 to 100 individual particle traces were obtained from the optical system during each test. While valid measurements were obtained for the particle temperature and velocity in all cases, accurate particle size measurements were not obtained for the low temperature, 40 µm tests or the higher pressures of 10 and 15 atm, due to limitations of the optical pyrometer. With the collection probe located 5.5 cm below the optical control volume for nearly all of the tests, the optical measurements were typically obtained near the midpoint of the particle residence time. Mean temperature and velocity measurements for each test are listed in Tables II.B-3 to II.B-5.

Individual particle measurements for a typical 70 µm particle test, U3.2, are presented in Figs. II.B-4 and II.B-5. Particle-to-particle variations in minerals, macerals and structure resulted in wide distributions in temperature and size. The variation in combustion behaviors was also evidenced by SEM photographs of particle samples. Fig. II.B-4a shows a nearly normal particle temperature distribution that spans a range of 300 K. The mean and median temperature values were essentially equivalent for this and all of the oxidation tests. Fig. II.B-4b shows a 700 K difference in particle and gas temperatures. This is due to the high reactivity of the char and the high oxygen concentration of the combustion environment. Little particle size dependence is observed in the measured temperatures.

Measured particle velocities followed a normal distribution with a small standard deviation (Fig. II.B-5a). Because of the small size of the particles, slip velocity was very low (ca. a few percent of gas velocity) and very little difference in slip velocity for the particle size distribution was seen. Since the gas movement is a developing laminar flow with a maximum velocity at the center of the reaction tube, particles slightly off center would move a little slower than those flowing along the axis. Thus, the particle velocity distribution was mainly dependent on the gas velocity profile.

The measured particle size distribution, Fig. II.B-5b, exhibited a wide variance and a skewing to the smaller sizes. This is a result of differences in the combustion of individual particles. While most of the particles seemed to burn in a decreasing density mode, a small portion burning with decreasing diameter would result in the smaller sizes measured. Fragmentation would also contribute to the number of smaller particles.

Char Structure Results - Structural changes in the chars were followed by densities (bulk, apparent and true), SEM photographs, and N_2 BET adsorption surface area measurements. These results are tabulated in Appendix A.

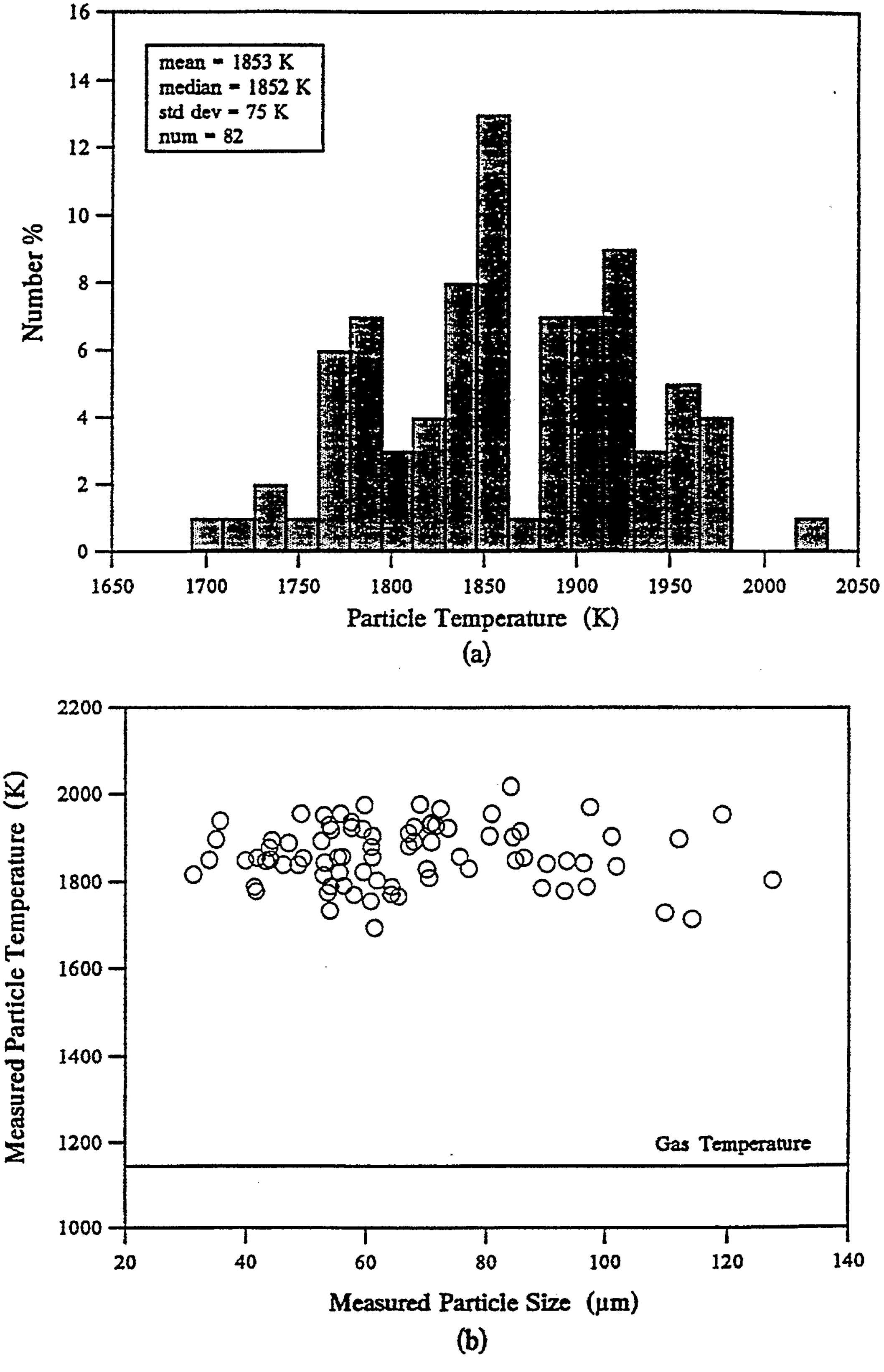

Figure II.B-4. Temperature measurement a) histogram and b) size dependence for a typical test (U3.2).

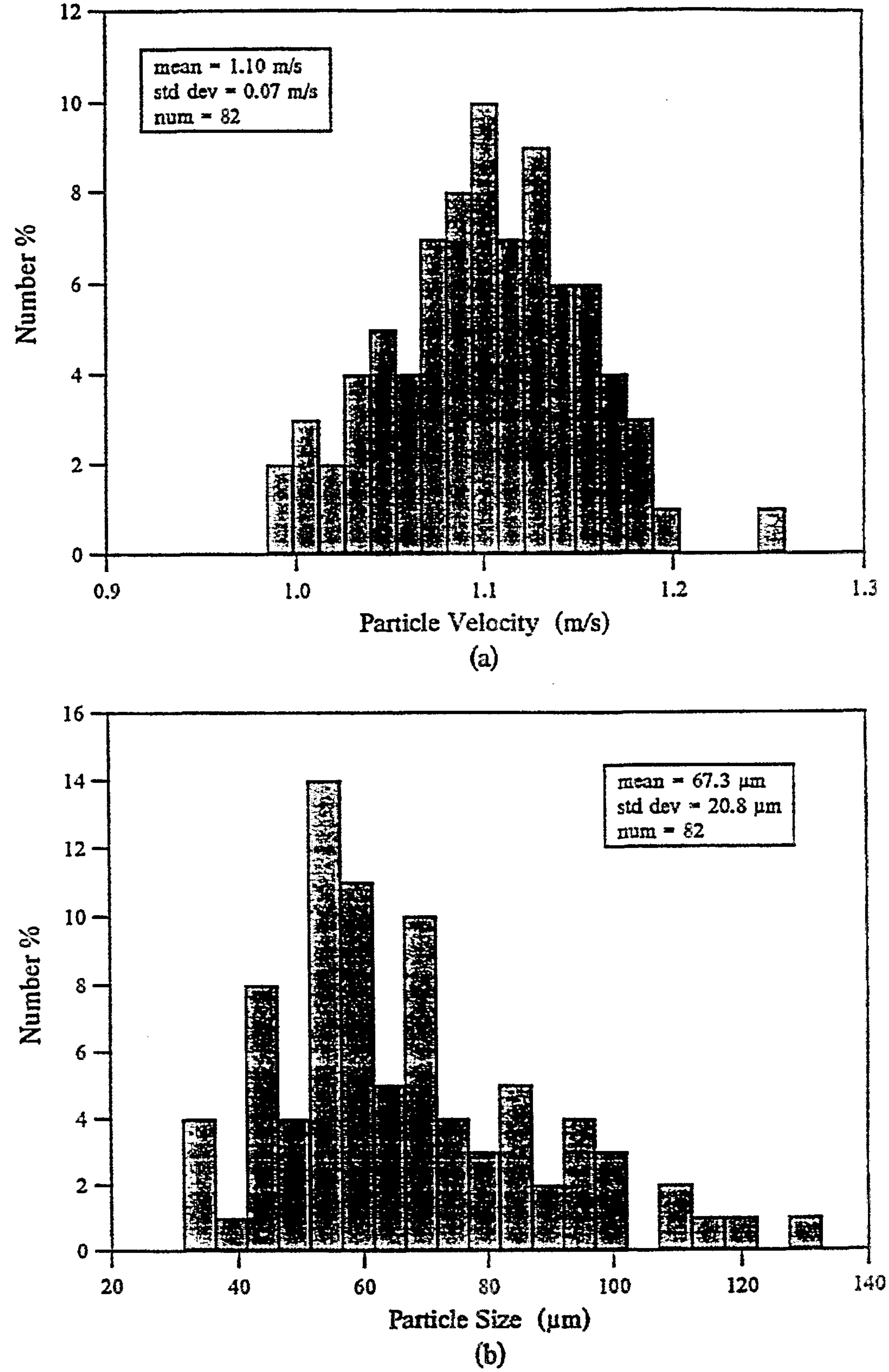

Figure II.B-5. Histograms of the a) velocity and b) size measurements for a typical test (U3.2).

Bulk densities were obtained for each test using a small graduated cylinder and a weight scale. The collected char residue was placed in the graduated cylinder and tapped until the minimum volume was obtained (typically 1-2 minutes). This volume, along with the weight of the sample, was used to calculate bulk density. Apparent densities were obtained from the bulk value by assuming the widely accepted interparticle void volume of 0.45 (Field, 1970).

$$\rho_{app} = \rho_b \frac{1}{(1-0.45)} \qquad \text{II.B-2}$$

The following correction was made for the ash content to yield the carbon apparent density, ρ_c (Hurt and Mitchell, 1992).

$$\rho_c = \frac{1-x_a}{\dfrac{1}{\rho_{app}} - \dfrac{x_a}{\rho_a}} \qquad \text{II.B-3}$$

The change in char density with burnoff is typically modelled by the burning mode parameter, α, as follows (Smith, 1982):

$$\frac{\rho_c}{\rho_{co}} = \left(\frac{m}{m_o}\right)_{daf}^{\alpha} \qquad \text{II.B-4}$$

Figure II.B-6 shows the effect of conversion on the carbon apparent density and the predicted density change from the model. The burning mode parameter most consistent with the 1 atm data (Fig. II.B-6a), determined from least- squares regression (excluding outlying points), was 0.65, while the higher pressure data were best fit by a value of 0.5. The 5 atm outliers at high burnout can be explained by small errors in the burnout measurements. A small percentage increase in the burnout values brings these points into conformance with the other data. Figures II.B-6b - II.B-6c present the same information for the 40 μm UT char and the Pitt. char. These fuels also exhibited nearly the same changes in structure with conversion. This reducing density, and reducing diameter burning, indicates that significant reaction was occurring within the particle pores (Zone II burning). Higher gas pressures did not significantly alter this mode of burning.

The trends in char structure indicated by the density analyses were consistent with the SEM photographs. Selected char samples were chosen to provide a range of burnoffs at two pressures for each of the fuels. Photographs of these samples are shown in Figs. II.B-7 to II.B-9. The variety of char structures present in each of the fuel types was most likely a result of varying maceral content in the particle populations (Tsai and Scaroni, 1987). The predominate structure in both UT chars was lacy cenospheres, while that of the Pitt. char was thin and thick walled cenospheres. As the chars burned, pore combustion resulted in fragile lacy structures, nearly the same size as the original chars. At high levels of conversion, these appear to have fragmented into smaller pieces. It is apparent that the char population was composed of particles exhibiting a wide range of reactivities. In the 1 atm, 0.15 conversion photograph in Fig. II.B-7, for example, some particles show no signs of any reaction while others show significant pore development and other signs of substantial conversion. It is also interesting to note that a few particles retained their original coal-like shape even at high burnoff values. In agreement with the density results, no pressure dependence is apparent in the photographs.

N_2 and CO_2 surface area measurements were used to estimate the mesopore and micropore areas of the original UT chars. The mesopore areas were fairly small, about 1 m^2/g, while the micropore

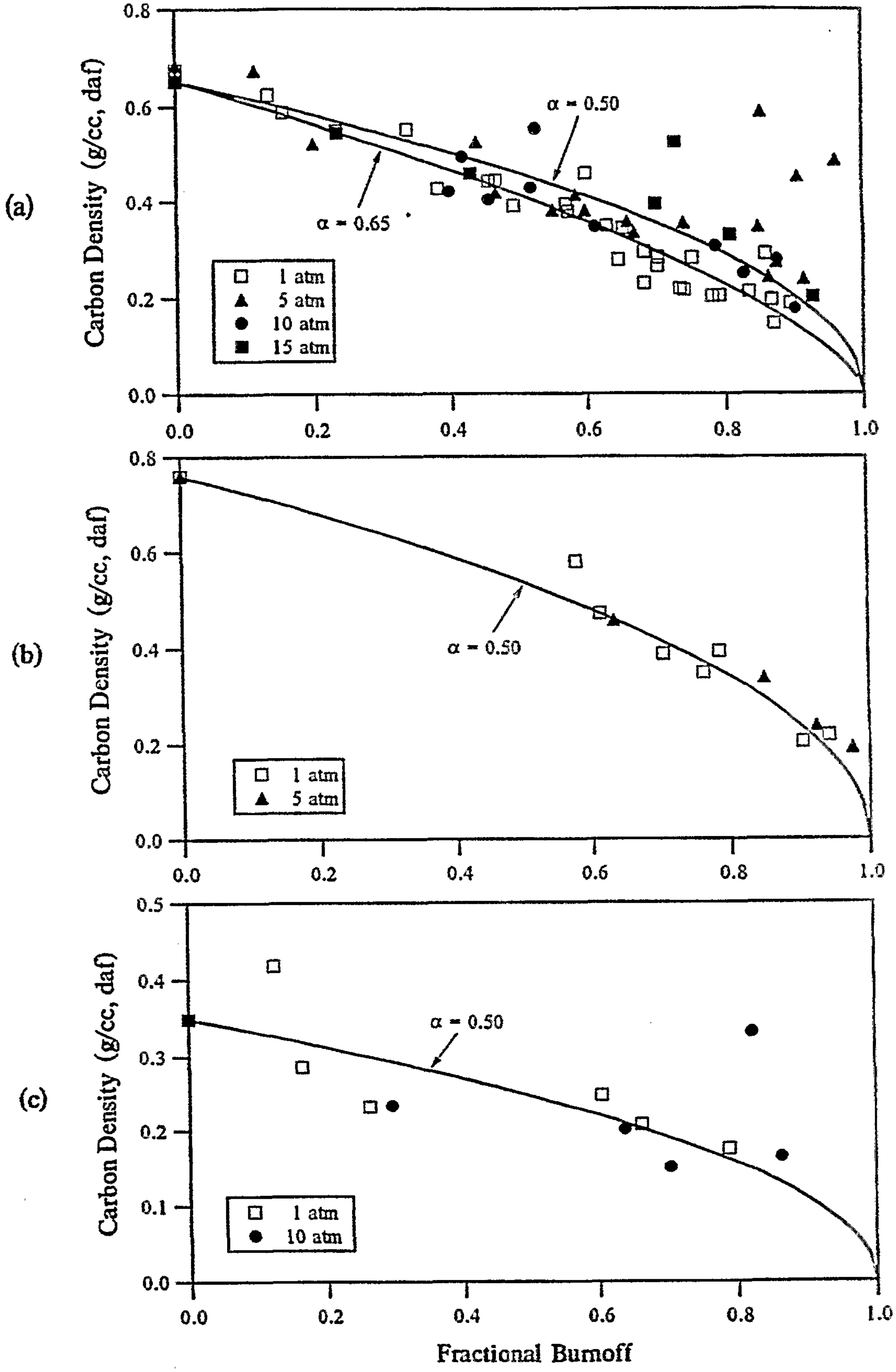

Figure II.B-6. The change in carbon density with burnoff for the a) 70 μm UT, b) 40 μm UT and c) 70 μm Pitt. Chars.

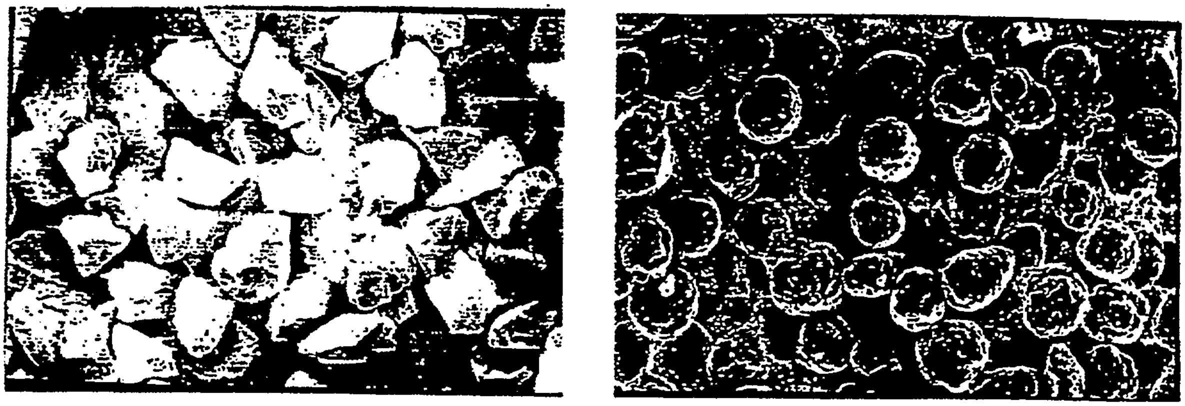

Raw Coal

Original Char

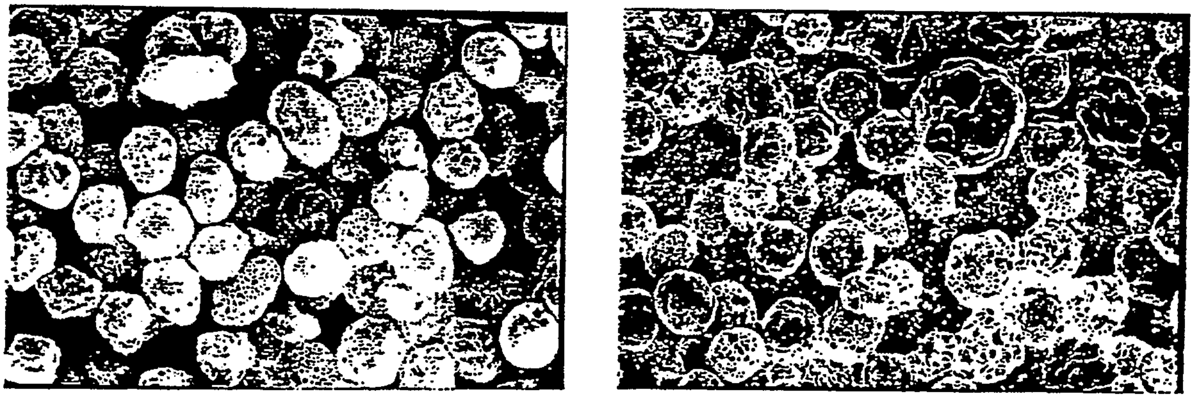

1 atm - 0.15 Conversion (U2.1)

10 atm - 0.42 Conversion (U17.1)

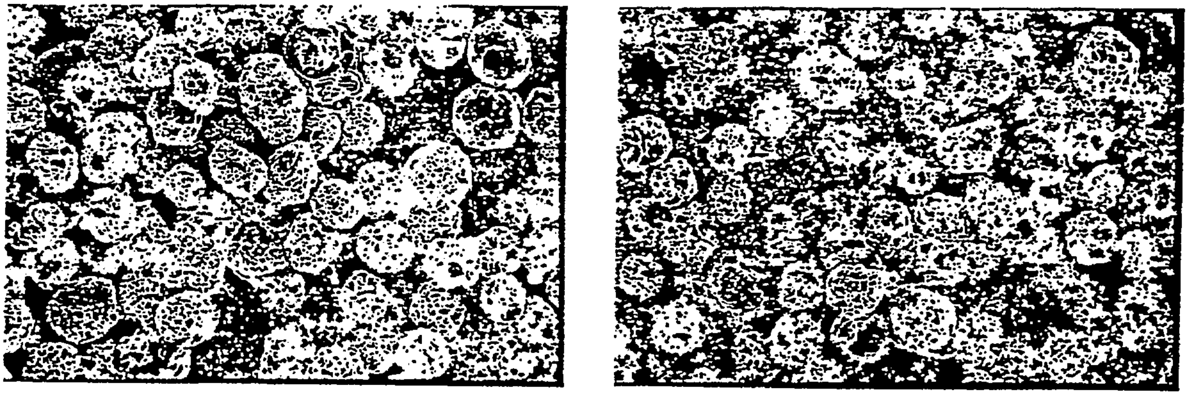

1 atm - 0.65 Conversion (U7.2)

10 atm - 0.83 Conversion (U21.1)

1 atm - 0.90 Conversion (U8.4)

10 atm - 0.88 Conversion (U19.2)

Figure II.B-7. SEM photographs of the 70 μm UT char as a function of conversion at 1 and 10 atm total pressure.
——————— 100 μm (x 130).

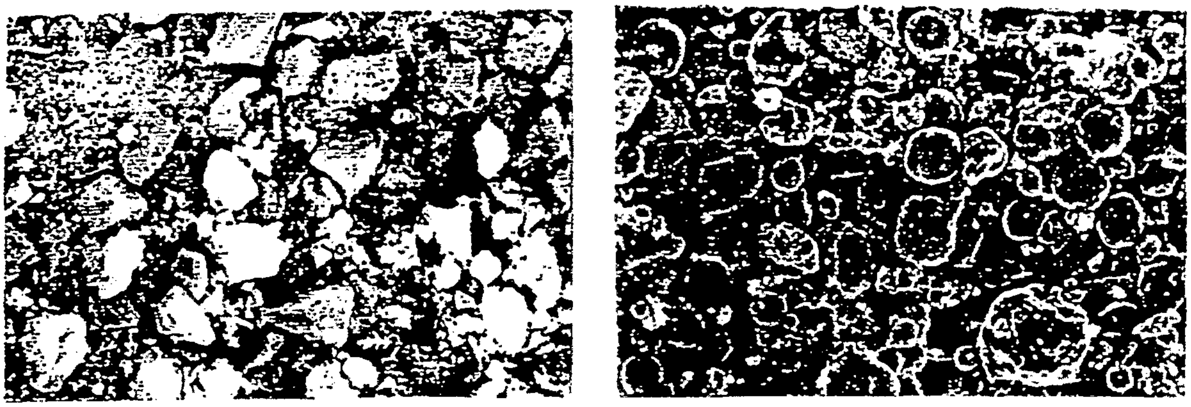

Raw Coal

Original Char

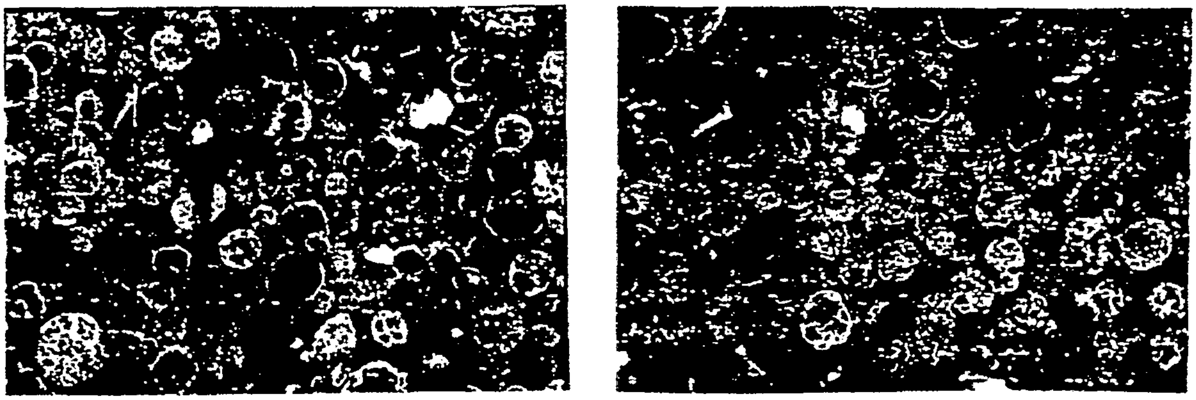

1 atm - 0.58 Conversion (U26.1)

5 atm - 0.63 Conversion (U28.1)

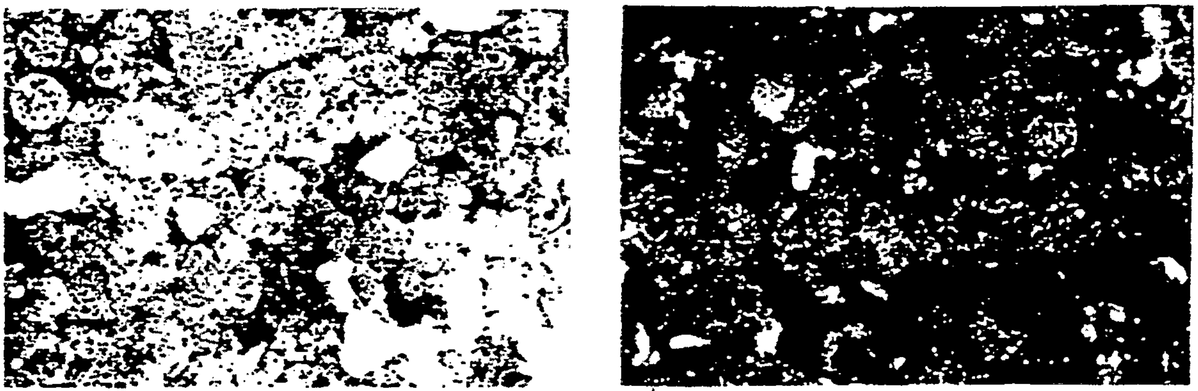

1 atm - 0.90 Conversion (U27.2)

5 atm - 0.85 Conversion (U28.2)

Figure II.B-8. SEM photographs of the 40 μm UT char as a function of conversion at 1 and 10 atm total pressure.
——————— 100 μm (x 200).

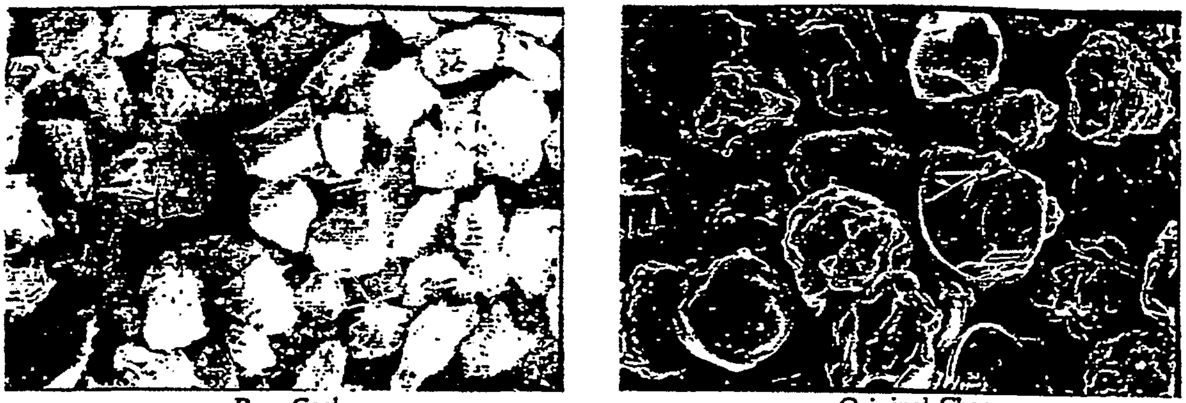

Raw Coal

Original Char

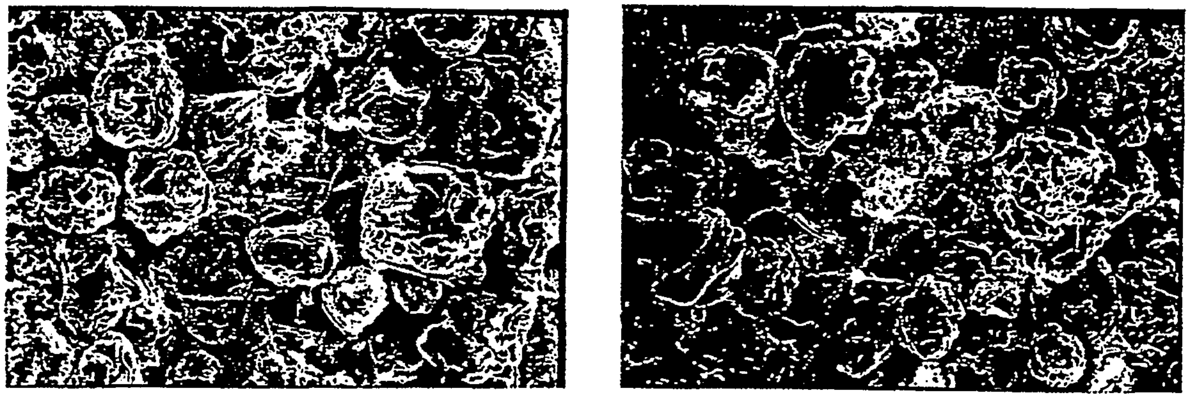

1 atm - 0.16 Conversion (P1.1)

10 atm - 0.40 Conversion (P5.1)

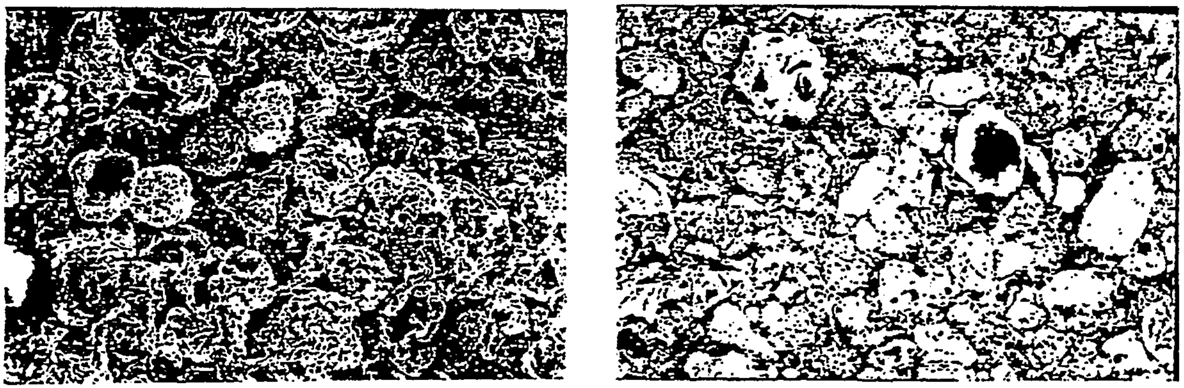

1 atm - 0.35 Conversion (P3.2)

10 atm - 0.78 Conversion (P7.2)

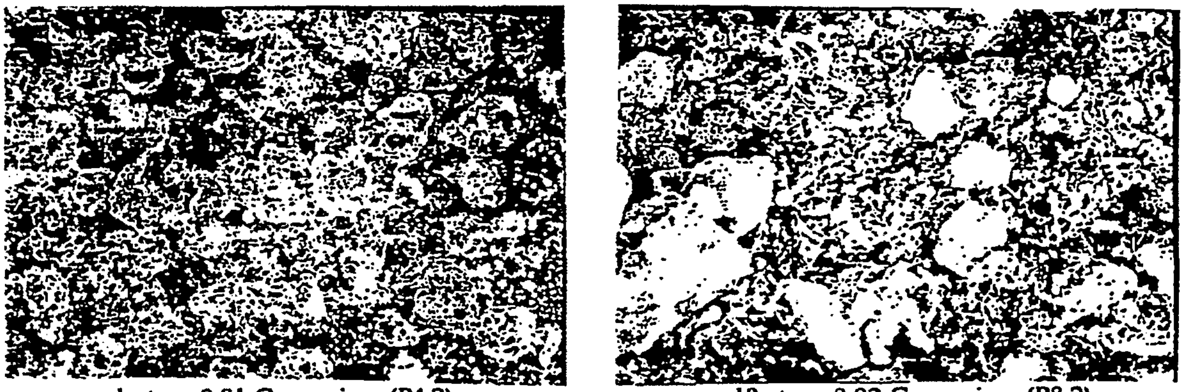

1 atm - 0.81 Conversion (P4.2)

10 atm - 0.92 Conversion (P8.2)

Figure II.B-9. SEM photographs of the 70 μm Pitt. char as a function of conversion at 1 and 10 atm total pressure.
——————— 100 μm (x 130).

areas where quite extensive, around 350 m^2/g. N_2 surface area measurements were also performed on selected chars as a function of burnoff and pressure. The samples used for these measurements corresponded to those used for the SEM photographs. These results are plotted in Fig. II.B-10. The pore evolution shows a maximum around mid-burnoff with little mesopore area in either the unoxidized or highly converted chars. Little pressure effect is seen in the surface areas.

All of the structure measurements are in agreement. The oxidation experiments occurred in a regime where internal burning was significant and the total pressure had no apparent effect on the char structure.

Char Reactivity - The overall chemical kinetics of char oxidation are usually described by the mass and area reactivities (Laurendeau, 1978). The mass reactivity, q_m, is defined by

$$q_m = \frac{1}{m}\frac{dm}{dt} \qquad \text{II.B-5}$$

Assuming the particle temperature remains constant during burnoff and taking the carbon mass at the midpoint of burnoff, the average mass reactivity can be determined from experimental measurement by

$$q_m = \frac{2B}{2-B}\frac{1}{t_r} \qquad \text{II.B-6}$$

In a manner similar to the mass reactivity, the overall reaction rate can also be described on a particle external surface area basis (assuming a spherical particle) by the area reactivity.

$$q_a = -\frac{1}{A_p}\frac{dm}{dt} \qquad \text{II.B-7}$$

Taking A_p at the midpoint of combustion, the time-averaged area reactivity can be determined from

$$q_a = -\frac{m_o}{A_{pm}}\frac{B}{t_r} \qquad \text{II.B-8}$$

The initial char apparent density and diameter can be used to calculate the initial particle mass, m_o, and A_{pm} can be calculated using Eqns. II.B-3, II.B-4, and geometry. Values for q_m and q_a for each test are listed in Tables II.B-3 - II.B-5. They are also plotted in Arrhenius form in Figs. II.B-11 to II.B-15.

Figure II.B-11 shows a comparison of area reactivities from the 1 atm UT char tests and from experiments conducted with UT chars at Sandia National Laboratories (Hurt et al., 1991) and Stanford University (Leslie et al., 1989). While the Sandia study did not report reactivities as a function of temperature, the basic measurements required to make these determinations (mass fractions of ash and tracers, residence time, diameter, density, and temperature) were reported. Thus, the Sandia reactivities shown in the figure were calculated from the reported measurements using the methods of this study. The Stanford reactivities in the figure are those reported by Leslie et al. (1989). It should be noted that the particle temperatures were calculated, not measured, in the Stanford study. Experiments at Sandia were carried out in laminar flows with gas O_2 pressures of 0.06 and 0.12 atm, while those at Stanford were performed in turbulent flows at 0.075 atm O_2 pressure. The data sets shown in the figure cover a particle size range of 40 to 116 µm.

Agreement between the similar-sized char data sets, 59 and 70 µm, is quite good and all the data sets agree within a factor of three. The differences could be attributed to a number of variables including

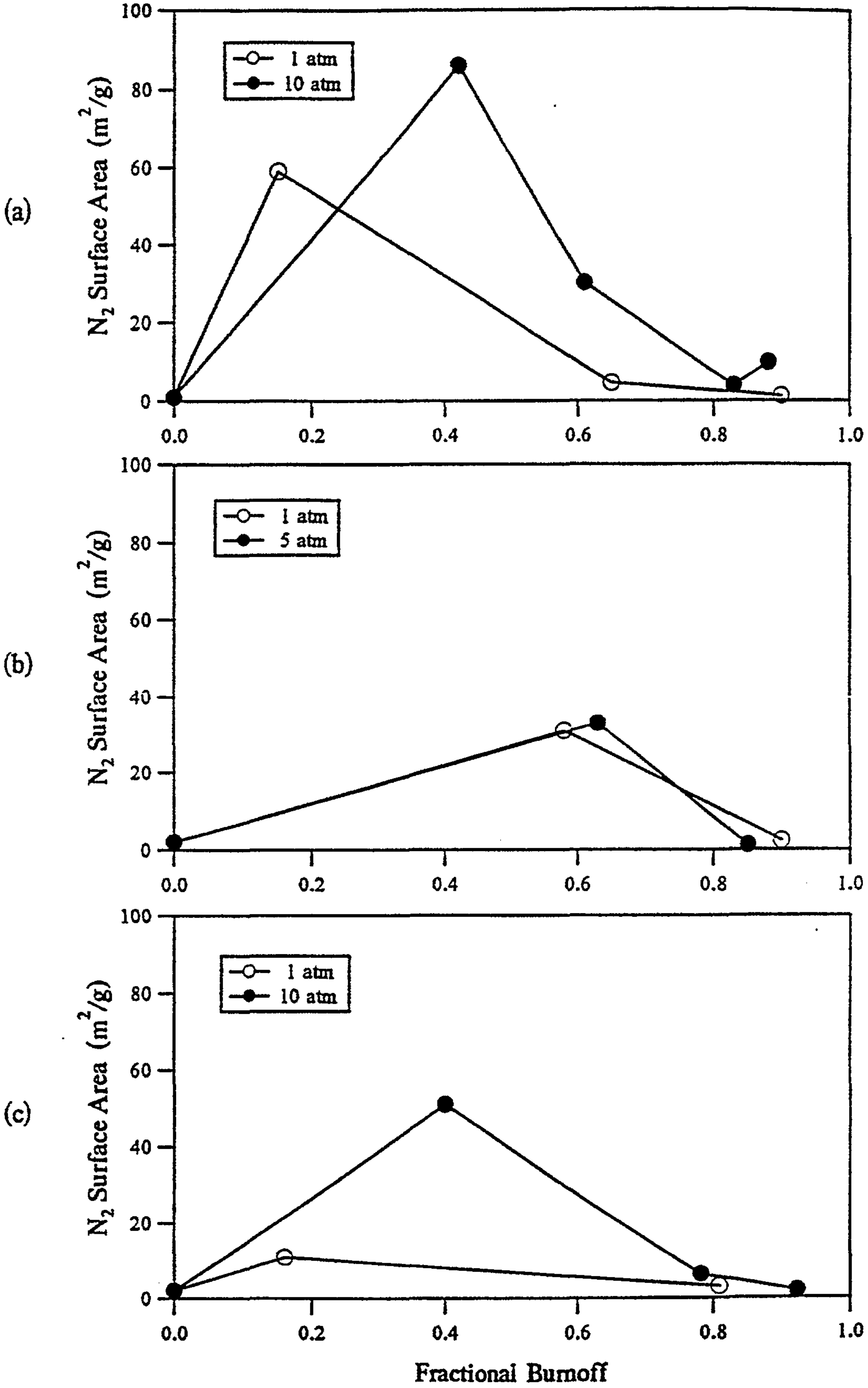

Figure II.B-10. The change in N2 surface area with burnoff for the a) 70 µm UT, b) 40 µm UT and c) 70 µm Pitts. chars.

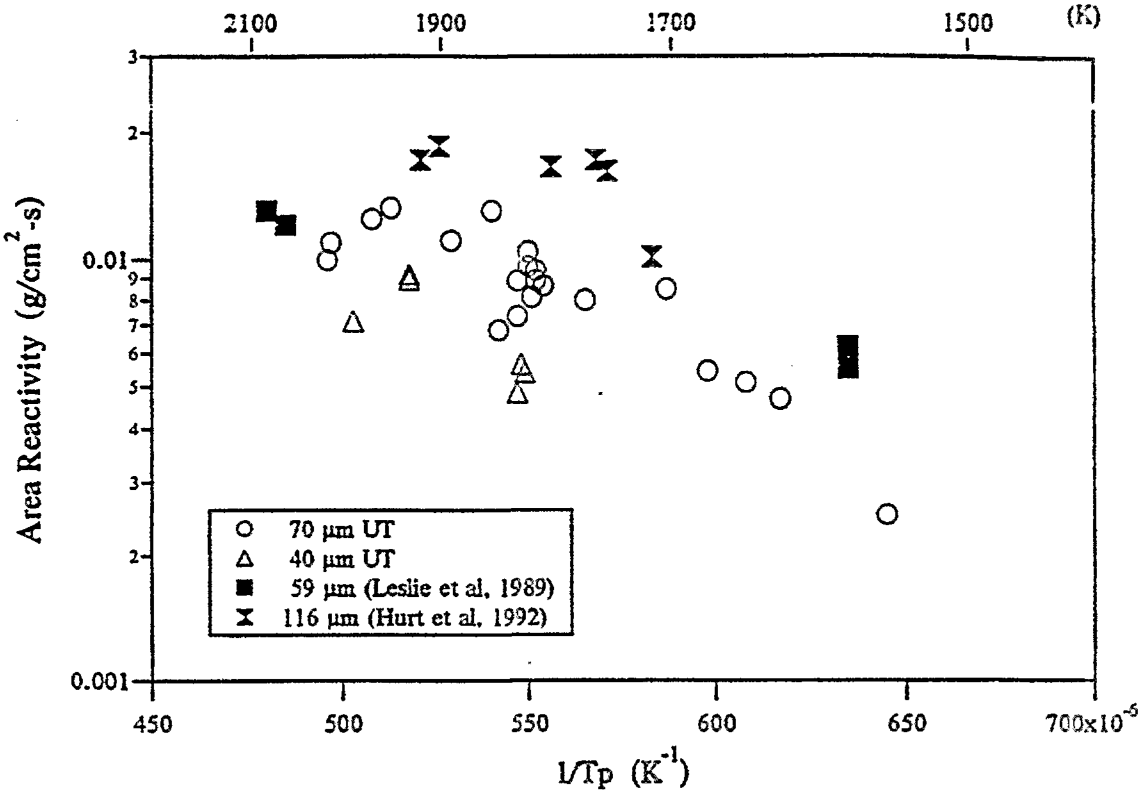

Figure II.B-11. Experimentally derived area reactivity for the UT Chars (at 1 atm) plotted with results from others' work with the same coal.

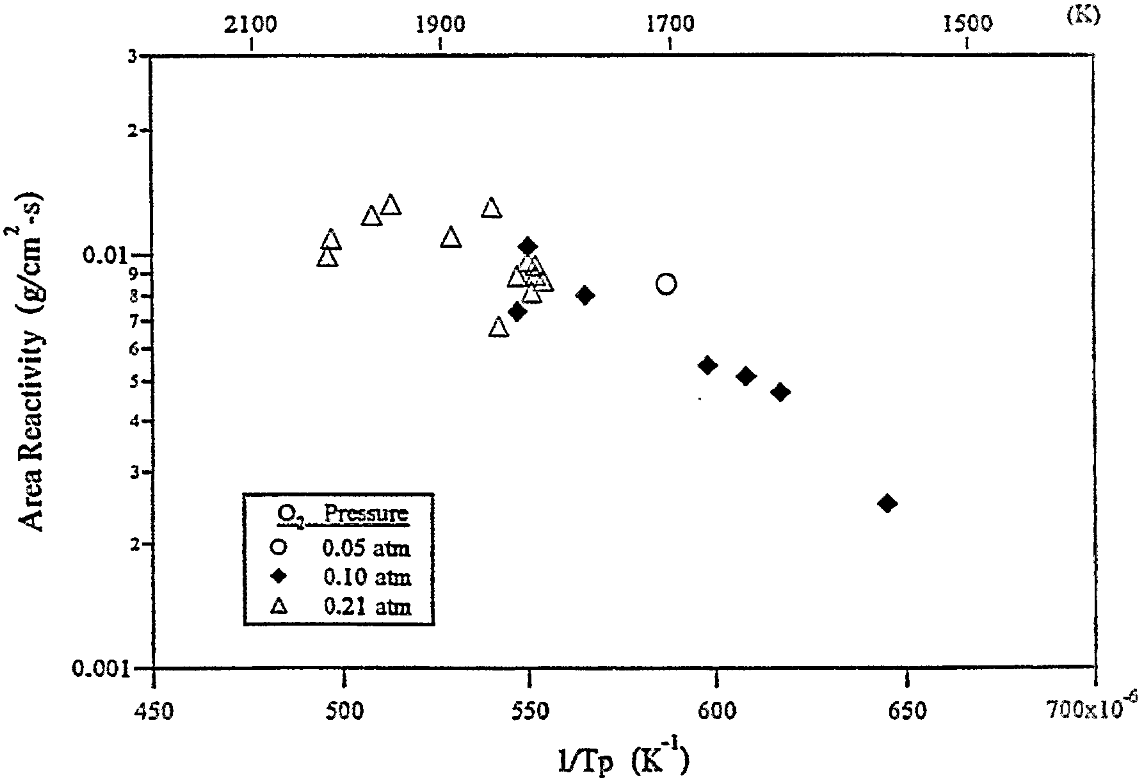

Figure II.B-12. Experimentally derived area reactivity for the 70 μm UT char (at 1 atm) as a function of bulk gas O_2 pressure.

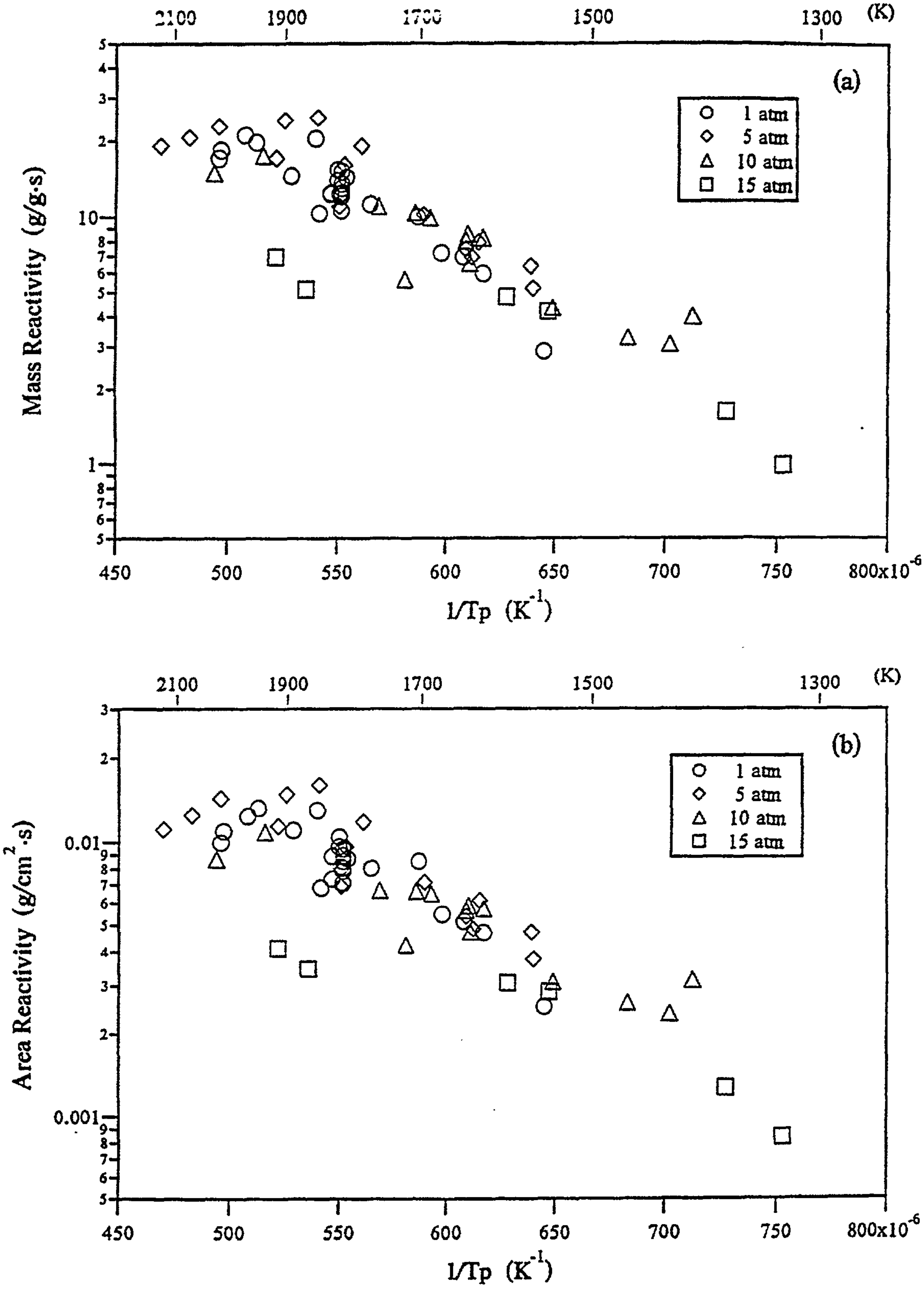

Figure II.B-13. Experimentally derived a) mass and b) area reactivities as functions of particle temperature for the 70 μm UT char.

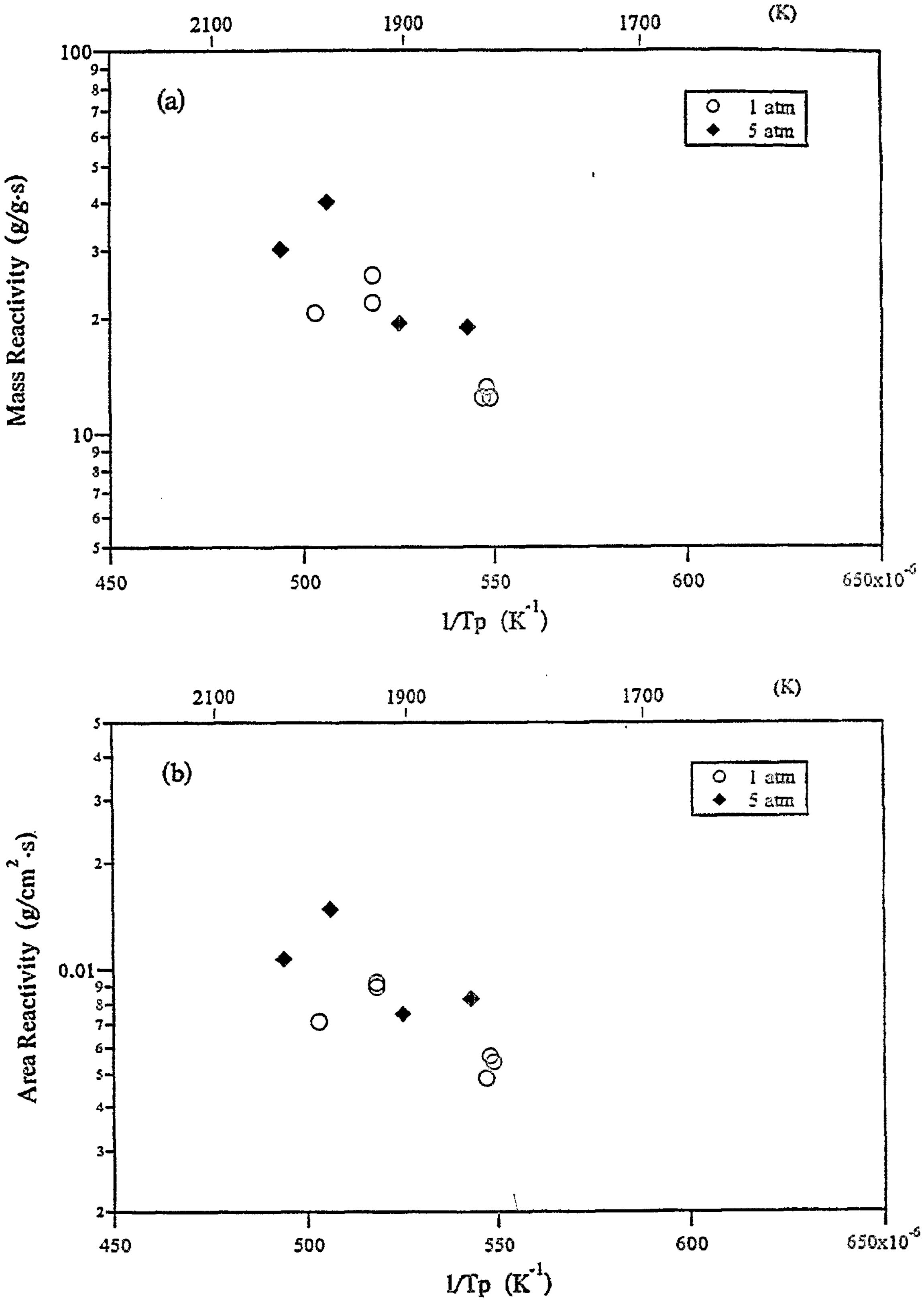

Figure II.B-14. Experimentally derived a) mass and b) area reactivities as functions of particle temperature for the 40 μm UT char.

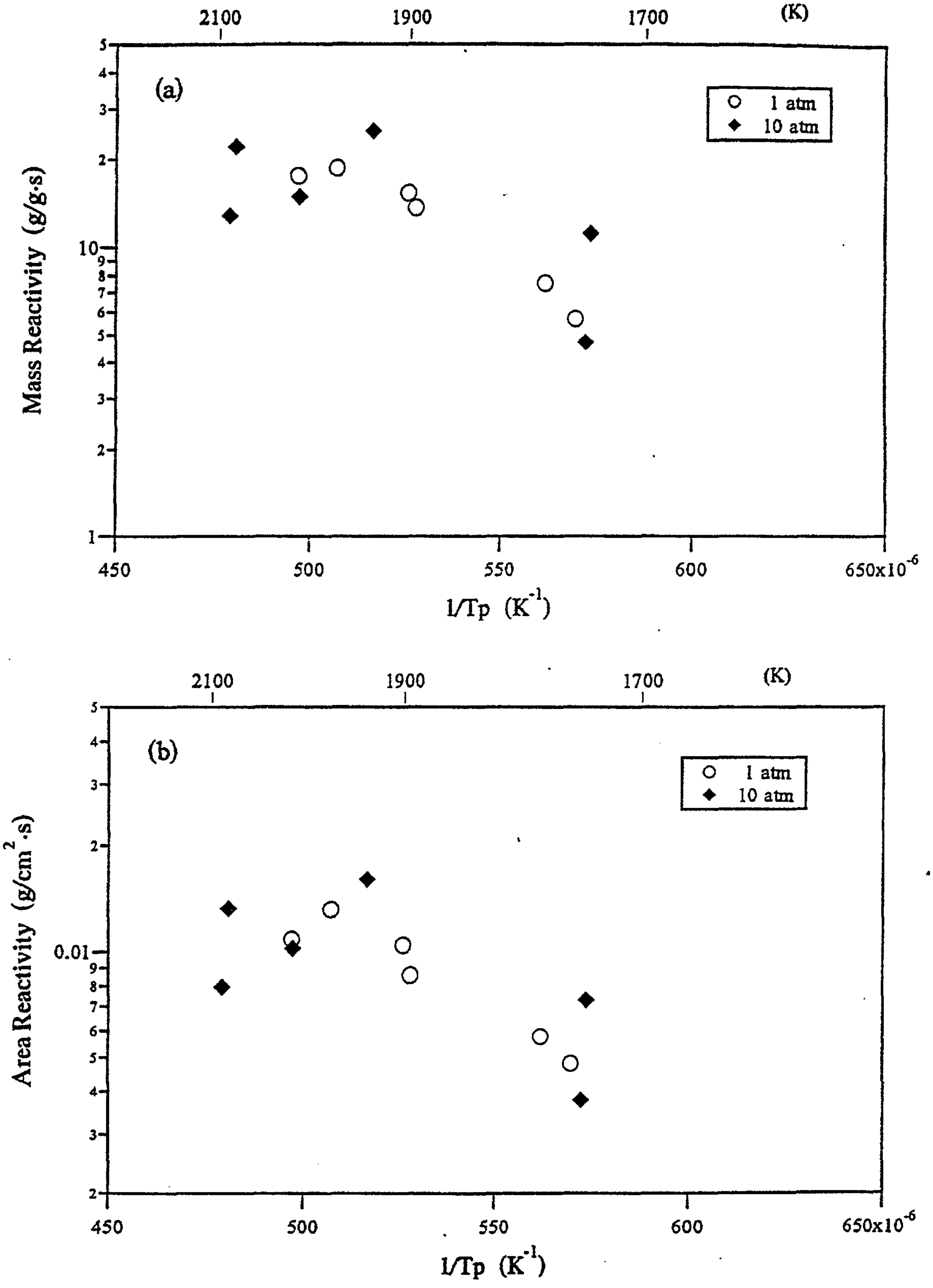

Figure II.B-15. Experimentally derived a) mass and b) area reactivities as functions of particle temperature for the 70 μm Pitt. char.

chars differing in chemical and structural properties as a result of coal variability and differing devolatilization conditions. Even if the starting chars were identical, differences between the data sets would be expected because of the dependence of the area reactivity on the diffusion rate and, hence, the particle size, gas O_2 concentration and flow characteristics. It was reported that the 116 μm char burned near the diffusion limit (Mitchell et al., 1992) and that the 59 μm char reacted in the pore diffusion regime(Leslie et al., 1989). While these two data sets were obtained at similar O_2 pressures, the smaller particle size and the turbulent flow of the Stanford experiments would move the combustion process away from the diffusion limit as compared to the Sandia study. The structural changes in the chars of this study indicate that combustion was occurring between the pore diffusion and kinetic regimes. This is plausible considering the small particle sizes and the higher O_2 pressures (0.21 atm) at the higher temperatures. The lower area reactivity of the 40 μm UT char as compared to the 70 μm UT char lends support to this burning regime. All of these results are consistent with the graphical position of the data sets in the Fig. II.B-11.

Figure II.B-12 shows the dependence of the area reactivity and particle temperature on the bulk gas O_2 pressure for the 70 μm UT char tests at 1 atm. As expected, higher O_2 pressures led to higher reaction rates. And thus, he various particle temperatures seen at the 10 and 21% O_2 concentrations resulted from varying the reactor temperature (gas and wall) from 1145 to 1460 K. Ignition was obtained in the 5% O_2 concentration environment at only the highest reactor temperature (this test turned out to be controlled by diffusion). Little temperature overlap is seen for the different oxygen concentration tests; the hottest reactor condition with 10% O_2 in the bulk gas produced particle temperatures equivalent to the lowest temperature reactor conditions with 21% O_2 in the bulk gas.

The mass and area reactivities for each of the three sets of chars are plotted in Figs. II.B-13 to II.B-15. Little difference is seen in the trends of the two reactivity types because of the use of common particle sizes for each fuel. Activation energies are slightly lower for the area reactivities because of the general trend of increasing burnoff with increasing temperature in the experiments. This results because a burning particle's mass decreases faster than its external surface area. Since an inverse relationship exists between these properties and the reactivities, the area reactivity decreases faster than the mass reactivity with burnoff.

Surprisingly, little total pressure effect is seen in the reactivities of any of the fuels. For the most part, the reactivities are grouped along the 1 atm line within the experimental error (about a factor of 1.5). The high temperature 15 atm points in Fig. II.B-13 are an exception to this, and low by about a factor of 3. This could be a pressure effect but is more likely a result of nonsteady particle temperatures at this extreme test condition. The combination of high pressure and high temperature resulted in a short reaction length for these tests. The assumption of a steadily burning particle would be invalid if the particle temperature peaked about halfway through the reaction zone (near the temperature measurement location) and then sharply fell during the remainder of the zone. The result would be a measured reactivity lower than expected for the measured temperature.

Pressure Effects on the Measured Particle Temperature - Measured particle temperature as a function of O_2 pressure and total pressure for the 70 μm UT char experiments is shown in Fig. II.B-16. Experiments performed at a fixed reactor temperature and pressure but with varying oxygen concentration (5, 10 and 21%) are joined by solid lines. Data from two reactor temperature settings are shown for all but the 15 atm pressure sets. Although the data points for the total pressures do not cover the same O_2 pressure range, strikingly large dependencies of the particle temperature on the total pressure and on oxygen partial pressure is apparent. At the same O_2 pressure and gas temperature, the particle temperature is typically several hundred degrees lower at the next higher total pressure level. The effect of the total pressure on the particle temperature was much larger than that due to changes in reactor temperature. Conversely, increasing oxygen partial pressure causes sharp increases in particle temperature at a fixed total pressure.

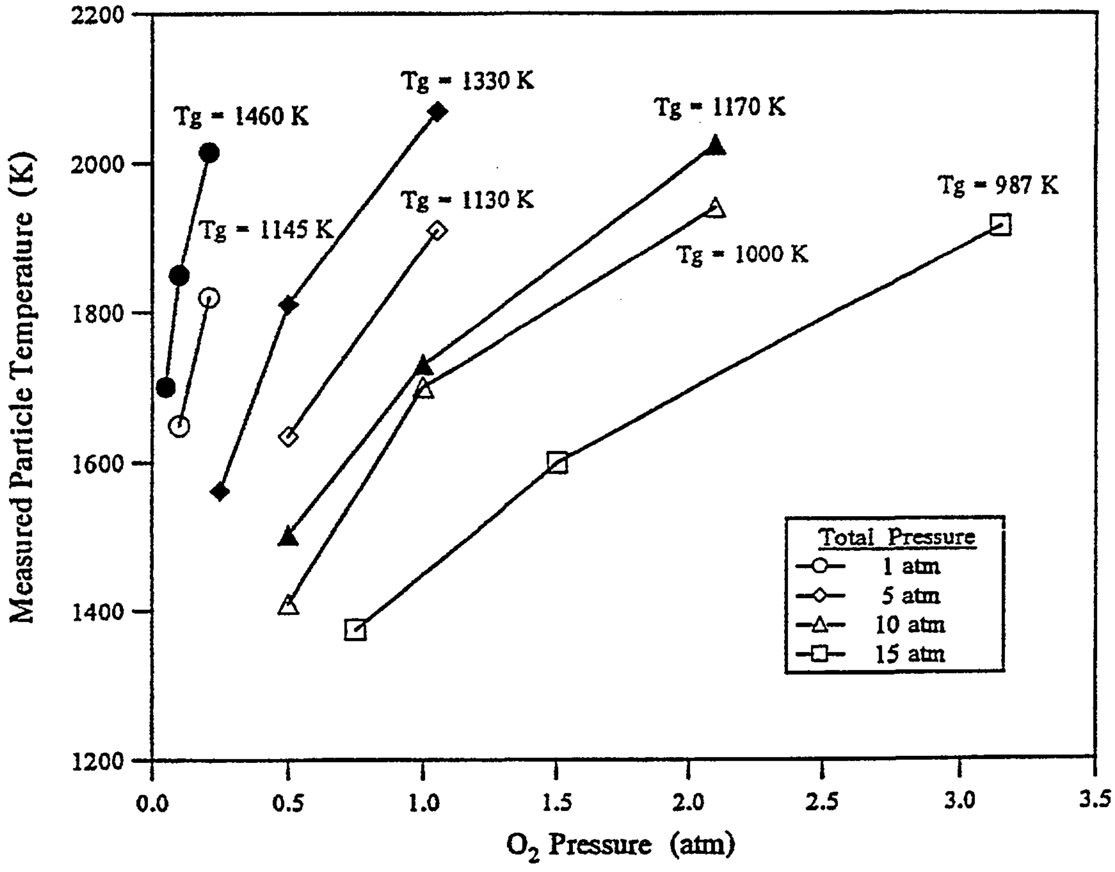

Figure II.B-16. The effects of O_2 pressure and total pressure on the measured particle temperature of the 70 μm UT char.

Global Char Oxidation Model

In high temperature char combustion processes, pore diffusion and internal reaction typically influence the overall reaction rate. Because the details of the complex particle pore structure and the accessibility of oxygen to these internal surfaces are usually not known, it has been common practice to relate the char reaction rate to the external surface area (Smith, 1982). In this model, diffusion across the boundary layer is treated but diffusion and burning within the particle pores is neglected. This global char oxidation model was used to correlate the results of this study. The wide range of conditions over which the oxidation experiments were performed provided a means of testing the validity of the n^{th} order rate equation.

Using the single film burning model and assuming a quasi-steady reaction, the global model equates the rate of carbon diffusion to the rate of carbon consumption. Using an n^{th} order power law, the following expression for the overall rate of carbon consumption per unit external surface area, q_a, is obtained:

$$q_a = k_c P_{os}{}^{n} \qquad \text{II.B-9}$$

he apparent chemical reaction rate coefficient, k_c, follows the Arrhenius form:

$$k_c = A\, e^{\frac{-E}{RT_p}} \qquad \text{II.B-10}$$

Experimental studies have indicated that, besides CO, some CO_2 is also a primary product of heterogeneous char oxidation (Mitchell, 1988, Waters *et al.*, 1988, Young and Niksa, 1988, Mitchell *et al.*, 1990b). This is significant because of the large heat of reaction (over 3 times greater than the CO reaction) and the stoichiometry of the CO_2 reaction (only half as much carbon consumed per oxygen molecule as compared to the CO reaction). The fraction of carbon converted to CO_2 is represented by ψ.

$$C + \frac{1}{2}(1+\psi)O_2 \rightarrow (1-\psi)CO + \psi CO_2 \qquad \text{II.B-11}$$

The rate of carbon diffusion on a particle-surface-area basis can be described by the following relation (Frank-Kamenetskii, 1969 and Mitchell, 1988). It allows for the formation of both CO and CO_2 and also accounts for the Stephan flow (the convective flow resulting from a change in the number of moles during the reaction).

$$q_a = \left(\frac{2}{1+\psi}\right)\frac{P}{R' T_p}\frac{2\, M_c D_{ox}}{d_p\ \gamma}\ln\left(\frac{1-\gamma\frac{P_{os}}{P}}{1-\gamma\frac{P_{og}}{P}}\right) \qquad \text{II.B-12}$$

where γ is defined as

$$\gamma = \frac{\psi-1}{\psi+1} \qquad \text{II.B-13}$$

The rate of carbon consumption (Eqn. II.B-9) and the rate of carbon diffusion (Eqn. II.B-12) are combined to eliminate the unknown P_{os}, yielding an implicit equation for q_a in terms of the apparent kinetic coefficients (A, E and n), the gas and particle properties, and ψ.

The particle temperature is described by the energy equation. In this study the particle temperature is assumed to remain fairly constant during the oxidation process. Thus, the inertial component can be neglected and the energy equation can be written as

$$0=-\frac{Nu\lambda\left(T_p-T_g\right)}{d_p}\left(\frac{B_f}{e^{B_f}-1}\right)+\varepsilon\sigma\left(T_p^4-T_w^4\right)-q_a\Delta H \qquad \text{II.B-14}$$

The Stephan flow is accounted for by the blowing factor, B.

$$B_f=\frac{C_{pg}\,q_a}{M_c\,h}\left(\frac{\psi-1}{2}\right) \qquad \text{II.B-15}$$

The heat of reaction is dependent on the fraction of CO_2 generated.

$$\Delta H=-26.4(1-\psi)-94.1\psi \qquad \text{II.B-16}$$

The model requires a number of temperature- and pressure-dependent gas properties: ρ, Cpg, μ, λ, and D_{ox}. These values were determined at the film temperature assuming ideal gas behavior, using curve fits from the JANAF Thermochemical Tables, and relying on molecular theory. The pressure dependence of C_{pg} and μ is very slight over the range of test conditions and, therefore, neglected. The strong dependence of D_{ox} on both temperature and pressure greatly affects the balance between the diffusion and kinetic rates. The thermal conductivity shows an almost proportional dependence on temperature and an almost negligible dependence on pressure.

The complex interaction between the three main equations in the model (Eqns. II.B-9, II.B-12, and II.B-14) and the variable gas properties make it difficult to accurately identify trends without a numerical simulation. The computer model was used to perform a number of simulations with the aim of examining the effect of O_2 and total pressure changes on char oxidation behavior. In these simulations it was assumed that the model and its kinetic parameters were valid over a wide range of combustion conditions.

Figure II.B-17a shows the predicted effect of increasing O_2 pressure at a constant total pressure of 1 atm. The parameters held constant are listed on the plot. Values of χ (ratio of observed rate to diffusion-limited rate) range from 0.35 to 0.6, indicating that neither the diffusion nor the chemical reaction rate control the combustion process in this case. χ experiences a minimum at a pressure just below 0.2, where the maximum amount of kinetic control occurs. At lower and higher oxygen concentrations the diffusion process increases its control on the overall reaction and χ increases moderately, tending to flatten out at higher O_2 pressures. The moderate rate of increase in χ with increasing O_2 pressure is not as large as expected. Other simulations showed that the average value of χ and the position of the minimum in χ vary considerably with changes in the combustion conditions and kinetic parameters. Also shown on the plot are the particle reaction rate and the diffusion-limited reaction rate. Both rates start at 0 with no oxygen in the gas and then increase substantially with increasing oxygen concentrations.

Figure II.B-17b shows the effect of the total gas pressure on the reaction rate. The solid lines represent constant mole fractions (Y_{O2}) and the dashed lines represent constant O_2 pressures (P_{O2}). As the total pressure is increased above 1 atm at a constant gas mole fraction, the reaction rate first increases fairly rapidly and then flattens off at higher pressures. The initial rise is more pronounced for higher oxygen gas compositions. In general, an increase in the O_2 mole fraction produces a substantially larger increase in rate than an increase in the total pressure. The constant O_2 pressure lines show the same unexpected trend as the temperature measurements of Fig. II.B-16: a decrease in the reaction rate with increasing total pressure. The pressure effect on the rate is quite marked at higher O_2 pressures.

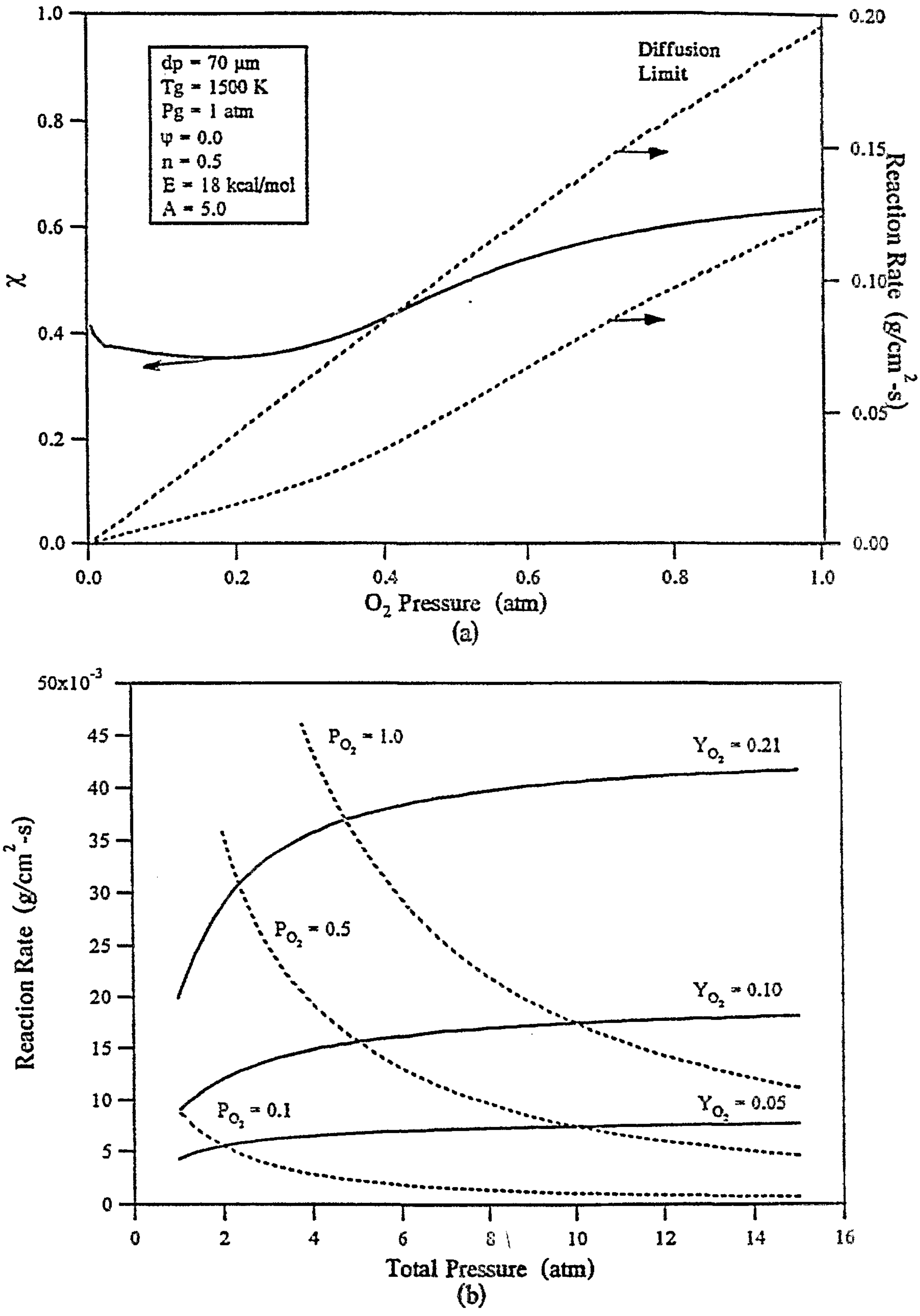

Figure II.B-17. Simulation results from the staeady state char oxidation model a) particle reactionr ate and χ at 1 atm total pressure b) particle reaction rate as a function of total pressure and gas composition.

These pressure effects on the reaction rate can be explained in the following manner. The decrease in diffusivity accompanying an increase in the total pressure slows the rate of O_2 diffusion to the particle, resulting in a lower O_2 pressure at the particle surface in the case of constant O_2 partial pressure. This decrease in the particle surface concentration slows the chemical reaction rate which, in turn, lowers the particle temperature and results in a further decrease in the oxygen diffusivity. The process of reducing reaction rate continues until a balance is obtained between the diffusion and kinetic rates and between the energy generated by the reacting particle and the energy lost by the particle through heat transfer. The final result is a decreasing particle reaction rate and temperature as the total pressure is increased. For the case of constant O_2 mole fraction, where the bulk O_2 pressure increases in proportion to the total pressure, the decrease in diffusivity leads to a very moderate increase in reaction rate and temperature. Most of changes due to pressure have occurred by 10 atm and further pressure increases produce little additional effect.

Elevated Pressure Data Analysis

Combustion Regime - Establishing the burning regime of the char experiments was an important step in analyzing the data. Had combustion occurred in the bulk diffusion controlled regime (Zone III) kinetic parameters could not have been determined. The ratio of the measured rate to the maximum rate, χ, was determined to help quantify the controlling processes. The maximum burning rate was calculated assuming complete conversion of carbon to CO at the diffusion limit, while allowing for the particle temperature increase due to the faster reaction. Hence, the diffusion and energy equations (Eqns. II.B-12 and II.B-14) were simultaneously solved for the given experimental conditions to determine the maximum rate. The value of χ determined from each test is listed in Tables II.B-3 to II.B-5. χ was typically in the range of 0.15-0.50 for the 70 µm char and somewhat lower for the 40 µm char. The decrease in χ with particle size was expected because the boundary layer depth also decreases with size, resulting in a faster diffusion rate. In only one test, U6.2, did the reaction occur near the diffusion limit. The effect of pressure on χ was masked by its dependence on the gas film temperature and O_2 pressure. χ seems to have slightly increased with pressure from 1 to 5 atm but further increases in pressure were accompanied by decreases in the film temperature and increases in O_2 pressure.

The χ values calculated for the tests, typically less than 0.5, indicate that the kinetic rates were exerting significant control over the combustion process. This result is consistent with the other experimental data. The slight decrease in the area reactivity of the smaller sized UT chars (Fig. II.B-11) indicates a burning regime between the kinetic (Zone I) and pore diffusion (Zone II) controlled zones (q_a is proportional to dp in zone I and independent of dp in Zone II). The particle density, SEM photographs, and calculated α's and activation energies also support this conclusion.

Interestingly, no significant total pressure effect on the burning regime was found. This result conflicts with the commonly held belief that higher pressures lead to complete diffusion control (zone III). Since the maximum (diffusion controlled) reaction rate is independent of pressure for a given gas composition (the diffusivity is inversely proportional and the O_2 pressure is directly proportional to the total pressure), the explanation must lie in the reaction rate behavior. Because the increase in overall rate with total pressure is much lower than expected, as a result of the pressure and temperature dependent diffusivity, the increase in χ with pressure is also much lower than expected. This leads to the conclusion that kinetic rates can exert significant control on the overall reaction rate at elevated pressures and that kinetic parameters can reasonably be extracted from the experimental data.

Reaction Products - CO/CO_2 - Although CO has commonly been accepted as the primary product of heterogeneous char oxidation, some researchers have found evidence for the formation of CO_2 as well. It was postulated by Arthur (1951) that the ratio of the CO to CO_2 formed was a function of the particle temperature and that it could be described by the Arrhenius law in the following manner.

$$\frac{\psi-1}{\psi} = A_c\, e^{\frac{-E_c}{RT_p}} \qquad \text{II.B-17}$$

In drop tube experiments, independent measurement of both the particle temperature and the rate of reaction is required to allow calculation of the fraction of CO_2 produced. With increases in CO_2 production the particle temperature is increased and the reaction rate is decreased. Thus, an energy balance will be consistent only for the proper ψ. With known particle temperature, reaction rate, and reactor conditions, ψ is calculated by solving the energy equation, Eqn II.B-14. Only researchers at Sandia National Laboratories have reported high temperature oxidation experiments where sufficient information was collected to allow these determinations (Mitchell, 1988, Waters *et al.*, 1988, Mitchell *et al.*, 1990, Hurt and Mitchell, 1992a).

Results from the determination of ψ for the 70 μm UT char data are shown in Fig. II.B-18 as a function of particle temperature. The results are somewhat scattered because of the sensitivity of the calculation to errors; any errors introduced by experimental measurements or shortcomings in the global model are included in the calculated ψ. In spite of the scattering, there is clearly a transition from CO_2 to CO production as the particle temperature increases from approximately 1500 to 1900 K. At temperatures below about 1700 K, oxidation rates are much too slow to produce the measured particle temperatures if CO is the only product considered. The solid line in the figure represents the best fit Arrhenius model to the data; agreement is seen to be quite good considering the uncertainties associated with the ψ determination. Agreement is also good with the parameters determined by Hurt and Mitchell (1992) for a UT char, $A_c = 3{\cdot}10^3$ and $E_c = 60$ kcal/mol. Surprisingly, ψ seems to be independent of the total gas pressure over the range covered in the experiments.

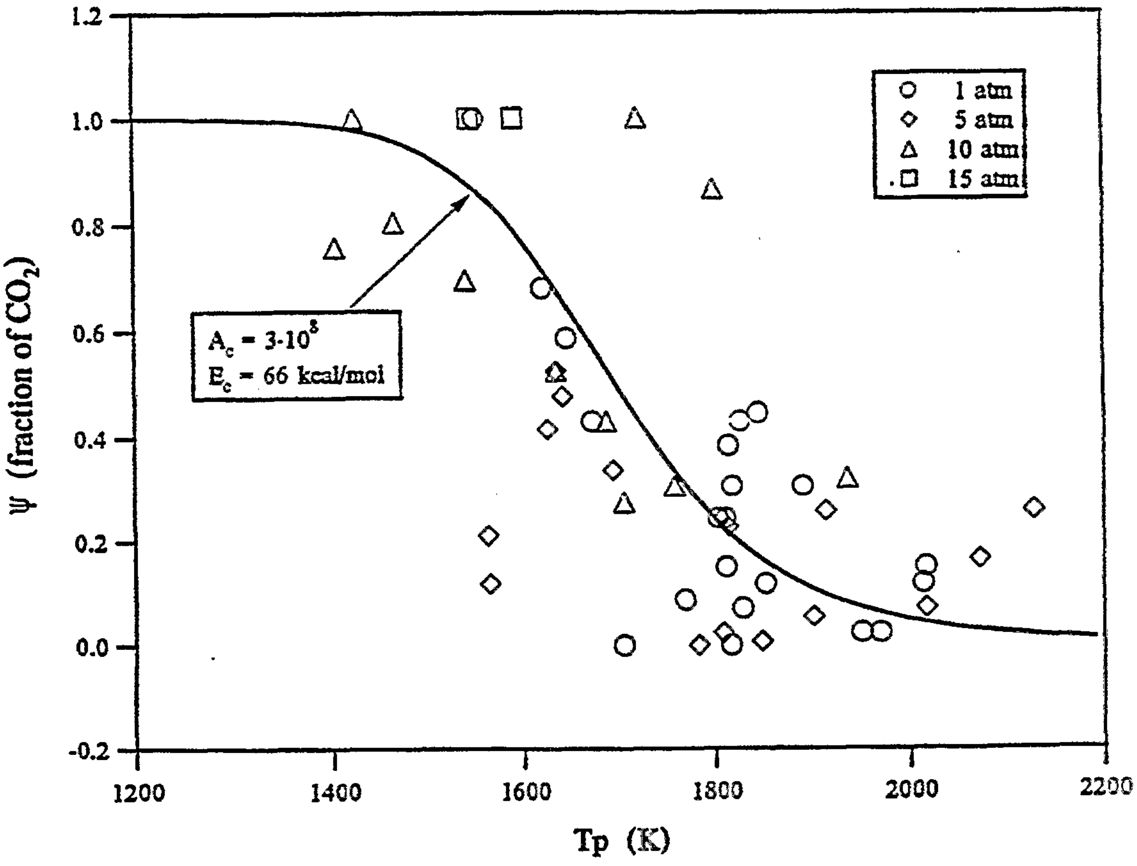

Figure II.B-18. Temperature dependence of φ for the 70 μm UT char.

It should be noted that while these results indicate that CO_2 may be formed heterogeneously, the global model is not sufficiently fundamental to prove this. Other explanations may also be plausible. For example, the same trend would be observed if only a portion of the particles ignited and temperature measurements were made on only burning particles. The collected char residue could contain a significant fraction of unreacted or partially reacted particles, resulting in a measured reaction rate lower than one corresponding to the measured temperatures.

Apparent Chemical Kinetics - The reaction rate coefficient, k_c, was determined from Eqn. II.B-9, using Eqns. II.B-10 and II.B-12 to determine P_{os}. Consistent with the previous work of other researchers (Young and Smith, 1981, Mitchell and McLean, 1982, and Hurt and Mitchell, 1992a) an apparent reaction order of 0.5 was used. Arrhenius plots of k_c are shown in Figs. II.B-19 and II.B-20. The activation energy and frequency factor at each total pressure were determined by a least squares regression of k_c vs. $1/T_p$, ignoring outlying points; these parameters are listed in Table II.B-6.

Interestingly, a significant pressure effect is seen on both the activation energy and frequency factor in each case. Both of these parameters are decreased at higher pressures. While the frequency factor decreases somewhat proportional to the pressure, the activation energy is significantly reduced at 5 atm and does not change with further pressure increases. This same pressure behavior is observed for each of the fuels.

The effect of fuel type on k_c is shown in Fig. II.B-20. The rate coefficients for all of the chars exhibit very similar temperature behavior and at any given pressure and temperature the rate coefficients for the chars agree within the experimental error. With this in mind, the larger 'best fit' Arrhenius parameters determined for the 40 µm UT char are most likely too high. A fairly large uncertainty was associated with the parameter determination for this fuel because of the small temperature range covered by the limited number of test conditions. The close agreement of the global rate coefficients for the three chars was expected because of their almost identical physical structures.

The large changes in Arrhenius parameters with pressure variations indicate an inadequacy in the model. Another observation further increases concern over the model adequacy. While little difference is seen in the overall reaction rates measured for a range of pressures (Figs. II.B-13 - II.B-15), after using the model to account for bulk diffusion effects, the reaction rate coefficients show a very pronounced pressure effect (Fig. II.B-19).

This could be a result of pressure related pore diffusion effects not accounted for in the global model if the pore area available to oxygen decreased with increasing pressure as Lester et al. (1981) conjectured. However, this would lead to an accompanying change in particle structure (a trend towards constant density burning with increasing pressure) and none of the structure measurements showed any significant effect of pressure. Also,unless the pore diffusion was also a complex function of temperature, a change in only the frequency factor, not the activation energy, would occur.

A more likely possibility is the inadequacy of the n^{th} order equation to predict changes with pressure. While it is commonly used and has proven adequate for predictive use at atmospheric pressure, the equation has no theoretical basis and has been shown to be invalid for atmospheric pressure char oxidation (Essenhigh, 1988 and 1991). Extrapolation of this empirical equation to elevated pressure would be valid only if it were consistent with experimental results. With the very limited research conducted at elevated pressures to date, the validity of the equation at these conditions has not been examined before. While the general trends of the model are consistent with the high pressure data obtained in this study, the variation in the kinetic coefficients with pressure indicate the inadequacy of the n^{th} order equation to model pressure changes. Use of a more fundamental rate equation, such as the Langmuir equation, may better describe the total pressure effects.

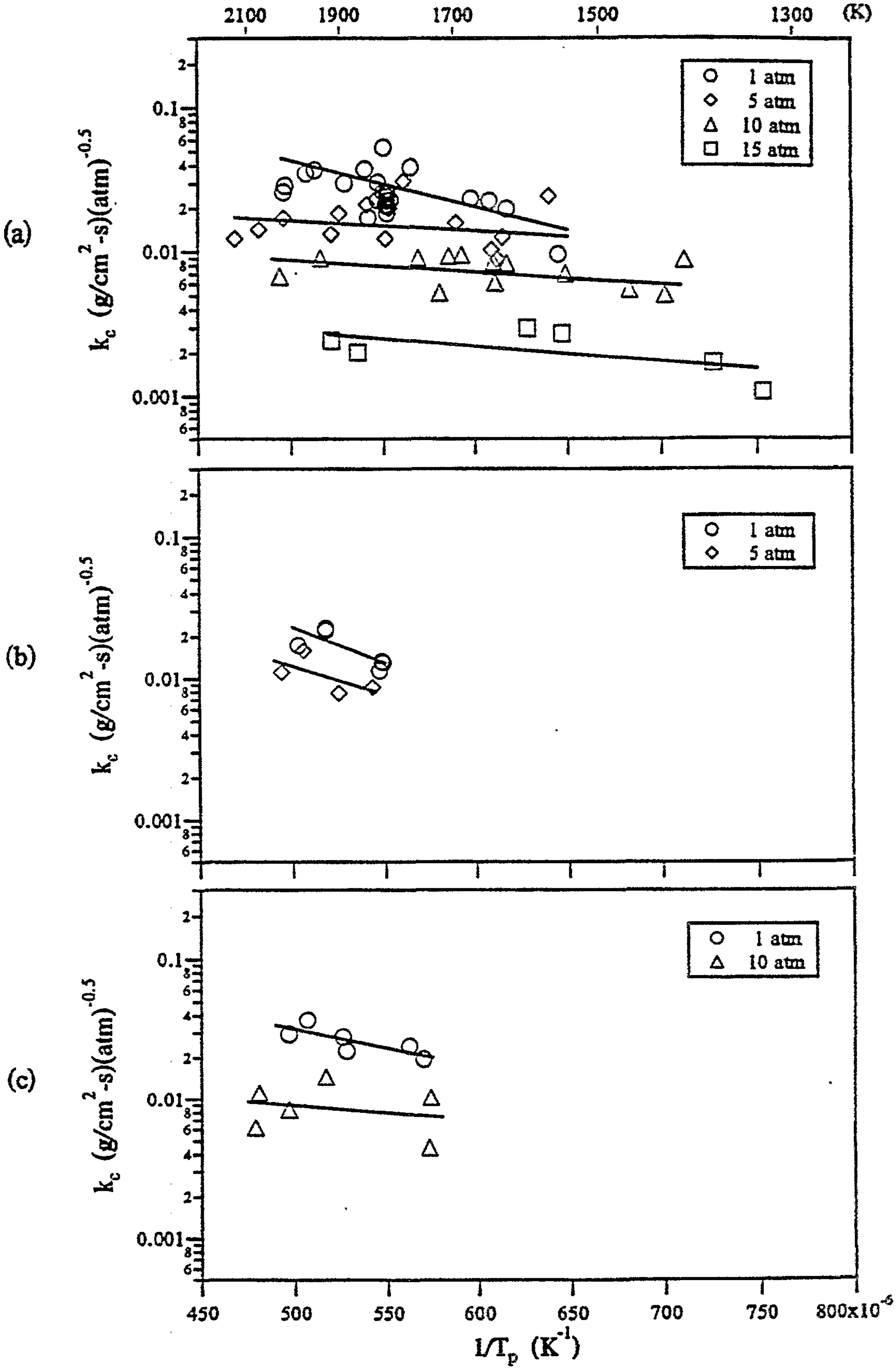

Figure II.B-19. Reaction rate coefficient as a function of particle temperature and total pressure for the a) 70 μm UT, b) 40 μm UT and c) 70 μm Pitt. Chars.

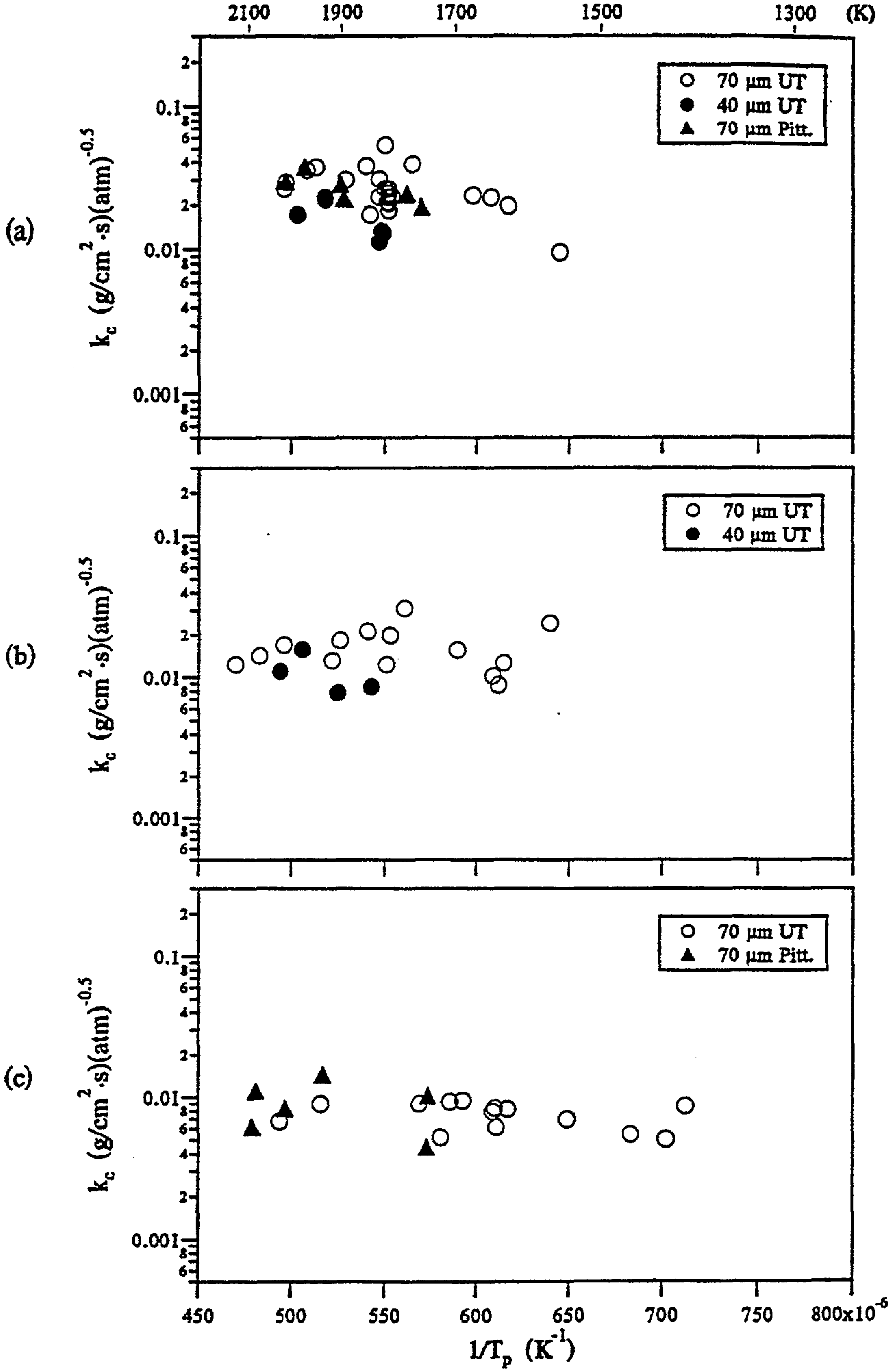

Figure II.B-20. Reaction rate coefficient as a function of particle temperature and char for a) 1 atm, b) 5 atm and c) 10 atm total pressures.

TABLE II.B-6

GLOBAL KINETIC PARAMETERS FOR AN APPARENT ORDER OF 1/2

Char	Pressure (atm)	A $(g/cm^{2}\cdot s)(atm)^{-0.5}$	E (kcal/mol)
70 µm UT	1	1.780	14.8
	5	0.0382	3.4
	10	0.0227	3.8
	15	0.00981	4.9
40 µm UT	1	8.38	23.4
	5	1.38	18.8
70 µm Pitt.	1	0.700	12.3
	10	0.029	4.7

Because the choice of apparent order exerts a great influence on the determined Arrhenius parameters, the use of 0.5 for the order in this study must be rationalized. While an assumed order of 0 leads to no total pressure dependence of the Arrhenius parameters (the reaction rate coefficients are equivalent to the area reactivities), the 0th order assumption is obviously erroneous as demonstrated by the unmistakable increase in experimentally observed reaction rates with increases in O_2 pressure. On the other hand, an assumed order of 1 leads to small and even negative activation energies. Model simulations have shown the predicted results to be fairly insensitive to the chosen order; assumed apparent orders from .5 to 1 lead to Arrhenius parameters that seem to fit the data equally well. Further, Essenhigh (1988) showed a smooth change in apparent order from 0 to 1 as char oxidation temperatures increased from 1000 to 2000 K. Thus the chosen order of 0.5 is a good average value and, as mentioned above, it has been used in recent atmospheric pressure char oxidation studies.

Model Predictions of the Elevated Pressure Data

The kinetic parameters derived from the data were used with the global model as a check on their predictive capabilities. Model simulations were performed for the conditions of the 70 µm UT char oxidation experiments. Fig. II.B-21 shows the model predictions.

The comparisons show that the model can be used to predict the data as long as adjustments are made in the kinetic parameters for differing total pressure (Table II.B-6). Assuming the chemistry of the carbon/oxygen reaction remains unchanged with pressure, the need to make adjustments in the kinetic parameters with pressure indicates some inadequacy in the model. Another observation increases concern over the model adequacy. While little difference is seen in the overall reaction rates measured for a range of pressures (Figs. II.B-13 - II.B-15), after using the model to account for bulk diffusion effects, the reaction rate coefficients show a very pronounced pressure effect (Fig. II.B-19).

This could be a result of pressure-related pore diffusion effects not accounted for in the global model such as the pore area available to oxygen decreasing with increasing pressure as Lester et al. (1981) conjectured. However, this would lead to an accompanying change in particle structure (a trend towards constant density burning with increasing pressure) and none of the structure measurements

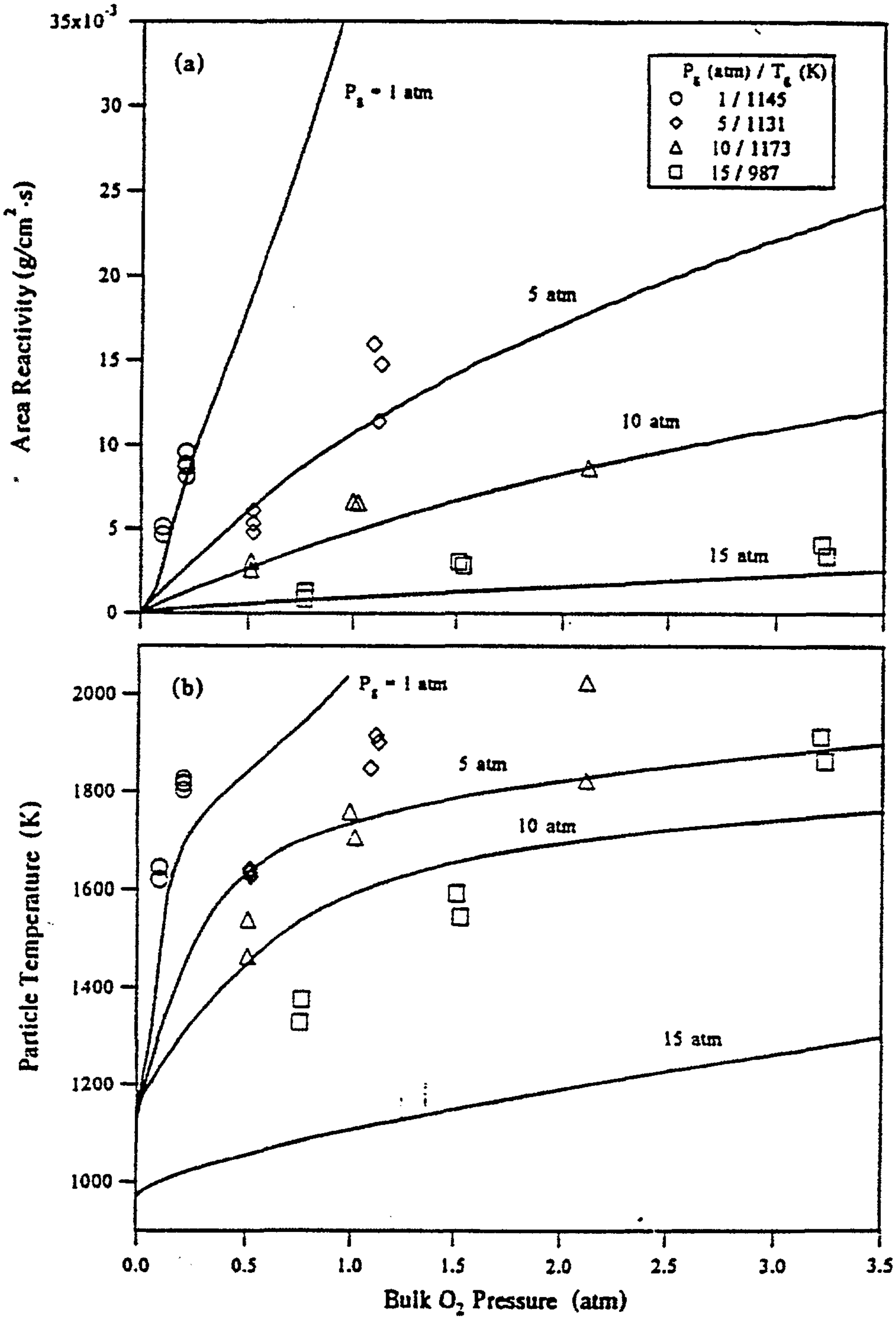

Figure II.B-21. Comparison of experimental data and model calculations for the 70 µm UT char. a) area reactivity and b) particle temperature. This is a check on consistency, not an independent prediction, since the model parameters were determined from these same data.

showed any significant effect of pressure. Also, unless the pore diffusion was also a complex function of temperature, a change in only the frequency factor, not the activation energy, would occur.

A more likely possibility is the inadequacy of the n^{th} order equation to predict changes with pressure. While it is commonly used and has proven adequate for predictive use at atmospheric pressure, the equation has no theoretical basis (Essenhigh, 1991). Extrapolation of this empirical equation to elevated pressure would be valid only if it were consistent with experimental results. With the very limited research conducted at elevated pressures to date, the validity of the equation at these conditions has not before been examined. While the general trends of the model are consistent with the high pressure data obtained in this study, the required variation of the kinetic coefficients with pressure to completely describe the data indicate the inadequacy of the n^{th} order equation to predict changes due to pressure effects. Use of a more fundamental rate equation, such as Langmuir- type kinetics, may better describe these total pressure effects.

Summary and Conclusions

The object of this study was to examine char oxidation at elevated pressure. To this end a high pressure facility was designed and constructed and char oxidation experiments were conducted at both atmospheric and elevated pressures.

The facility consists of a high pressure drop tube reactor, an optical pyrometer and support equipment. The electrically heated, computer controlled reactor has the following capabilities: pressure from 1 to 30 atm, temperature from 1000 to 1700 K, controllable temperature profile along the reaction tube length, particle residence times from 30 to 1000 ms, variable gas compositions of inert and oxidizing gases, and optical access ports for *in-situ* diagnostics. A particle imaging system providing *in-situ*, simultaneous measurement of individual particle temperature, size and velocity was developed for use in conjunction with the reactor. The pyrometer was shown to be both precise and accurate for the intended operating conditions (particles ranging from 30 to 150 µm at temperatures above 1500 K and velocities under 5 m/s). High quality temperature and velocity measurements were obtained over the entire design range, while high quality size measurements were obtained for all but the smallest particles and lowest temperatures. The size measurements were also limited to pressures below 10 atm.

Approximately 100 oxidation experiments were performed with two sizes of UT and Pitt. bituminous coal chars at 1, 5, 10, and 15 atm total pressure. Reactor temperatures were varied between 1000 and 1500 K and bulk gas compositions ranged from 5 to 21%, resulting in average particle temperatures ranged from 1400 to 2100 K with burnouts from 15 to 96%. Individual particle temperature, size and velocity were determined for approximately 75 particles at each test condition and overall reaction rates were independently determined from mass loss measurements. This allowed an internal check of the data consistency and insight into the products of combustion. Significant particle-to-particle variations were observed at each test condition. The results from the 1 atm UT char oxidation results were shown to be consistent with results obtained by other researchers using the same coal. The chars were found to be burning in mainly a reducing density mode in a regime intermediate between the kinetic and pore diffusion zones, irrespective of total pressure. While the global model was used to correlate the results of the study, the extrapolation of the n^{th} order rate equation to pressures higher than atmospheric was found to be invalid.

The effect of increasing total pressure on char oxidation at a constant gas composition can be summarized as follows. Raising total pressure also necessarily increases the bulk gas O_2 pressure, leading to an increase in the reaction rate. However, this increase is tempered by the decrease in oxygen diffusivity that also accompanies increases in pressure. The overall result is a slight increase in rate with increasing total pressure. Most of this change has occurred by 10 atm and further increases in total pressure produce little effect on the rate.

The major findings of the study are as follows:

1. In spite of careful size classification and char preparation, the resulting particle population exhibited substantial variation in combustion behavior.
2. Increasing total pressure in an environment of constant gas composition leads to modest increases in the reaction rate and particle temperature.
3. Significant kinetic control of the char oxidation process is exhibited at elevated pressures.
4. The global model kinetic parameters were found to be strongly dependent on the total pressure. This indicates that the empirical n^{th} order equation is not completely valid over the range of pressures covered in the experiments.
5. CO_2 formation must be accounted for at particle temperatures below about 1700 K. This is true regardless of the pressure.
6. Independent particle temperature and mass loss measurements are both experimental necessities to fully describe combustion behavior.

With little high pressure char oxidation data available in the literature, this study has begun to fill a much neglected area of coal combustion and gasification. Insight into the fundamentals of char oxidation at both atmospheric and elevated pressure has been gained. Practically, the results are directly applicable to pressurized coal combustion. Accurate high pressure oxidation predictions could be made using the nth order global model as long as the Arrhenius parameters were adjusted not only for coal types but for pressure as well. However, a number of issues still remain unresolved: Do Langmuir or other types of kinetics better explain the total pressure behavior?, Do other coal chars exhibit similar pressure effects?, How do pore diffusion characteristics change with pressure?, Do chars of different sizes behave similarly at elevated pressures?, can these trends be extrapolated to higher pressures?, What effects do different gas environments have at pressure? Further work is also necessary to quantify the effects of pressure on devolatilization as well as simultaneous devolatilization/oxidation before a complete understanding of the coal combustion process can be obtained.

NOMENCLATURE

A	apparent frequency factor	$(g_C/cm^2 \cdot s)(1/atm)^n$
A_c	CO/CO_2 apparent frequency factor	
A_p	particle external surface area	(cm^2)
A_{pm}	mean particle external surface area	(cm^2)
B	carbon burnoff	(%)
B_f	blowing factor	
C_{pg}	gas specific heat	$(cal/mole \cdot K)$
D_{ox}	oxygen diffusivity	(cm^2/sec)
d_p	particle diameter	(cm)
E	apparent activation energy	(cal/mole)
E_c	CO/CO_2 activation energy	(cal/mole)
h	convection heat transfer coefficient	$(cal/cm^2 \cdot s \cdot K)$
ΔH	heat of reaction	(cal/g_C)
k_c	apparent chemical reaction rate coefficient	$(g_C/cm^2 \cdot s)(1/atm)^n$
k_d	film diffusion rate coefficient	$(g_C/cm^2 \cdot s)(1/atm)$
m	mass of carbon	(g)
M_C	carbon molecular weight (12)	$(g/g \cdot mole)$
m_o	initial mass of carbon	(g)
n	apparent reaction order	
Nu	Nusselt number	
P	total gas pressure	(atm)
P_{og}	oxygen partial pressure in the bulk gas	(atm)
P_{os}	oxygen partial pressure at the particle surface	(atm)
q_a	overall rate of carbon consumption per unit external surface area (area reactivity)	$(g_C/cm^2 \cdot s)$
q_m	mass reactivity	$(g/g \cdot s)$
Pr	Prandtl number	
R	gas constant (1.9859)	$(cal/mole \cdot K)$
R'	gas constant (82.32)	$(atm \cdot cm^3/mole \cdot K)$
Re	Reynolds number	
t	time	(s)
T_g	gas temperature	(K)
T_p	particle temperature	(K)
t_r	particle residence time	(s)
T_w	wall temperature	(K)
v_p	particle velocity	(cm/s)
v_∞	particle terminal velocity	(cm/s)
x_a	mass fraction of ash	
α	burning mode parameter	
γ	intermediate factor based on ψ (Eq. 4)	
ε	particle emissivity	
λ	gas thermal conductivity	$(cal/cm \cdot s \cdot K)$
μ	gas viscosity	$(g/cm \cdot sec)$
ρ	gas density	(g/cm^3)
ρ_a	ash apparent density (1.5)	(g/cc)
ρ_{app}	particle apparent density	(g/cc)
ρ_b	bulk density	(g/cc)

ρ_c	carbon density	(g/cc)
ρ_{co}	initial carbon density	(g/cc)
σ	Stefan-Boltzmann constant ($1.345 \cdot 10^{-12}$)	($cal/cm^2 \cdot s \cdot K^4$)
χ	fraction of measured to CO diffusion limited rate	
ψ	fraction of CO_2 production	

References for Section 2.b.

Annamalai K. and Ramalingham S.C., Group Combustion of Char/Carbon Particles, Combustion and Flame, **70**, 307 (1987).

Arthur, J.R., Reaction Between Carbon and Oxygen, Transactions of the Faraday Society, **47**, 164, (1951).

Essenhigh, R.H., An Integration Path for the Carbon-Oxygen Reaction with Internal Reaction, Twenty-Second Symposium on Combustion/The Combustion Institute, 89 (1988).

Essenhigh, R.H., Rate Equations for the Carbon-Oxygen Reaction: An Evaluation of the Langmuir Adsorption Isotherm at Atmospheric Pressure, Energy and Fuels, **5**, 41 (1991).

Field, M. A., Measurement of the Effect of Rank on the Combustion Rates of Pulverized Coal, Combustion and Flame, **14**, 237 (1970).

Frank-Kamenetskii, D.A., *Diffusion and Heat Transfer in Chemical Kinetics*, Plenum Press, New York - London, 1969.

Hurt, R.H and Mitchell, R.E., Unified High-Temperature Char Combustion Kinetics for a Suite of Coals of Various Ranks, Twenty Fourth International Symposium on Combustion, The Combustion Institute, Pittsburgh, PA, (1992a).

Laurendeau, N.M., Heterogeneous Kinetics of Coal Char Gasification and Combustion, Progress in Energy and Combustion Science, **4**, 221 (1978).

Leslie, I.H., Jost, M., Kruger, C.H., Measured and Predicted Char Reactivity of Three U.S. Coals, Combustion and Flame, **78**, 195 (1989).

Lester, T.W., Seeker, W.R. and Merklin, J.F. , The Influence of Oxygen and Total Pressure on the Surface Oxidation Rate of Bituminous Coal, Eighteenth Symposium on Combustion/The Combustion Institute, 1257 (1981).

Mitchell, R.E.and McLean, W.J., On the Temperature and Reaction Rate of Burning Pulverized Fuels, Nineteenth International Symposium on Combustion, The Combustion Institute, Pittsburgh, PA, 1113 (1982).

Mitchell, R.E., On the Products of the Heterogeneous Oxidation Reaction at the Surfaces of Burning Coal Char Particles, Twenty Second International Symposium on Combustion, The Combustion Institute, Pittsburgh, PA, 69 (1988).

Mitchell, R.E., Kee, R.J., Glarborg, P., and Coltrin, M.E. The Effect of CO Conversion in the Boundary Layers Surrounding Pulverized-Coal Char Particles, Twenty Third International Symposium on Combustion, The Combustion Institute, Pittsburgh, PA, (1990b).

Mitchell, R.E., Hurt, R.H., Baxter, L.L., Hardesty, D.R. Compilation of Sandia Coal Char Combustion Data and Kinetic Analyses, Milestone Report, Sand92-8208, Sandia National Laboratories at Livermore, September 1991.

Niksa, S., Mitchell, R.E., Hencken, K.R., and Tichenor, D.A., Optically Determined Temperatures, Sizes and Velocities of Individual Carbon Particles under Typical Combustion Conditions, Combustion and Flame, **60**, 183 (1984).

Pace, R.S., Titanium as a Tracer for Determining Coal Burnout, M.S. Thesis, Brigham Young University, Dept. of Chem. Eng., Provo, UT (1982).

Smith, I.W., The Combustion Rates of Coal Chars: A Review, Nineteenth International Symposium on Combustion, The Combustion Institute, Pittsburgh PA, 1045 (1982).

Solomon, P.R., Serio, M.A., Hamblen, D.G., Smoot, L.D. and Brewster, B.S., Measurement and Modeling of Advanced Coal Conversion Processes, 5th Annual Report, DOE-METC Contract No. DE-AC21-86MC23075, Advanced Fuel Research, Hartford, CT, (1991).

Solomon, P.R., Serio, M.A., Hamblen, D.G., Smoot, L.D. and Brewster B.S., Measurement and Modeling of Advanced Coal Conversion Processes, 5th Annual Report, DOE-METC Contract No. DE-AC21-86MC23075, Advanced Fuel Research, Hartford, CT, (1990).

Solomon, P.R., Serio, M.A., Hamblen, D.G., Smoot, L.D. and Brewster B.S., Measurement and Modeling of Advanced Coal Conversion Processes, 5th Annual Report, DOE-METC Contract No. DE-AC21-86MC23075, Advanced Fuel Research, Hartford, CT, (1991).

Tichenor, D.A., Mitchell, K.R., Hencken, K.R., Niksa, S., Simultaneous In Situ Measurement of the Size, Temperature and Velocity of Particles in a Combustion Environment, Twentieth International Symposium on Combustion, The Combustion Institute, Pittsburgh, PA, 1213 (1984).

Tsai, C.Y., Scaroni, A.W., The Structural Changes of Bituminous Coal Particles During the Initial Stages of Pulverized-Coal Combustion, Fuel, **66**, 200 (1987).

Waters, B.J., Squires, R.G., Laurendeau, N.M., and Mitchell, R.E., Evidence for Formation of CO_2 in the Vicinity of Burning Pulverized Carbon Particles, Combustion and Flame, **74**, 91 (1988).

Young, B.C. and Smith, I.W., The Kinetics of Combustion of Petroleum Coke Particles at 1000 to 1800 K: The Reaction Order, Eighteenth Symposium on Combustion/The Combustion Institute, 1249 (1981).

Young, B.C.and Niksa, S., Combustion Rates for Selected Low-Rank Coal Chars, Fuel, **67**, 155 (1988).

II.C. SUBTASK 2.c. - SECONDARY REACTION OF PYROLYSIS PRODUCTS AND CHAR BURNOUT SUBMODEL

Senior Investigators - Peter R. Solomon, James R. Markham, and Michael A. Serio
Advanced Fuel Research, Inc.
87 Church Street, East Hartford, CT 06108
(203) 528-906

Objective

The objective of this subtask was to develop and evaluate by comparison with laboratory experiments, an integrated and compatible submodel to describe the secondary reactions of volatile pyrolysis products and char burnout during coal conversion processes. Experiments on tar cracking, soot formation, tar/gas reactions, char burnout, and ignition were done in order to allow validation of submodels.

Summary of Accomplishments

The processes addressed under this subtask were:

- ignition
- soot formation
- soot radiation
- char burnout

These processes were studied using a new laminar coal flame experiment developed at AFR known as the Transparent Wall Reactor (TWR) and a novel diagnostic method known as Fourier Transform Infrared (FT-IR) Emission/Transmission (E/T) Tomography. This work is described in a number of publications and papers that resulted from this contract:

- Solomon, P.R., Chien, P.L., Carangelo, R.M., Best, P.E., and Markham, J.R., Application of FT-IR E/T Spectroscopy to Study Coal Combustion Phenomena, paper presented at the Int. Coal Combustion Symposium, Beijing, China (1987).
- Solomon, P.R., Chien, P.L., Carangelo, R.M., Best, P.E., and Markham, J.R., Application of FT-IR Emission/Transmission (E/T) Spectroscopy to Study Coal Combustion Phenomena, The 22nd Symposium (Int) on Combustion, The Combustion Institute, Pittsburgh, PA, p. 211 (1988).
- Solomon, P.R., Best, P.E., Markham, J.R., and Klapheke, J., The Study of Coal Flames Using FT-IR Emission/Transmission Tomography, Int. Conference on Coal Science Proceedings, IEA, Tokyo, Japan, p. 329 (October 23-27, 1989).
- Solomon, P.R., Serio, M.A., and Markham, J.R., Kinetics of Coal Pyrolysis, Int. Conference on Coal Science Proceedings, IEA, Tokyo, Japan, p. 575, (October 23-27, 1989).
- Brewster, B.S., Smoot, L.D., and Solomon, P.R., Structure of a Near Laminar Coal Jet Diffusion Flame, Poster Session, 23rd Symposium (Int) on Combustion, The Combustion Institute, Orleans, France (1990).
- Solomon, P.R., Chien, P.L., Carangelo, R.M., Serio, M.A., and Markham, J.R., New Ignition Phenomenon in Coal Combustion, Combustion & Flame, 79, 214 (1990a).

- Solomon, P.R., Markham, J.R., Zhang, Y.P., and Carangelo, R.M., FT-IR Emission/Transmission Tomography of Coal Flames, ACS Div. of Fuel Chem. Preprints, **35**, (3), 746, (1990).
- Markham, J.R., Zhang., Y.P., Carangelo, R.M., and Solomon, P.R., FT-IR Emission/Transmission Tomography of a Coal Flame, 23rd Symposium (Int) on Combustion, The Combustion Institute, Orleans, France, pp 1869-1875 (1990).
- Solomon, P.R., and Best, P.E., Fourier Transform Infrared Emission/Transmission Spectroscopy in Flames, in *Combustion Measurements*, (N. Chigier, Ed.), Hemisphere Publishing Corp. pp. 385-344 (1991).
- Brewster, B.S., Smoot, L.D., Solomon, P.R., and Markham, J.R., Structure of a Near-Laminar Coal Jet Flame, Energy and Fuels 7 (6), 884 (1993).
- Solomon, P.R., On-Line Fourier Transform Infrared Spectroscopy in Coal Research, in *Advances in Coal Spectroscopy*, (H.L.C. Meuzelaar, Ed.), Plenum Publishing Corp. pp. 341-371 (1992).

The work done under this subtask is described below. In cases where the work has been well documented in the open literature, reference has been made to the appropriate publications and only the abstracts are included. Details of the work can also be found in the Quarterly and Annual reports for this contract. Additional studies of char burnout were performed under Subtasks 2.a., 2.b., and 2.f. Studies of tar cracking were also made under Subtask 2.e.

II.C.1. Application of FT-IR Emission/Transmission (E/T) Spectroscopy to Study Coal Combustion Phenomena

This work was described in Solomon et al. (1988). The abstract for this paper is given below.

Abstract

This paper describes the application of a recently described Fourier Transform Infrared (FT-IR) Emission and Transmission (E/T) technique to study coal flames produced in a transparent wall reactor. Comparisons are made for the ignition, soot formation, particle temperature and gas temperature for a number of coals varying in rank from lignite to low volatile bituminous. Samples of chars prepared at different temperatures and demineralized coals were also studied. Flame properties were compared with characteristics of the samples to determine the factors which control flame behavior. A comparison of the ignition of several samples suggests that the rate of ignition correlates with the initial rate of weight loss in air in a TGA experiment at lower temperatures. Ignition of chars is heterogeneous; ignition of high rank coals is homogeneous; but low rank coals exhibit both homogeneous and heterogeneous contributions to ignition. Soot formation in combustion correlates well with the tar yield in pyrolysis, suggesting that tar is the chief precursor of soot.

This work is also discussed in a paper by Solomon et al. (1987) and in review articles by Solomon and Best (1991) and Solomon (1992).

II.C.2. FT-IR E/T Tomography of a Coal Flame

This work is discussed briefly in Solomon et al. (1989) and in more detail by Markham et al. (1990). The abstract for the latter paper is given below:

Abstract

Fourier Transform Infrared (FT-IR) Emission/Transmission (E/T) spectroscopy has recently been shown to be a versatile technique for coal combustion diagnostics by allowing for measurements of particle concentrations and temperatures, and gas compositions, concentrations, and temperatures. These measurements are for the ensemble of particles and gases along a line-of-sight in the flame. In this paper, tomographic reconstruction techniques have been applied to line-of-sight FT-IR E/T measurements to derive spectra that correspond to small volumes within a coal flame. From these spectra, spatially resolved point values for species temperature and relative concentrations can be determined. The technique was used to study the combustion of Montana Rosebud subbituminous coal burned in a transparent wall reactor. The coal is injected into the center of an up-flowing preheated air stream to create a stable flame. Values for particle temperature, relative radiance intensity, the relative CO_2 concentrations and the CO_2 temperature have been obtained as functions of distance from the flame axis and height above the coal injector nozzle. The spectroscopic data are in good agreement with visual observations and thermocouple measurements. The data present a picture of the coal burning in a shrinking region which collapses to the center at the tip of the flame. The highest CO_2 temperatures are 2200 to 2600 K. The highest particle temperatures are 1900 to 2000 K with occasional temperatures up to 2400 K.

This work is discussed further Solomon et al. (1990), where a second Rosebud subbituminous coal flame was studied which was produced using a slower flow of preheated gas, along with a third flame produced from Pittsburgh Seam bituminous coal under the same conditions. The three flames showed both coal and flow dependent phenomena. The slow flow cases showed reduced mixing (more soot and more variations in flame properties with radius) compared to the fast flow case. The Pittsburgh Seam coal produced higher soot yields, higher particle swelling, lower particle temperatures and lower char reactivity when compared to the Rosebud coal.

II.C.3. New Ignition Phenomenon in Coal Combustion

A new ignition phenomenon has been observed during the studies of coal combustion in the TWR. The experiment, which was described in several publications (Solomon et. al., 1988; Markham el al., 1990), injects coal particles suspended in a room-temperature carrier gas as a jet into a flowing preheated air stream. The new phenomenon is shown in Fig. II.C-1, which is a photograph of several ignited coal or char particles traveling upward. The particles of interest are at the edge of the cold particle stream and have first contact with the surrounding hot preheated gas stream. They ignite and appear to burn on the particle's surface, as indicated by the fact that the width of the luminosity is roughly that of the particle diameter. The particles become hotter with increasing distance.

The new ignition phenomenon occurs after the particles have burned for a short time. Under these conditions there is often a secondary ignition event. To the unaided eye, it looks like a bright flash of light at the end of a long luminous trajectory. When viewed through a microscope, this event has the following characteristics.

1. The dimension of the second flame zone increased to about 3 times the original dimension.
2. The second flame appears to be hotter than the original.
3. The second flame often ends with particle fragmentation, suggesting burnout of the char.
4. The duration of the flame is on the order of a few milliseconds.
5. The flame appears to oscillate or spiral around the particle in almost all (90%) cases.

The effect has been observed for chars as well as coals, so it is not associated with volatiles. The effect has been observed for demineralized coals and thus is not a mineral effect.

One possibility is that the flame results from CO burning in a sheath surrounding the particle rather than well away from the particle. This would transfer the heat from the $CO \rightarrow CO_2$ flame back to the particle

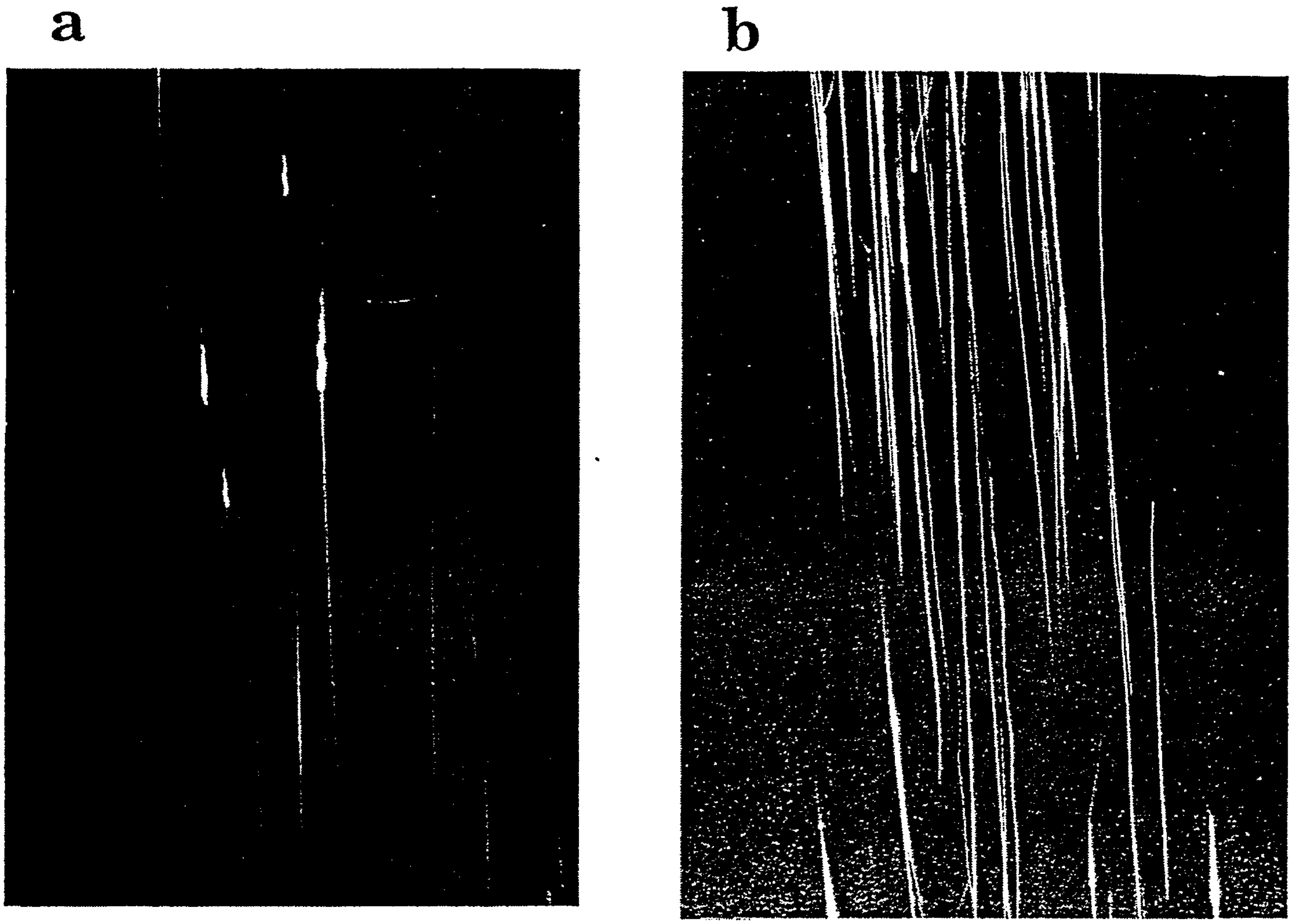

Figure II.C-1. Secondary Ignition Observed for a) Coal and b) Char Particles.

and result in a more intense flame with the possibility of more rapid burnout. However, this mechanism requires that the chief heterogeneous reaction be CO_2 gasification on the coal particles surface. The higher temperature may make this slower reaction possible.

This work is discussed further in Solomon et al. (1990a). Further work is required to more fully characterize and explain this new phenomenon.

II.C.4. Pyrolysis Experiments with In-Situ FT-IR Diagnostics in the TWR

Introduction

In the literature, there are orders of magnitude discrepancies in the reported rates for coal pyrolysis weight loss or tar loss. The conflict in values and the reasons for the conflict have been discussed previously (Solomon and Hamblen, 1985; Solomon and Serio, 1987; Solomon et. al., 1992). These studies concluded that inaccurate knowledge of coal particle temperatures was the chief cause of the variations.

To improve the knowledge of particle temperatures, a new method was developed which employs a Fourier Transform Infrared (FT-IR) spectrometer to measure the emission and transmission (E/T) in a reacting particle stream (Solomon and Hamblen, 1985; Serio et al., 1987). This technique has been applied to measure the temperature of coal particles in an entrained flow reactor (EFR) (Best et al., 1986; Solomon et al., 1987a) and a heated tube reactor (HTR) (Solomon et al. 1986). The kinetic rate, determined from these experiments for a number of coals and lignites was $8.6 \times 10^{14} \exp(-228{,}500/RT)$ sec^{-1} for tar loss (or approximately half this value for weight loss) and was the highest ever reported at temperatures above 600°C. There were, however, some limitations to these experiments. The EFR experiments only allowed optical access for temperature measurement at one position and the HTR was limited to non-swelling coals. Recent experiments by Fletcher (1989) in an apparatus which does not have these limitations and which employs temperature measurements by 2-color pyrometry have confirmed these high rates within a factor of 2 for both low and high rank coals.

Under this subtask, kinetic rate measurements were made on a Zap North Dakota lignite and a Pittsburgh Seam bituminous coal in the transparent wall reactor (TWR) which does not have the limitations of the HTR or EFR. The temperature measurements were made with the FT-IR E/T technique. This reactor, with the in-situ FT-IR diagnostics, was used under this subtask to make spatially resolved measurements on coal flames using a tomographic technique, as discussed above. These measurements provide fundamental data on the processes of ignition, soot formation, and char burnout for submodel validation. The pyrolysis experiments allow a test of the experimental and optical systems for a simpler set of conditions.

Experimental

The measurement of particle temperatures from the particle's emitted radiation is difficult if the pyrolysis reactor has hot walls. In this case, wall radiation scattered by the particles interferes with the emitted radiation. To overcome this problem, the pyrolysis experiments in this study were performed in a reactor with relatively cold walls. The apparatus is a transparent wall reactor (TWR) which has been discussed above and in the literature (Solomon et al., 1989c). Nitrogen is passed through a heat exchanger and enters a reaction section at approximately 850°C. Coal entrained in cold nitrogen carrier gas is injected through a co-axial 7 mm diameter tube into the preheated stream. An octagonal glass enclosure shields the pyrolyzing stream from room air currents. The glass enclosure has movable KBr windows to allow access to the flame for radiation measurements. Particle velocities were measured using a video camera under slightly oxidizing conditions which allowed a small percentage of the particles to ignite.

To measure temperatures of pyrolyzing coal particles, several other problems had to be overcome.

Because pyrolysis in this reactor occurs at relatively low temperatures (600-800°C), the measurements are made in the mid-infrared where sufficient energy is emitted. In addition, coal is not a gray-body and its emissivity changes during pyrolysis. To overcome this problem, the temperature has been measured using the amplitude of the radiated energy in a frequency range where the emissivity is close to one and independent of the extent of pyrolysis. The transmission is used to determine the emitting surface area of the particles. Finally, soot radiation can make the particle temperature appear much higher than it really is. Measurements have been made with a gas temperature of 850°C, so soot formation did not occur.

The coals studied in this work were a dried Zap North Dakota lignite and a Pittsburgh Seam bituminous coal. The ultimate analyses are approximately those reported in Serio et al. (1987). Both samples were sized to 200 x 325 mesh. Weight loss was determined from captured char particles, by ash tracer analysis, using a Perkin Elmer TGA.

Results and Discussion

The emission spectra for the pyrolyzing particles at 15 cm above the injector are presented in Solomon et al. (1989) and Solomon (1992). The spectra are normalized by the emitting surface area using the measured attenuation at 3500 cm^{-1} assuming a total extinction efficiency of 1.2. The spectra are not gray-body. They reveal the infrared absorption bands in the char, such as the higher hydroxyl and carbonyl bands in the lignite and the higher aliphatic and aromatic C-H bands in the bituminous coal. Bands for pyrolysis water, CO_2, and CO are also apparent. Particle temperatures were determined by matching the theoretical black-body curves curves to the radiance at 1600 cm^{-1}, where the emissivity is approximately 1.0 (Best et al., 1986).

Spectra such as these were obtained for both coals at positions between 5 and 40 cm. In addition, char samples were captured at a number of locations and the FT-IR E/T technique was used to determine both particle and CO_2 temperatures (Solomon et al., 1987a,1989c). The CO_2 and particle temperatures agree to within 100°C. The thermocouple temperature measurements averaged across the estimated width of the particle stream are also in reasonable agreement, except early in the early stages when the particles are heating and in the later stages when the gas is cooling. The particle's heating rate is about 5000°C/sec. Data were also obtained for the weight loss determined by ash tracer analysis, which are compared to predictions of the FG-DVC model (Solomon et al., 1988).

As discussed in Solomon et al. (1989) and Solomon (1992), the high kinetic rates for tar evolution or weight loss recently reported by Solomon et al. (1985,1986a), Serio et al. (1987) and Fletcher (1989) are supported by these TWR measurements. At high heating rates, significant pyrolysis occurs within 100 ms at temperatures between 700 and 1000 K for both a lignite and a bituminous coal. At lower heating rates, the differences in rate between coals of different rank are more readily apparent (see subtask 2.a.).

II.C.5. Gas Flow Characteristics and Sample Burnout Profiles in the TWR

Introduction

In order to provide data for validation of the PCGC-2 code predictions (reported under Subtask 3.a.) and discussed in Brewster et al. (1990, 1993) an effort was directed at characterizing the TWR with regard to air and particle velocities, gas temperature profiles, particle spreading, and char burnout as a function of distance from the nozzle.

Results and Discussion

Radial gas temperature measurements were taken by thermocouples with and without coal being injected. Figure II.C-2, for the no coal case, shows measurements done from 2 mm above the nozzle to 70 cm above the nozzle. The measurements were taken with a bare 0.005" diameter bead chromel-alumel thermocouple, which was corrected for radiation loss to the cold walls, and for thermocouple surface

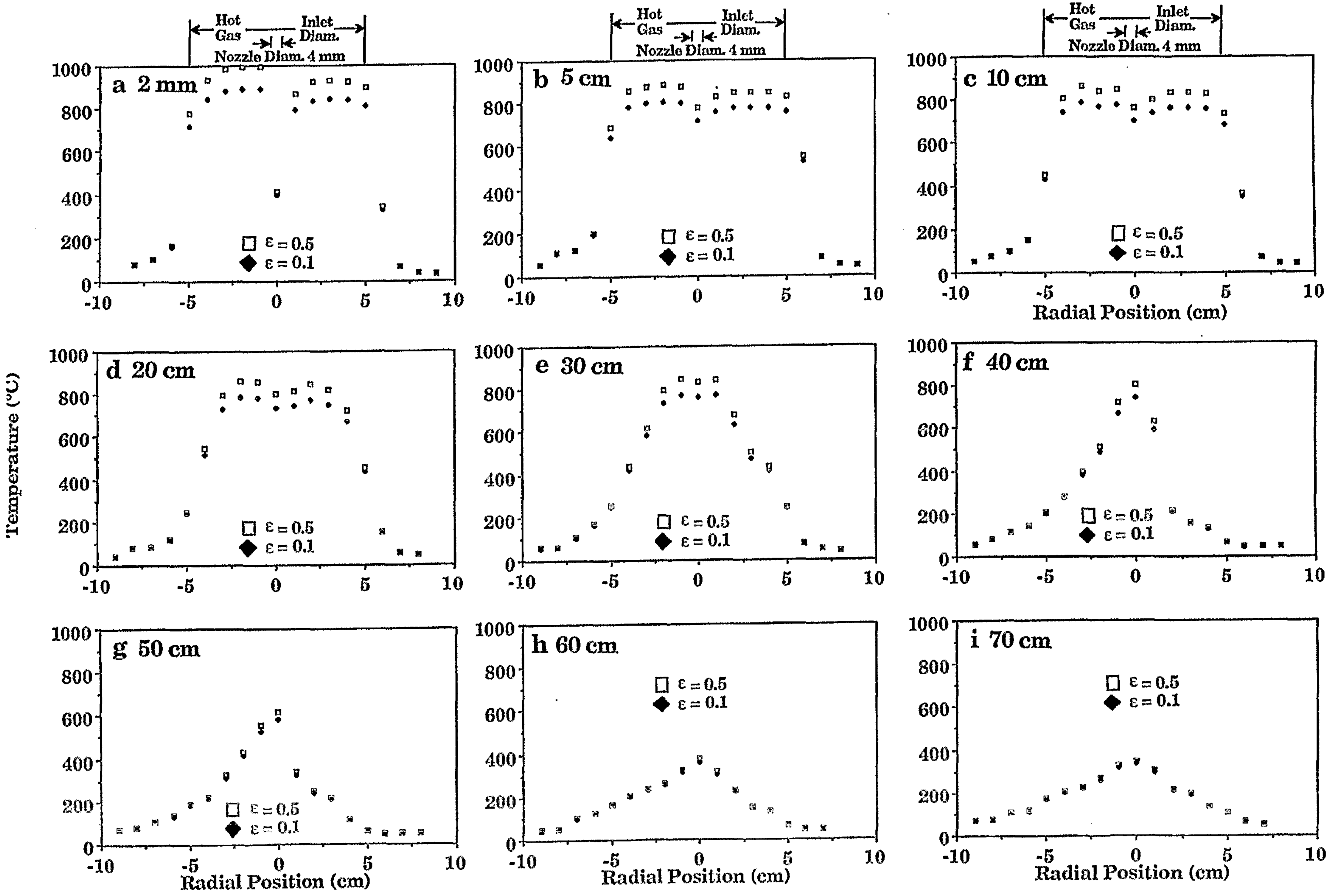

Figure II.C-2. Radial Gas Temperature Profile in the TWR, No Coal Case.

emissivity. Emissivity values of 0.1 and 0.5 were used, based on a literature value range for shiny to oxidized surfaces of this material. The figure clearly shows the region where cold gas is injected through the nozzle and that the integrity of the hot gas column is maintained through 20 cm.

Figure II.C-3 again profiles the gas temperature, but with 200 x 325 mesh Montana Rosebud coal injected into the TWR. For this case a 0.015" diameter platinum - 13% rhodium/platinum thermocouple was used. Surface emissivity values of 0.1 and 0.9 were used, based on the extremes of shiny metal to a soot/carbon coated surface. Profiles similar to the no coal case were observed, except for in the coal region, where the temperature greatly increases upon ignition of the coal at 10 cm above the nozzle.

The dimensions of the particle stream for the Rosebud flame were measured with a video camera. A schematic is shown in Fig. II.C-4. Above the ignition point, direct recording of the flame width was possible; below the ignition point, a He-Ne laser was directed through the particle stream and the laser light that was scattered by the particles was used to define the stream boundaries. The dimensions determined by the video camera were in agreement with spectroscopic detection of particles during the tomography measurements, and for detection of trace amounts of SO_2 fed through the nozzle.

Particle velocities as a function of distance from the nozzle are shown in Fig. II.C-5 for pyrolysis (N_2) and combustion (air) conditions. These were measured from particle tracks that were recorded with the video camera at a known shutter speed. For pyrolysis conditions, a small amount of oxygen was added to the gas stream to allow a small percentage of the particles to ignite. The particle velocities for each case are similar until beyond 20 cm above the nozzle. At this point the pyrolyzing stream approaches the calculated velocity of the hot gas at the nozzle region. Under combustion conditions, however, the energy released upon ignition drives the particles to higher velocities.

Particle burnouts as a function of distance from the nozzle were measured for 200 x 325 mesh samples of a dry Zap lignite, dry Rosebud subbituminous coal, and Pittsburgh Seam bituminous coal. Char collections were achieved with a 5/8" diameter water cooled extractor that adds cold helium gas to the removed hot particle stream as it is aspirated to a cyclone separator. The extractor inlet temperature was maintained below 300°C by the helium addition

Percent burnout was determined by ash tracer analysis of the collected char. The results are presented in Fig. II.C-6. One observation is the rank dependent effect on char reactivity, as indicated by the interval of time necessary to achieve 100% burnout: Zap < Rosebud < Pittsburgh.

II.C.6 In-Situ FT-IR Diagnostics in BYU Gasifier

An optical path was added to the BYU gasifier to allow the FT-IR transmission and emission measurements, as shown in Figs. II.C-7 and II.C-8. Figure II.C-7 shows the location of the optical path for the gasifier, while Fig. II.C-8 shows the schematic details of the spectrometer optics. The method requires two basic measurements: an emission spectrum from the flame through the spectrometer to the emission detector, and a transmission spectrum using the IR source within the spectrometer through the flame to the transmission detector. Several calibration spectra are also required: 1) a background emission spectra from the hot gasifier without a flame (to correct the emission spectra for gasifier wall radiation); 2) an emission spectrum from a black-body source (to correct the emission spectrum from instrument losses and detector sensitivity, etc.); and 3) a transmission spectrum without a flame (to correct the transmission spectrum from instrument and optical path effects).

An example of the corrected transmission ($1-\tau$) and emission (E) spectra are shown in Fig. II.C-9a,b. The emission (radiance) curve represents the radiation per unit area of the flame. The normalized emission, $E/(1-\tau)$, has the effect of normalizing to effective area of the radiating particles to provide the radiation per unit area of radiating particles and gases (Fig. II.C-9c). In the regions of the spectrum in Fig. II.C-9c where there are no gas absorptions, the curve can be fit by a black-body Planck function, scaled

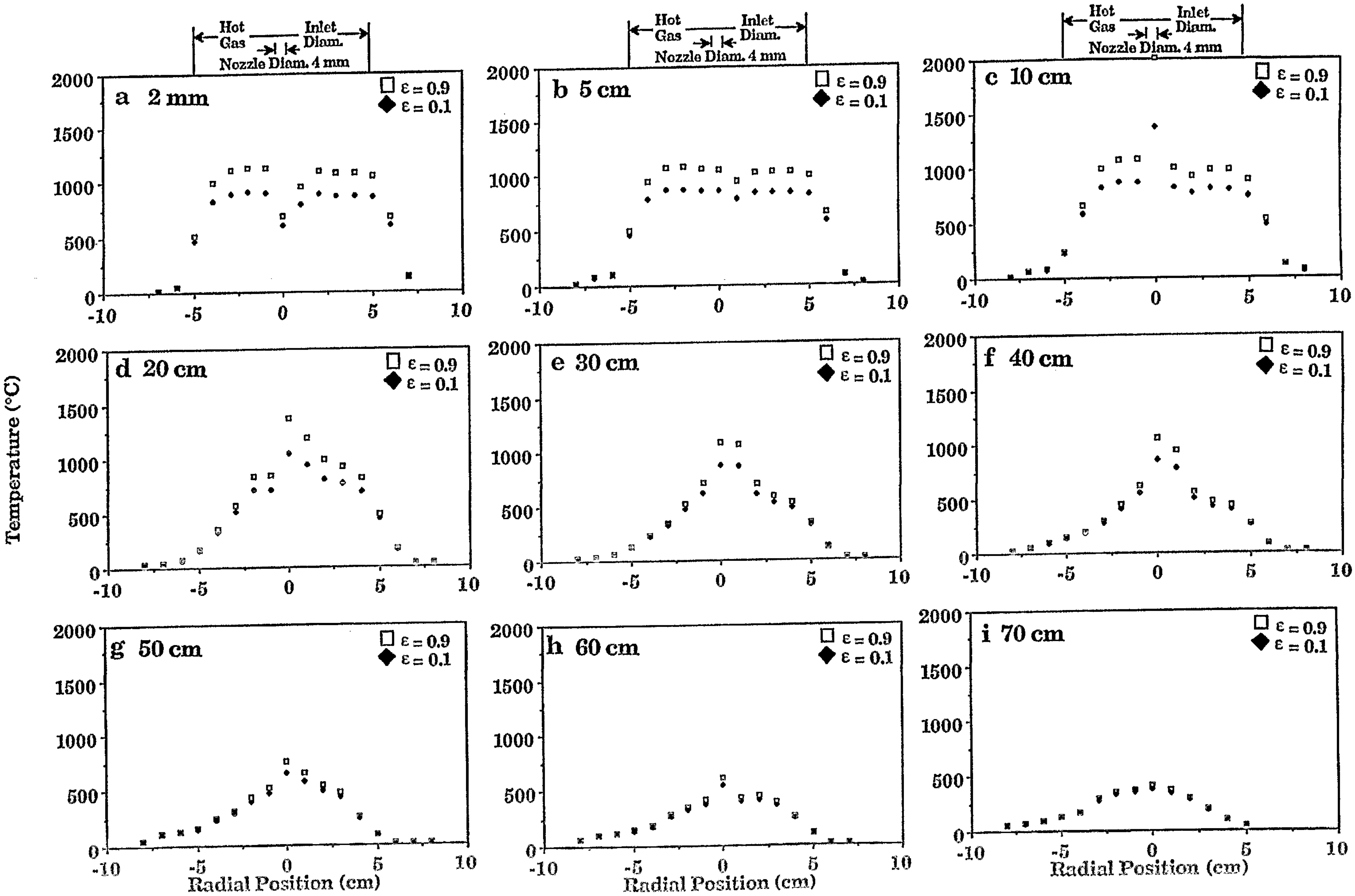

Figure II.C-3. Radial Gas Temperature Profile in the TWR During Combustion of Montana Rosebud Coal.

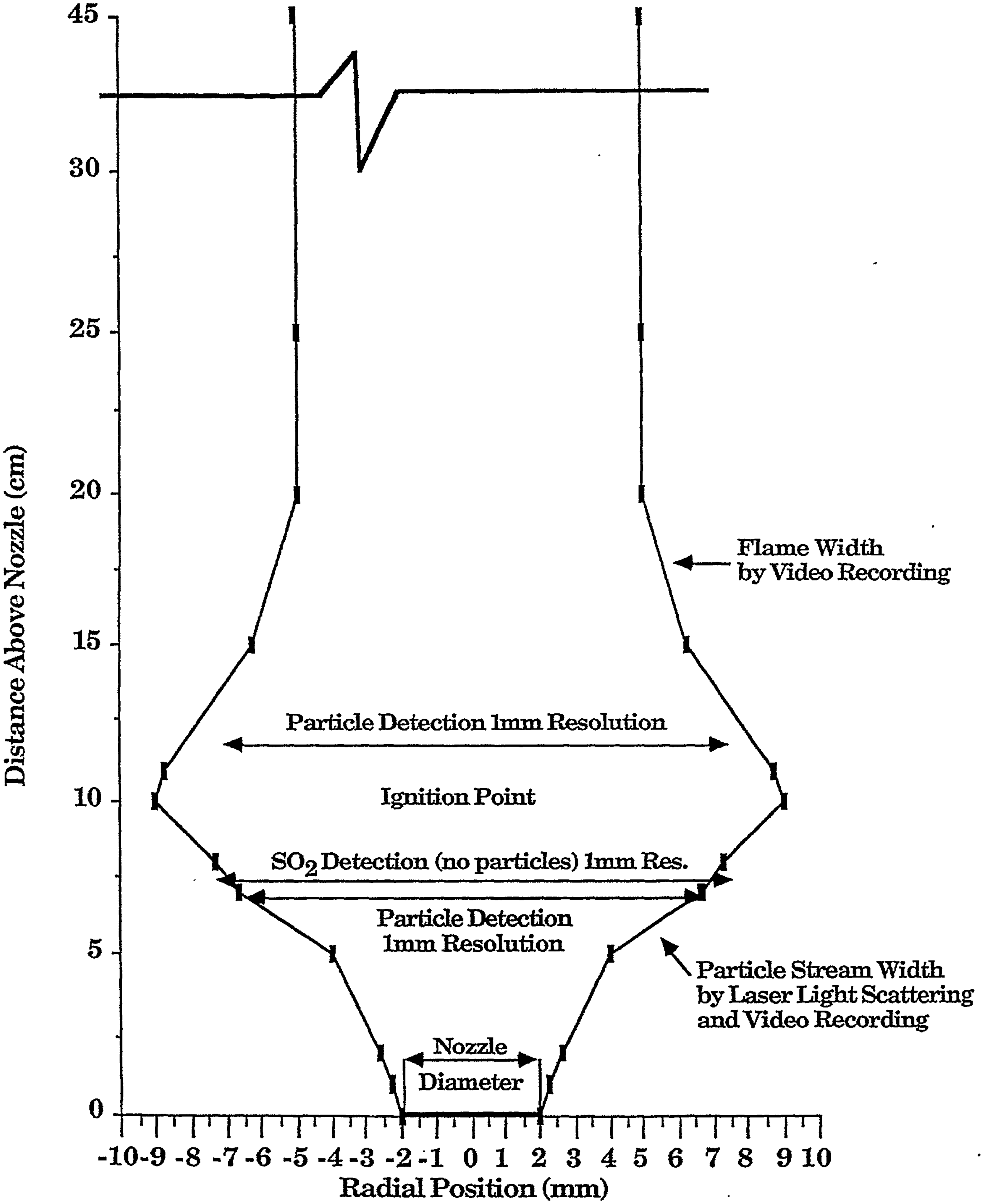

Figure II.C-4. Schematic of Montana Rosebud Particle Stream Boundaries before and after Ignition.

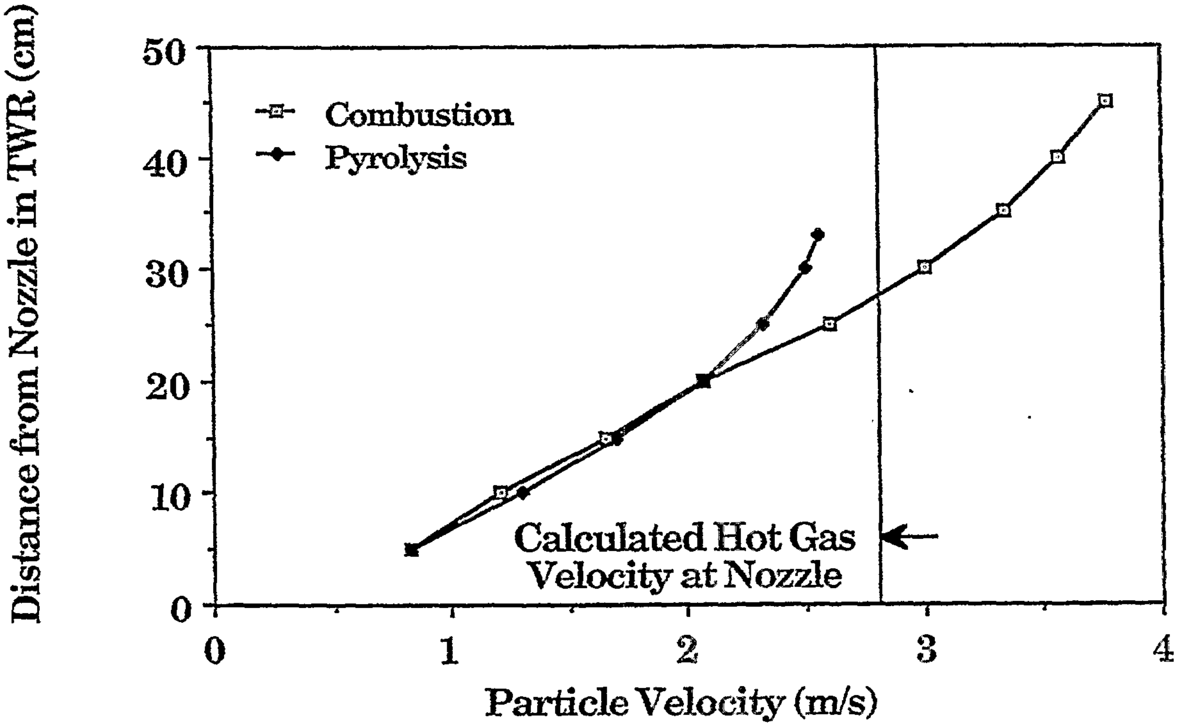

Figure II.C-5. Velocity of 200 x 325 mesh Montana Rosebud Particles in the TWR. Velocities were Measured by a Video Recording of Particle Tracks.

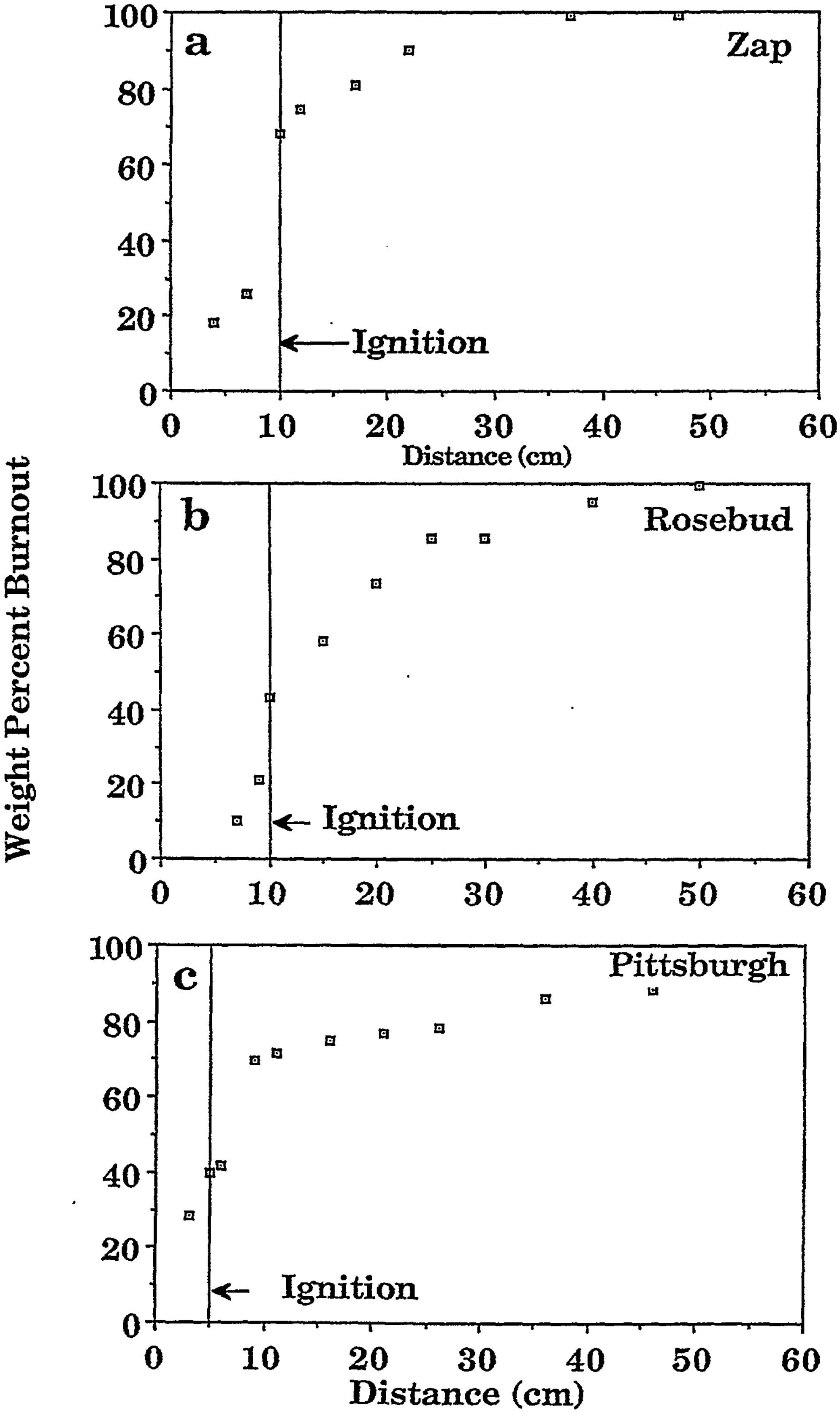

Figure II.C-6. Particle Burnout for Combustion of a) Zap Lignite, b) Montana Rosebud SubbituminousCoal and c) Pittsburgh Seam Bituminous Coal in the TWR.

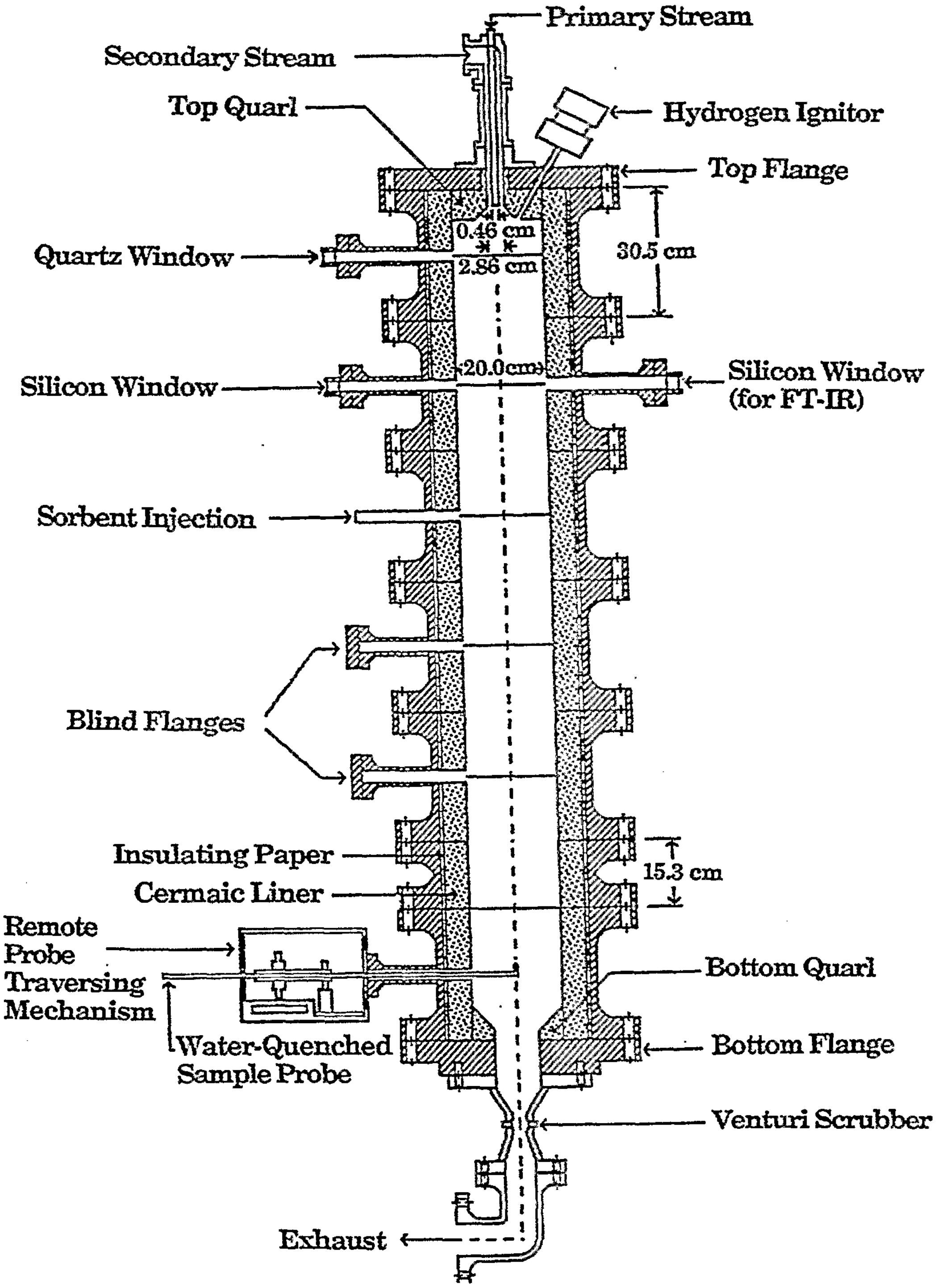

Figure II.C- 7. Modified Gasifier for Sorbent Injection and FT-IR Measurements.

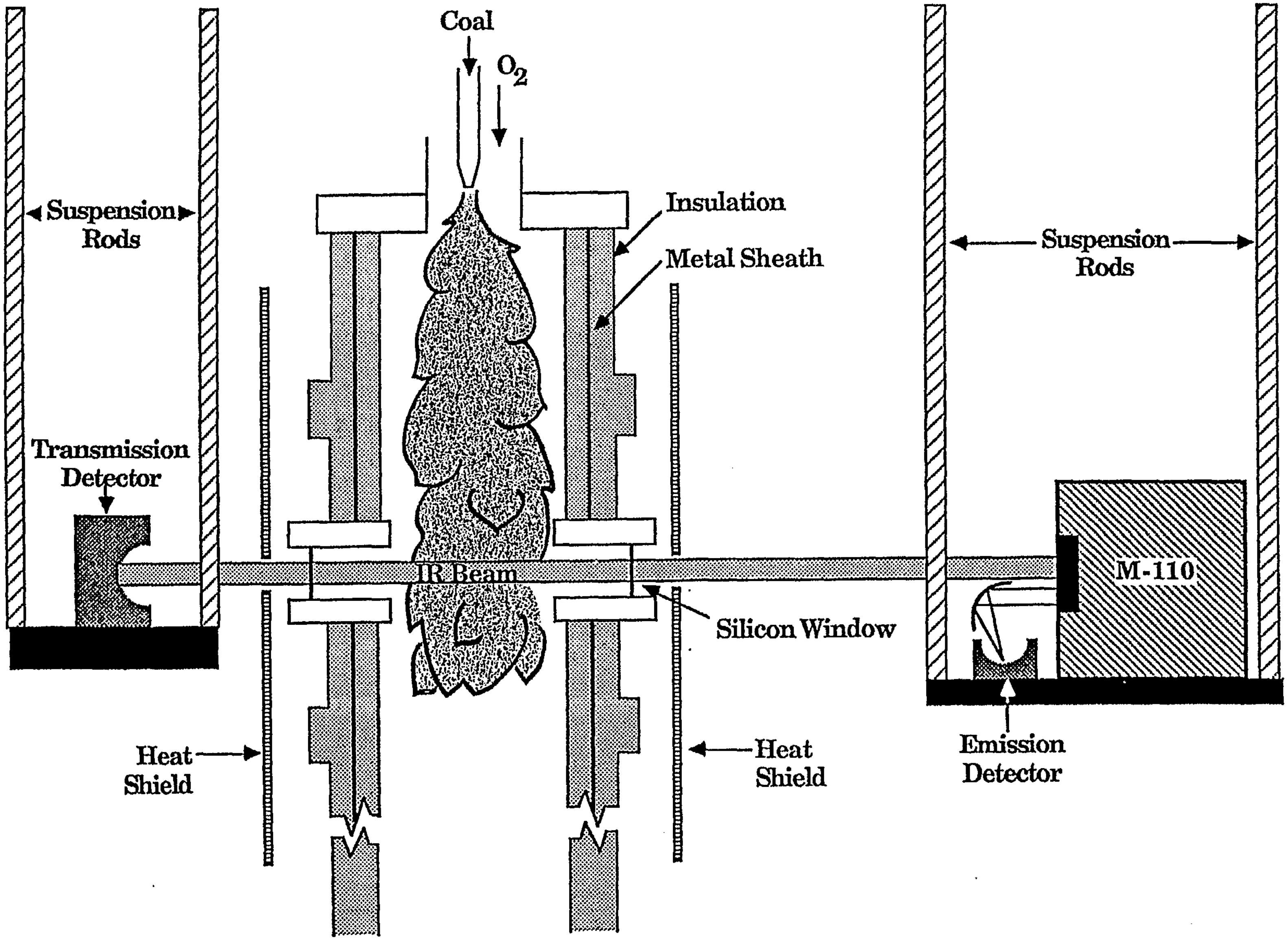

Figure II.C-8. Schematic of BYU Gasifier with In-Situ FT-IR Diagnostics.

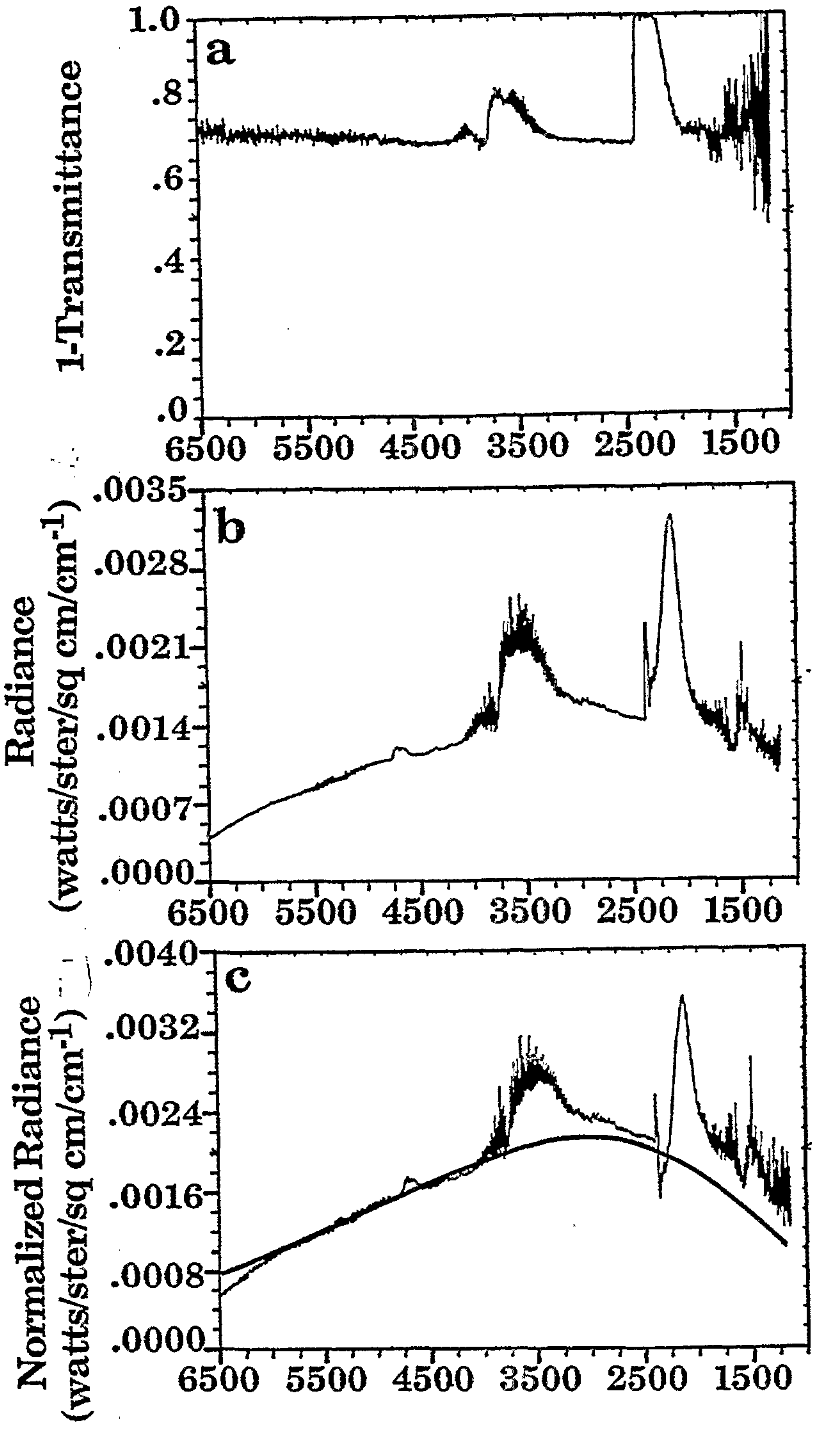

Figure II.C-9. Transmission, Emission and Normalized Emission Spectra through the Flame of the BYU Pilot Flame for the Combustion of Pulverized Coal.